SURFACE INITIATED POLYMERIZATION OF CONJUGATED POLYMERS BY KCTP (KUMADA CATALYST TRANSFER POLYCONDENSATION) EFFICIENT GRAFTING METHODOLOGIES, STRUCTURE FUNCTION RELATIONSHIP AND ORGANIC ELECTRONIC DEVICE FABRICATION

by

ANANDI ROY

(Under the Direction of JASON LOCKLIN)

ABSTRACT

In this dissertation, synthesis of conjugated polymer brushes of poly(3-methylthiophene) (P3MT) via SI-KCTP (Surface Initiated Kumada Catalyst Transfer Polycondensation) and their applications is discussed. These conjugated polymer brushes have unique optical and electronic properties and hence they are thoroughly investigated for applications in fabrication of more efficient organic electronic devices (OEDs). These devices have definite requirements in terms of grafting densities and directionality of polymer brushes. Therefore to have a thorough understanding, their unique properties are evaluated by systematic analysis of their structure-function relationship and limitations. The current problems associated with their limited applicability in OED fabrication are also studied. With this thorough understanding, optimal P3MT brushes have been developed and applied for successful OED fabrication. Covalent immobilization of polymer chains to substrates prevents delamination and provides a method to make uniform coatings on objects of complex geometries. Utilization of "grafting from" approach has proved to be efficient towards producing uniform and mechanically robust films.

SI-KCTP begins with fabrication of reactive initiator monolayers from substrate surfaces and uses highly reactive catalysts like Ni(0) or Pd(0). The catalyst centers are prone to enter into a competitive side reaction called disproportionation, whereby catalyst concentration on the surface is reduced. This reduces grafting density and also indirectly affects the directionality of polymer brushes. The structure of these monolayers highly influences the rates of disproportionation reactions. A detailed systematic study is performed in order to understand the structure-function relationship of reactive initiator monolayers to the nature of P3MT brushes grown. This led us to develop the optimal initiator monolayer which produced P3MT brushes, appropriate for usage in OEDs.

To prove the efficiency of the new reactive initiator monolayer towards OED fabrication, organic spin valve devices (OSVs) are fabricated with P3MT brush acting as the non-magnetic spacer layer covalently bound to ferromagnetic electrode. The device showed highly enhanced magnetoresistance response. This encouraging result proves the potential of the new monolayer. It also justifies the hypothesis that spin coating produces more disordered layers, reducing device efficiency by poor contact with surfaces and enhancing intermolecular rather than intra molecular carrier transport. Further, these brushes are considered for potential application towards heat conducting devices since they have shown high thermal conductivities on measurement by the time domain thermoreflactance (TDTR) technique. Rapid and efficient electrochemical techniques are also examined to overcome problems associated with traditional solution deposition ones.

INDEX WORDS: Kumada coupling transfer polycondensation, P3MT, P3HT, Polymer brush, H-aggregation, Magnetoresistance, Thermal conductivity

SURFACE INITIATED POLYMERIZATION OF CONJUGATED POLYMERS BY KCTP (KUMADA CATALYST TRANSFER POLYCONDENSATION): EFFICIENT GRAFTING METHODOLOGIES, STRUCTURE FUNCTION RELATIONSHIP AND ORGANIC ELECTRONIC DEVICE FABRICATION

by

ANANDI ROY

B.Sc. Chemistry, University of Delhi, India, 2009

M.Sc. Chemistry, University of Delhi, India, 2011

A Dissertation Submitted to the Graduate Faculty of The University of Georgia in Partial Fulfillment of the Requirements for the Degree

DOCTOR OF PHILOSOPHY

ATHENS, GEORGIA

2016

SURFACE INITIATED POLYMERIZATION OF CONJUGATED POLYMERS BY KCTP (KUMADA CATALYST TRANSFER POLYCONDENSATION): EFFICIENT GRAFTING METHODOLOGIES, STRUCTURE FUNCTION RELATIONSHIP AND ORGANIC ELECTRONIC DEVICE FABRICATION

by

ANANDI ROY

Major Professor:	Jason Locklin
Committee:	Tina Salguero
	Jin Xie

Electronic Version Approved:

Suzanne Barbour
Dean of the Graduate School
The University of Georgia
August 2016

DEDICATION

To my mother, father and husband. Thank you for believing in me and my goals. Dad, who is my biggest guide in life and who helped me to follow my dreams. For my Mom who always gave me confidence and advice to deal with all kinds of challenges I had to face, staying far away from home. For my husband who took care of me through my good and bad days during PhD and gave me immense mental support.

ACKNOWLEDGEMENTS

I would like to thank my parents for their constant support and guidance throughout my PhD, for bearing with me and encouraging me to keep working hard during all the times in these five years when I could not go home and missed all family celebrations. I could not have done my PhD without their support. I would also like to thank my husband, who has given me moral support and always given me strength to go on even after when I had failures during this journey. We have been living far apart but, he always made it a point to stay connected to me during difficult times. Thank you for being so kind and considerate and letting me run my research ideas by you.

My advisor Dr. Jason Locklin has been by my side always. He gave me the opportunity to work on interesting projects and guided me throughout. I would like to thank him for not only teaching me science and how to think creatively but also for guiding me with so many other facets of life helping me grow to not only become mentally stronger but also to become an independent scientist. You are a man of principles, I really admire that and I will always have great respect for you and for everything you have done for me.

My collaborators have been immensely supportive and helpful. I would like to thank Rugang Geng, Dr. Tho Nguyen, Dr. Thomas Bougher and Dr. Baratunde Cola for their help and advice. Running experiments and having discussions at odd hours and working hard to make our collaborative projects successful have been challenging, but with all your help we have successfully come through.

I would also like to thank my committee members, Dr. Tina Salguero and Dr. Jin Xie for their guidance and investing their time in me. Your comments have been very valuable towards developing my creative thinking. Finally I would like to thank my labmates, especially my dear friend Jing Gao. You have been one of my closest friends here in Athens. You and I practically shared each and every day of our lives in the lab, dealing with our day to day challenges and beyond. It has been a tough journey but we helped and supported each other out to get through tough times. My labmates and friends Jeremy, Josh, Karson, Deb, Li and Qiaohong, I will always be grateful to all of you and thank you for your friendship. We have had fun as well as stressful times but we stuck together as a family. My seniors Rachelle, Kyle, Gareth, Evan, Joe, Jenna and Eric; You have taught me so much. Kyle for teaching me and getting me interested in KCTP, Eric for teaching me interesting synthetic techniques, Gareth for teaching me analytical techniques and Evan for letting me bounce of ideas and drafts by you and critiquing on my talks. Joe, you have not been my labmate but like my own brother. You helped me deal with so many important things about life outside the lab. You were always ready to help and support me whenever I needed you, irrespective of what time it was. I wish I can do the same for you. You are a really good man and I am lucky to have you in my life. Jenna, you have given me so much advice on writing, and helped me understand a lot of challenging concepts in KCTP, even when you graduated. Thank you very much for your advice and for the time you invested in me. Finally Rachelle, you have been my dear friend and helped me through so many things in lab I cannot even mention. Thank you very much for being my friend. My dear friends in Athens who helped me stay happy and cheerful, took immense care of me when I was sick or upset and celebrated with me during my good times, Dipesh, Abhinav, Dipanwita, Shubhankar, Maria and Madhumati. I can’t thank you enough for all your support. I could not have done this without you.

TABLE OF CONTENTS

Page

LIST OF TABLES

Page

LIST OF FIGURES

Page

CHAPTER 1

INTRODUCTION AND LITERATURE REVIEW

Conjugated Polymers

Conjugated polymers (CPs) were discovered in the 1970s by Alan Heeger, Alan MacDiarmid, and Hideki Shirakawa. They noted that π-conjugated polymeric materials (e.g., polyacetylene) can be made electrically conductive. Commonly known polymers (e.g., plastics) are considered "insulating" because they are bad conductors of electricity, this surprising discovery immensely diversified the field of polymer chemistry. For this revolutionary discovery, they were awarded the Nobel prize in 2000.[1] Since then, CPs have attracted a lot of attention due to their immense potential in fabrication of OEDs. They show a unique blend in characteristics of metals/inorganic semiconductors which exhibit interesting optical and electronic properties while retaining the identity of synthetic polymers. This imparts mechanical flexibility and causes potential reduction in processing expenses of organic photovoltaic devices. Since they can be processed in solution and therefore can be easily coated on surfaces of OEDs with complex geometries by spin coating, inkjet printing etc.[2] All these interesting properties make CPs a class of attractive materials. The development of CPs was accidental to a certain extent. One day, Shirakawa's student from Tokyo Institute of Technology was attempting to synthesize polyacetylene by the Ziegler Natta polymerization technique. Polyacetylene was already knows as a black powdery material with high crystallinity but little applications due to its limited solubility and air sensitivity. In this process he accidentally used huge excess of catalyst as opposed to the millimolar concentration he was required to use. This led to the production of a polymeric thin

film with a metallic-foil like appearance instead of the dark powdery material that was expected.[3] The polyacetylene film produced was analyzed further when Prof. A.G. MacDiarmid (Department of Chemistry, University of Pennsylvania) invited Prof. H. Shirakawa to investigate more about the film that they had prepared. Later these professors collaborated with Prof. Alan Heeger and reported that the conductivity of this CP significantly increased (about a million-fold) when doped by iodine or bromine. This collaborative discovery pioneered the fascinating field of conjugated polymers. This spurred a lot of research in this field focusing on developing more stable and useful conductive CPs.

CPs are semiconductors in their native or undoped state. They contain alternating single and double bonds in their backbone. The carbon atoms are sp_2 hybridized, each forming one localized sigma bond which is a strong chemical bond and another weaker double bond which contains delocalized π-electrons. The presence of multiple double bonds close to one another produce extended molecular orbitals by their efficient overlap. Plastic materials, consist primarily of sp_3-hybridized carbon atoms, causing a large energy difference between the highest occupied molecular orbital (HOMO) and the lowest un-occupied molecular orbital (LUMO). Unlike in plastics, CPs have low lying HOMOs due to extended electron delocalization. However delocalization of π electrons is not enough to impart high conductivity to a polymeric material. These materials need to be doped i.e., extra charge carriers (electrons or holes) need to be added to make them more conductive. There are several ways of doping. Addition of electrons (n-type) or addition of holes (removal of electrons, p-type) can both cause doping facilitating transport of charge carriers over long distances. Another possible way is electrochemical doping. Owing to the extensive conjugation of electrons in CPs, they can be easily oxidized or reduced whereby the polymer can either act as an electron donor or an acceptor. This kind of doping process gives more

precise control over doping level, by adjusting the current. With increasing research in this field, a lot of other conjugated and aromatic compounds were developed. The prime interest was in potentially lowering the cost of manufacturing and improving the processing of these polymers. This was projected for applications in the fabrication of new and efficient OEDs with improved mechanical flexibility. Organic materials have very high absorption cross sections allowing them to absorb a huge fraction of solar energy. Since they also have much lower densities compared to inorganic materials, CPs stand out as ideal candidates for making lightweight and efficient OEDs. Some of the important CPs developed were polythiophene(PT), poly(p-phenylene)(PPP), polyphenylenevinylene (PPV), polycarbazole (PCbz), polyfluorene(PPF), polypyrrole, polyaniline etc. as listed in Table 1.1.

Name	**Structure**
Polythiophene	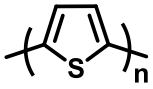
Poly(p-phenylene)	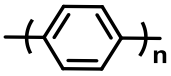
Polyphenylenevinylene	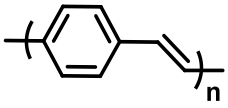
Polycarbazole	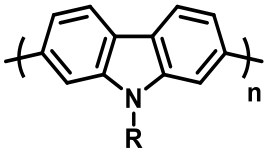
Polyfluorene	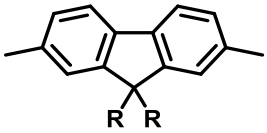
Polypyrrole	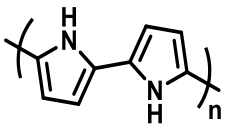
Polyaniline	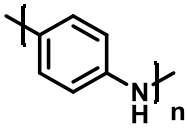

Table 1.1. Examples of commonly used conjugated polymers and their chemical structures

Polythiophenes are used to make OEDs such as organic solar cells, fuel cells, sensors, and field effect transistors. Polyphenylenevinylidene is used as the active layer in electroluminescent displays of mobile phones. Polycarbazoles are used for efficient processing of organic solar cells. Polyfluorenes have interesting opto-electronic properties and are therefore used in light emitting diodes (LEDs) and transistors etc. Doped polyaniline is used as a conductor and for electromagnetic shielding of electronic circuits.

Polythiophenes (PTs) in particular are attractive candidates for usage in OEDs as they are optically transparent, easier to process in the solution, and offer high degree of stability in both doped and un-doped states.[4] They are a very important class of linear conjugated polymers that can be synthesized by chemical as well as electrochemical techniques and can be functionalized easily. Their electronic and optical properties can be tuned for fabricating several optoelectronic devices. PTs can also be doped easily owing to the presence of the electron rich thiophene rings. Presently, a lot of research is ongoing in order to diversify the use of CPs in various OEDs to provide better flexibility, lower costs of processing and easy tunability. So far they have shown very promising results and efficiencies of OEDs fabricated with PTs are rapidly growing.

Synthetic methodologies of conjugated polymers

Cross coupling reactions have grown into an extremely powerful tool to form carbon-carbon bonds and a widely accepted strategy for synthesizing conjugated polymers. Many cross coupling reactions exist, which usually proceeding via step growth polymerization, e.g., Kumada, Stille, Suzuki, Heck, Negishi and Sonogashira reactions.[5-9] All of these reactions proceed by employing M(0) catalysts for e.g. Ni(0) or Pd(0) catalysts in the reaction cycle. The basic catalytic cycle followed in a cross coupling reaction is shown in Figure 1.1. They follow a procedure

involving a cycle of three major steps: oxidative addition and transmetallation followed by reductive elimination. In the oxidative addition step, an active M(0) (M = Ni/ Pd) catalyst inserts across an aryl-halide bond which acts as an electrophilic center, whereby catalyst changes its oxidation state to M(II) and forms an ArM(II)Br complex. This undergoes transmetallation with another nucleophilic organometallic reagent (which varies depending on the specific type of catalytic cycle). Transmetallation produces an unstable aryl-M(II)-aryl species which undergoes reductive elimination to release M(0) to form a dimeric species. The formation of the new C-C bond is the driving force towards this reaction. The catalytic cycle then repeats to produce the polymer in solution.

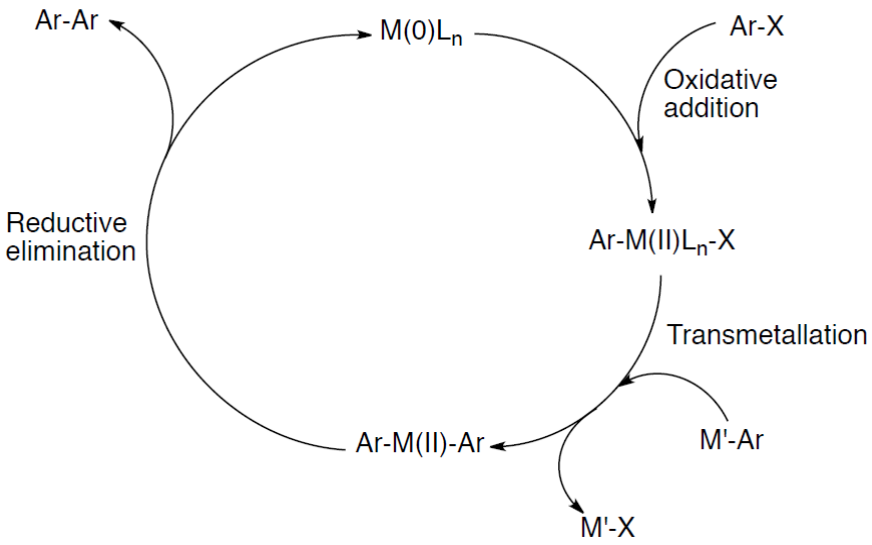

Figure 1.1. Catalytic cycle of a typical metal catalyzed cross coupling reaction

Usually this kind of cross coupling reaction generates polymers in solution by step growth mechanism. But this method is proved to be inefficient because it lacked control. High molecular weights could only be attained at very high monomer conversions. It also didn't provide control over end group functionality. Chain growth polymerization on the other hand can generate

polymers with greater control. Each monomer unit can react only with a propagating chain, with one catalyst responsible for initiating one particular chain. It uses A-B type bifunctional monomers containing both electrophilic and nucleophilic reaction sites, as opposed to A-A/B-B type monomers commonly employed in the step growth process. Bifunctional A-B type monomers provide both electrophilic aryl halide center and metal nucleophilic center on the same molecule which paves the way for cross coupling reaction to proceed in a chain growth fashion. These types of polymers can be synthesized in a more consistent fashion with reproducible molecular weight and end group functionality, which are important factors to consider while employing in device fabrication for optimizing efficiency. One of the most widely used class of conjugated polymers for OEDs is poly(3-alkylthiophenes) (P3ATs). This is because they show unique physical properties like crystallinity and high carrier mobilities. Synthesis of regioregular P3ATs was first demonstrated by McCullough and coworkers in 1992 via Kumada coupling reactions.[10,11] The Kumada coupling reaction is one of the most important cross coupling reactions and hence will be discussed in detail in the following section.

Kumada coupling reaction

In 1972, Kumada and Corriu independently reported cross coupling reactions of Grignard reagents with aryl and alkenyl halides catalyzed by nickel(II) halide catalysts.[6,12,13] This process proceeds through a double transmetallation step. Ni(II) species reacts with organic electrophilic species to form a diorganonickel intermediate where both the aryl centers are bound to the Ni center by sigma bonds. The spatial arrangement of ligands diphenylphosphinoethane or diphenylphosphinopropane (dppe or dppp) around the metal center forces the aryl species to take a cis configuration. This produces unstable intermediate, making it susceptible to reductive

elimination. Therefore, in the next step, Ni(0) is generated by reduction of the unstable Ni(II) complex, which subsequently undergoes intramolecular oxidative addition to the nearest available aryl halide bond. The process then continues as shown in the cycle above to generate polymer in solution. Active catalyst in the Kumada coupling cycle is generated in the following way (as explained above) (Figure 1.2)

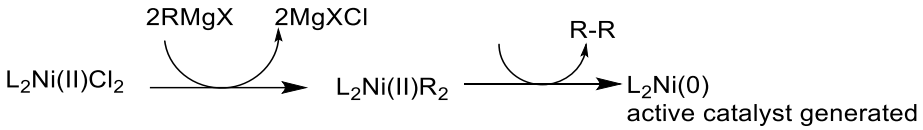

Figure 1.2. Generation of active catalyst in KCTP cycle

McCullough and co-workers synthesized regioregular head to tail (H-T) coupled poly(3-alkylthiophenes) (P3ATs). Their procedure involved lithiation of 2-bromo-3-alkylthiophenes with LDA at cryogenic temperatures, further transmetallating with $MgBr_2 \bullet Et_2O$ to produce 2-bromo-5-(bromomagnesio)-3-alkylthiophenes. This monomer was then polymerized with catalytic amounts of $Ni(dppp)Cl_2$ to give P3AT) which was analyzed to contain 98-100% HT-HT coupling. Later his group discovered another approach to produce regioregular P3ATs at room temperature and at larger scales to avoid usage of cryogenic temperatures. This followed the Grignard metathesis reaction (GRIM), where 2,5-dibromo-3-alkylthiophene monomer was treated with one equivalent of alkyl Grignard reagent causing a magnesium halogen exchange reaction either at the 2 or 5 positions in a ratio of 85:15 to 75:25, respectively.[14] A certain degree of undesired isomers were formed, but regioregular P3AT was produced over at 99%.[15]

With further research and development in this field, McCullough and Yokozhawa independently reported the synthesis of regioregular, low dispersity, high molecular weight P3HT (poly(3-hexylthiophene)) which is not what is expected out of the step growth mechanism.

Yokozawa had reported that this polymerization carried out by Kumada catalyst transfer polycondensation proceeds via chain growth mechanism and that nickel catalyzed cross-coupling polymerization of 2-bromo-5-iodo-3-hexylthiophene showed "living" behavior.[16] McCullough and coworkers also reported later, that this reaction showed some "living" characteristics, which generates end functionalized polymers having well defined molecular weights and narrow dispersity.[17] It was also observed that the molecular weight of the polymer increased linearly with monomer conversion, further proving chain growth characteristics. Subsequent work by Luscombe, Kiriy, Locklin, and McNeils' groups provided additional evidences of chain growth mechanism, and provided more insight into the mechanism.[18-20] They reported the formation of an associated pair between the Ni(0) catalyst and the aryl ring in the growing chain, preventing possibility of the diffusion of Ni(0) away from the growing chain and adding across different monomer units. This imparts more control in the reaction and gives it "living" characteristics. It also prevents several side reactions that could limit the living nature of the polymer growth.

To probe into the possibility of end group functionalization of the polymers formed by this technique, various other Grignard reagents were added to the active chain ends. It was found that they resulted in the formation of end functionalized polymers successfully. Triblock copolymers were also synthesized e.g., poly(3-dodecylthiophene)-b-poly(thiophene)-b-poly(3-dodecylthiophene), in order to prove the living nature of polymerzation and to show the existence of active chain ends after initial monomer has been completely consumed.

To summarize the explanation on chain growth nature of KCTP, it can be claimed to proceed through a double transmetallation step where Ni(II) precatalsyt reacts with two units of bifunctional AB type monomer, at their organometallic nucleophilic site forming an unstable aryl-Ni(II)-aryl species. On the subsequent reductive elimination of the unstable species to produce the

active Ni(0) in situ, the active catalyst stays associated with the growing chain and adds across the nearest available aryl-halide bond to cause intramolecular oxidative addition.

The association of the Ni(0) with the growing chain has been investigated in several studies, both theoretical and experimental (kinetic isotope effect studies).[21,22] This is the key step responsible for making the polymerization process chain growth rather than step growth. It has been claimed that the first irreversible step is the oxidative addition of Ni(0) across the aryl-halide bond. Continuation of this process to cause sequential transmetallation, reductive elimination and intramolecular oxidative addition produces high molecular weight polymer in a chain growth fashion. The proposed mechanism is described in Figure 2.

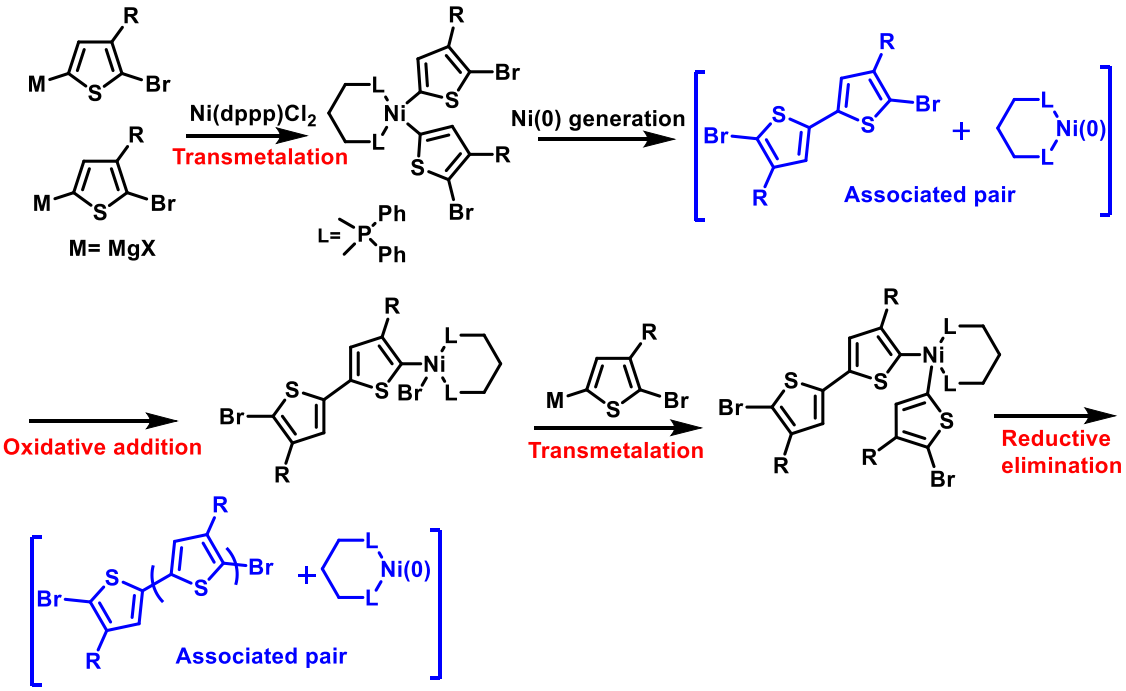

Figure 1.3. Proposed mechanism for Kumada Catalyst Transfer Polycondensation (KCTP) by McCullough and Yokozawa.

Development of "external initiation" by KCTP

The drawback of this synthetic methodology was its inability to initiate the polymerization from an external moiety, as had been shown for other CPs. To synthesize polymers with more complex polymer architectures external initiation is favorable.[23] In external initiation, the catalyst system in the form of (Ph)M(II)L_2-X is prepared separately before polymerization usually by (a) oxidative addition of M(0) to aryl halides or (b) transmetallation of an organolithium/organomagnesium species with M(II) species and then externally added to the monomer solution to initiate polymerization.[18,24,25]

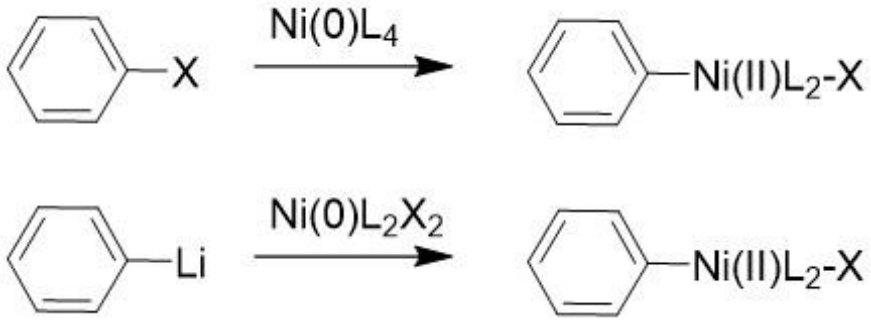

Figure 1.4. Possible routes to prepare external initiators for KCTP

Senkovsky et al. first demonstrated the synthesis of externally initiated P3HT.[26,27] They reported chain growth polymerization of P3HT from a Ni(II) macroinitiator prepared by the reaction of Ni(PPh3)4 with photocross-linked poly(4-bromostyrene) films. On reacting the monomer with this macroinitiator via KCTP, regioregular P3HT was produced by chain growth mechanism with narrow dispersity of 1.6. It provided a way to selectively polymerize off of a surface rather than in bulk solution and hence giving a method for surface initiated polymerization. It also gave a way to synthesize end-functionalized polymers.[28] Luscombe and coworkers also investigated external initiation of P3HT and the effects of varying the initiating aryl halide moieties.[24] They reported that the presence of strongly electron donating substituents reduce the

efficiency of the external initiation process. Through all these studies a lot could be understood about intricacies of KCTP mechanism, including how the electronic and steric factors affect the efficiencies of such reactions. They also demonstrated the polymerization of 3HT via external initiation with cis chloro(aryl)(dppp)nickel(II) complex, which produced regioregular P3HT with controlled molecular weights and narrow dispersities.[29]

Kiriy et al. further developed strategies to improve efficiency of the external initiation process as well as making it more universally applicable.[26] They carried out the polymerization of 2-bromo-5-chloromagnesio-3-hexylthiophene using Ni(bpy)Cl_2. Regioregular head-to-tail (HT) P3HT was produced by a chain growth mechanism over a wide range of temperature and with a gradual growth of M_n with polymerization time. Dispersities of 1.4 - 1.6 were achieved by such polymerization. Although these bpy based species were very attractive owing to their ability to form several ArNi(bpy)Br species in high purity and yield, on close analysis by NMR, they found that the products contained significant amounts of unwanted H/Br termination rather than Ph/H termination. In comparison, Ni(dppp)Cl_2 based polymerizations perform much better than the bpy based systems. This need for phosphorous based ligands led to the Kiriy group develop a "ligand exchange technique" to exchange bpy with dppp/dppe ligands. The initiating species produced this way were found to be more efficient, barring the requirement of ortho-stabilizers and provided a more universal method for external initiation of KCTP.

In further studies, Kiriy et al. investigated the robustness of the chain growth mechanism on using monomers with more than one thiophene ring.[30] McCullough had previously suggested that the Ni(0) species formed from reductive elimination stays associated with the growing chain and then "ring walks" to the nearest chain end, where it intramolecularly oxidatively adds to the

aryl-halide bond.[31] This was claimed to be responsible for chain growth characteristics. To prove the validity of this concept for lengthier monomers, Kiriy group attempted polymerization with mono-, bis-, and trithiophenic monomers by externally initiating with a Ph-Ni(PPh_3)$_2$-Br initiator.[30] The polymeric products were isolated and characterized thoroughly by NMR. They reported the predominant formation of Ph terminated products which can be possible only if the polymerization was chain growth. Even though the amount of Ph terminated products decreased somewhat by increase in monomer length (most likely due to chain transfer reactions), the chain growth step products predominate. This proved that chain growth mechanism is valid and robust even for lengthy monomers, and that the association followed by ring walking of Ni(0) over several nanometers of the growing chain, is the pivotal step in maintaining chain growth. It was however not clear if the ring walking was unidirectional or bidirectional. To probe into this mechanism, Kiriy group used Br-Ph-Ni(dppe)-Br to externally initiate polymerization of 3HT.[31] The presence of the initiator moiety can be detected in the polymer usually as an end group. But in this case, due to the presence of an extra C-Br bond para to the Ni substituent in the initiator, two different types of products were expected: One being the usual product i.e. P3HT with p-bromophenyl end group. This will show that unidirectional ring walking has occurred. The second product expected will have the initiator phenyl ring located within the chain showing evidence for bidirectional walking. On analysis, it was observed that the content of the product with initiator within the chain increases with degree of polymerization. This proves that the Ni(0) catalyst is able to ring walk over long distances of tens of nanometers and cause initiation at the C-Br bond available there. They also proved that the catalyst Ni(0) has higher affinity for thienyl rings than phenyl rings, since the major product obtained was the polymeric product with initiator present at the chain end (when DP goes to 40) favoring unidirectional growth. [26]

SI-KCTP for surface modification with conjugated polymers

External initiation studies gave a lot of insight into the mechanistic pathways of KCTP, which eventually led to the discovery and development of surface initiated polymerization techniques, referred to as SI-KCTP or Surface Initiated-Kumada Transfer Polycondensation.[18,19,32,33] On grafting conjugated polymer chains (P3ATs) from surface of various metal or metal oxide substrates, they show several interesting optical and electronic properties which can be exploited to make efficient organic electronic devices e.g., organic solar cell devices, fuel cells, sensors, heat conducting devices etc.[19,34-36] Surface immobilization offers ways to obtain uniform coatings on objects of complex geometries. It also prevents delamination of polymer from the surface of substrates and provides better control over the inorganic-organic interface. Covalently binding polymer to substrate surface also prevents thermal expansion/contraction and abrasion that usually occurs in spin casted films. Therefore irreversible surface immobilization of polymer chains is very valuable especially for the purpose of making OEDs.

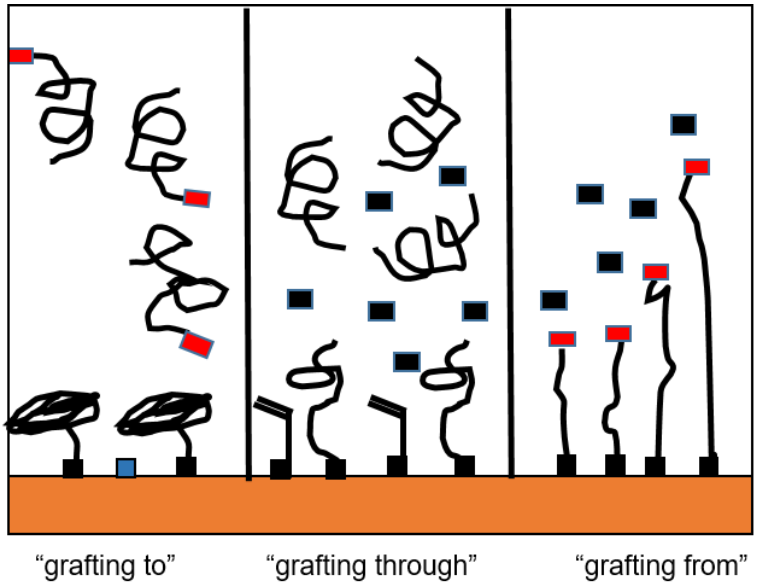

Figure 1.5. Surface bound polymer chains: techniques of grafting polymers to surfaces

Polymer chains can be grafted on a solid substrate primarily by three techniques: (a) grafting to, (b) grafting from, (c) grafting through. In "grafting to" processes, polymer is synthesized in solution that is either end functionalized by post polymerization modification or has a reactive functionality on one end. This functionality/end group can further react with a complimentary functional group that is bound to the surface. This process limits grafting density severely both kinetically and thermodynamically.[37] The reason behind that is the existence of the polymer chains in random coil conformation (in the mushroom regime) before and after polymerization, the process being entropy driven. This prevents the diffusion of the incoming end functionalized polymer to approach the initiating sites, as they get blocked by the random coil structure of the existing attached polymer chains. Therefore this technique produces low density films. An important demonstration of such a *grafting to* technique was shown by Prucker et al. where they introduced a way to attach polymer films (e.g. polystyrene) to a surface via monolayers of a photoreactive group like benzophenone by UV illumination for a certain time.[38] This method is very versatile and makes polymeric films with good thicknesses as compared to other graft to films. But these thicknesses are still way lower in comparison to films produced by "Grafting from" techniques.

In *grafting from* technique, polymerization is initiated from a surface which is fabricated with reactive initiator monolayers. Surfaces with reactive initiator monolayers are fabricated through chemical self-assembly and monomer in solution reacts with this surface to produce polymer that is therefore grafted from the surface. This process gives very high grafting densities of covalently immobilized polymer chains. With increasing grafting density, due to excluded volume effects, polymer chains in random coils start to extend into a stretched configuration and they push against each other. This leads to cross over into a regime which has highly stretched

polymer chains rather than random coil mushroom like configuration. This regime is known as the "brush" regime and hence these structures are called "polymer brushes". The stretched chains can interact with each other in various ways and they show lot of interesting optical and electronic properties which would otherwise not be observable in random coil configuration. However, there are certain limitations to this process too: (a) it involves more intricate experimental setup than in *grafting to* technique, (b) it is limited to polymerizations that are chain growth in nature, (c) an additional reactive initiator fabrication step is required which usually takes several hours. Usually "living" polymerizations are appropriate for "grafting from" technique as it requires an active end group after addition of each monomer unit that facilitates chain growth polymerization. SI-KCTP is one the most important examples of grafting from approach, by which P3AT brushes are grown. These have important applications in making OEDs. Other examples include ring opening metathesis polymerization (ROMP), atom transfer radical polymerization (ATRP) etc.[39,40] The Locklin group has developed this technique further to synthesize polymer brushes of P3MT and polyphenylenes by SI-KCTP.[19] [18] Here the initiator was fabricated on various substrates by solution deposition of phosphonic acid or thiol based aryl halide molecules, depending on the type of substrate. This initiator is then made reactive by oxidatively adding highly active Ni(0) i.e. Ni(cyclooctadiene)$_2$ (Ni(COD)$_2$) with a supporting ligand bpy (bipyridine). This was made to undergo ligand exchange with higher bite angle ligand dppp. This initiator was then reacted with a solution of monomer that reacts by magnesium halogen exchange at the surface. The polymer chains continue to grow from the anchoring point through chain growth polymerization. Polymer brushes with thicknesses of about 50 nm could be generated by this technique. Further studies on brush growth mechanisms revealed that a competitive side reaction occurs at high grafting densities. This type of side reaction, also known as Yamamoto type homocoupling can occur if the

catalyst centers are in close proximity to each other whereby the come together and disproportionate.[41] Unfortunately, this leads to the production of several dead initiator sites, ultimately reducing grafting density. It was also shown that "ortho" substituents to the catalyst centers can improve stability and can reduce disproportionation.

A third approach is intermediary of the above mentioned techniques. It is known as the *grafting through* approach.[42] This technique involves surfaces that have self-assembled monolayers containing polymerizable groups. It proceeds initially by solution polymerization and this solution polymer is made to react with a surface bound monomeric unit which gets integrated into the growing polymer chain. This way, polymer chain gets directly grafted from the surface of a substrate.[43] This reaction pathway is expected to be a little simpler in its procedure, the reaction being "one-pot", but still complex in its mechanism. This also follows chain growth mechanism and can provide sufficiently high grafting densities, but it is never as high as that produced from *grafting from* techniques. This process is a mixture of both *grafting to* and *grafting from* techniques. A detailed study has been performed by Jurgen Rühe's group to analyze the reaction mechanism and study several parameters such as the temperature, time of polymerization, concentration of initiator and monomer concentration etc. that affect the grafting density of the polymer grafted from a surface.[43] However, there are limitations in this process too. This polymerization is diffusion limited, as the growing surface bound layer poses hindrance to the income of further new polymeric chains that are forming in solution. Hence high molecular weight chains have difficulties in penetrating through to the surface. Therefore, the reaction starts showing *grafting to* characteristics and the kinetics of attachment are severely slowed down. This is one of the primary reasons for low grafting densities by this technique.

Solubility is another issue, especially for conjugated polymers which are highly insoluble in most of the common solvents used. This limits the reaction of the conjugated polymer chains (which often form aggregates due to solubility issues) at the surface.

Objectives and outline of this dissertation

In this dissertation, SI-KCTP is used to synthesize P3MT by the *grafting from* approach from surface of different substrates. The overall goal was to develop and improve the SI-KCTP technique to grow P3MT brushes that can be applied in fabrication of efficient OEDs. The process, as mentioned earlier has its limitations like disproportionation reactions and it is also very time consuming since the entire process spans over 72 hours. A detailed investigation was performed to find alternative routes that could improve the efficiency of the reaction. This could be done by reducing the rates of competitive side reactions as well as making the process significantly rapid. The role of the structure of the initiator monolayers in the growth of polymer brushes was also investigated in regard to their effect on grafting density and directionality. After performing a detailed study to optimize the reaction, develop the most appropriate initiator monolayer and fabricating the P3MT brushes through the developed technique, application of these polymer brushes towards making OEDs was explored.

Chapter 2 discusses electrochemical reduction techniques those are used to rapidly generate reactive initiator monolayers (in the order of seconds) from the substrate of substrates (e.g., gold). This process is designed in a way that it can avoid the entire ligand exchange process and hence cause a significant reduction in disproportionation reaction. This leads to a significant improvement in the grafting density of the polymer brushes. The density of initiators on the surface

is estimated using previously used ferrocene quenching technique. Surface plasmon resonance spectroscopy is used in parallel to monitor the surface binding events.

Chapter 3 discusses the structure and function relationship of reactive initiator monolayers towards the grafting densities and directionality of polymer brushes. On modification of the geometries of the initiator monolayer, the rates of competitive side reactions can be influenced, thereby modifying the catalyst coverage at the surface. This, in turn, influences several other interaction parameters between the growing chains and affects the directionality/orientation of the brushes. This understanding helps in designing the ideal reactive initiator monolayer for making P3MT brushes that can be used to make efficient OEDs. Several analytical characterization techniques were utilized for this study. Cyclic voltammetry, Drop- shape analysis, UV-VIS (Ultraviolet-Visible) spectroscopy, NEXAFS (Near Edge X-Ray Absorption Fine Structure), AFM (Atomic Force Microscopy) were used to characterize the monolayers and the polymer brushes grown from them.

Chapter 4 demonstrates the application of above studies to synthesize P3MT brushes by SI-KCTP for fabrication of successful organic spintronic/spin valve devices (OSV). The idea was to covalently immobilize P3MT brushes directly from the surface of a ferromagnetic electrode (LSMO- $La_{0.67}Sr_{0.33}MnO_3$) in OSV, rather than performing thermal evaporation or spin coating of organic molecules. The aim was to determine if/how this covalent attachment of conjugated polymer brushes to LSMO improves magnetoresistance (MR) response of the device. On successful device fabrication, we obtained a huge MR response (70% at 20K) showing that the brushes indeed provided much better intimate contact with the substrate surface than spin coated polymer films. It improves spin injection and also provides more order in the organic layer.

This facilitates more intra chain carrier (electron spin) transport rather than inter chain hopping, which is usually responsible for reducing device efficiency. We did several characterizations of the device, and modified several parameters that can significantly affect the device efficiency.

Chapter 5 further discusses the potential application of the P3MT brushes developed, in fabricating heat conducting devices. With the ultimate goal of fabricating heat sinks/heat conductive devices with these conjugated polymer brushes, the thermal conductivities of the P3MT brushes made from structurally different initiator monolayers were measured. This was done by TDTR measurement technique. Spin coated P3HT films were then compared to determine if covalent immobilization of oriented P3MT brushes leads to improvement in thermal conductivity. We observed that indeed the P3MT brushes showed very high thermal conductivities, with the oriented brush showing higher conductivity than the un-oriented brush. The spin coated films however showed the least conductivity owing to extensive loss of vibrational energy due to non-intimate contact with the surface. More disorder among the entangled chains provides several coupling spots within the chains causing further loss of vibrational energy.

Chapter 6 summarizes all the work reported in this dissertation and provides and outlook on the new dimensions and potential applications of these studies in future.

References:

(1) Chiang, C. K.; Fincher, C. R.; Park, Y. W.; Heeger, A. J.; Shirakawa, H.; Louis, E. J.; Gau, S. C.; MacDiarmid, A. G. *Physical Review Letters* **1977**, *39*, 1098.

(2) Lecrec *Chapitre de livre*.

(3) Shirakawa, H.; Louis, E. J.; MacDiarmid, A. G.; Chiang, C. K.; Heeger, A. J. *Journal of the Chemical Society, Chemical Communications* **1977**, 578.

(4) McCullough, R. D. In *Handbook of Oligo- and Polythiophenes*; Wiley-VCH Verlag GmbH: 1998, p 1.

(5) Miyaura, N.; Suzuki, A. *Chemical Reviews* **1995**, *95*, 2457.

(6) Tamao, K.; Sumitani, K.; Kumada, M. *Journal of the American Chemical Society* **1972**, *94*, 4374.

(7) Heck, R. F.; Nolley, J. P. *The Journal of Organic Chemistry* **1972**, *37*, 2320.

(8) Espinet, P.; Echavarren, A. M. *Angewandte Chemie International Edition* **2004**, *43*, 4704.

(9) Stille, J. K. *Angewandte Chemie International Edition in English* **1986**, *25*, 508.

(10) McCullough, R. D.; Lowe, R. D. *Journal of the Chemical Society, Chemical Communications* **1992**, 70.

(11) McCullough, R. D.; Lowe, R. D.; Jayaraman, M.; Anderson, D. L. *The Journal of Organic Chemistry* **1993**, *58*, 904.

(12) Kiso, Y.; Tamao, K.; Miyake, N.; Yamamoto, K.; Kumada, M. *Tetrahedron Letters* **1974**, *15*, 3.

(13) Thorsett, E. D.; Stermitz, F. R. *Journal of Heterocyclic Chemistry* **1973**, *10*, 243.

(14) McCullogh, R. D.; Williams, S. P.; Tristam-Nagle, S.; Jayaraman, M.; Ewbank, P. C.; Miller, L. *Synthetic Metals* **1995**, *69*, 279.

(15) Sato, M.; Morii, H. *Macromolecules* **1991**, *24*, 1196.

(16) Yokoyama, A.; Miyakoshi, R.; Yokozawa, T. *Macromolecules* **2004**, *37*, 1169.

(17) Iovu, M. C.; Sheina, E. E.; Gil, R. R.; McCullough, R. D. *Macromolecules* **2005**, *38*, 8649.

(18) Marshall, N.; Sontag, S. K.; Locklin, J. *Chemical Communications* **2011**, *47*, 5681.

(19) Sontag, S. K.; Sheppard, G. R.; Usselman, N. M.; Marshall, N.; Locklin, J. *Langmuir* **2011**, *27*, 12033.

(20) Bryan, Z. J.; McNeil, A. J. *Macromolecules* **2013**, *46*, 8395.

(21) Yoshikai, N.; Matsuda, H.; Nakamura, E. *Journal of the American Chemical Society* **2008**, *130*, 15258.

(22) Sontag, S. K.; Bilbrey, J. A.; Huddleston, N. E.; Sheppard, G. R.; Allen, W. D.; Locklin, J. *The Journal of Organic Chemistry* **2014**, *79*, 1836.

(23) Bronstein, H. A.; Luscombe, C. K. *Journal of the American Chemical Society* **2009**, *131*, 12894.

(24) Doubina, N.; Ho, A.; Jen, A. K. Y.; Luscombe, C. K. *Macromolecules* **2009**, *42*, 7670.

(25) Senkovskyy, V.; Sommer, M.; Tkachov, R.; Komber, H.; Huck, W. T. S.; Kiriy, A. *Macromolecules* **2010**, *43*, 10157.

(26) Senkovskyy, V.; Tkachov, R.; Beryozkina, T.; Komber, H.; Oertel, U.; Horecha, M.; Bocharova, V.; Stamm, M.; Gevorgyan, S. A.; Krebs, F. C.; Kiriy, A. *Journal of the American Chemical Society* **2009**, *131*, 16445.

(27) Senkovskyy, V.; Khanduyeva, N.; Komber, H.; Oertel, U.; Stamm, M.; Kuckling, D.; Kiriy, A. *Journal of the American Chemical Society* **2007**, *129*, 6626.

(28) Smeets, A.; Van den Bergh, K.; De Winter, J.; Gerbaux, P.; Verbiest, T.; Koeckelberghs, G. *Macromolecules* **2009**, *42*, 7638.

(29) Doubina, N.; Paniagua, S. A.; Soldatova, A. V.; Jen, A. K. Y.; Marder, S. R.; Luscombe, C. K. *Macromolecules* **2011**, *44*, 512.

(30) Beryozkina, T.; Senkovskyy, V.; Kaul, E.; Kiriy, A. *Macromolecules* **2008**, *41*, 7817.

(31) Tkachov, R.; Senkovskyy, V.; Komber, H.; Sommer, J.-U.; Kiriy, A. *Journal of the American Chemical Society* **2010**, *132*, 7803.

(32) Huddleston, N. E.; Sontag, S. K.; Bilbrey, J. A.; Sheppard, G. R.; Locklin, J. *Macromolecular Rapid Communications* **2012**, *33*, 2115.

(33) Roy, A.; Gao, J.; Bilbrey, J. A.; Huddleston, N. E.; Locklin, J. *Langmuir* **2014**, *30*, 10465.

(34) Yang, L.; Sontag, S. K.; LaJoie, T. W.; Li, W.; Huddleston, N. E.; Locklin, J.; You, W. *ACS Applied Materials & Interfaces* **2012**, *4*, 5069.

(35) Singh, V.; Bougher, T. L.; Weathers, A.; Cai, Y.; Bi, K.; Pettes, M.; Wei, L.; Resler, D. P.; Gattuso, T. R.; Altman, D. H.; Sandage, K. H.; Shi, L.; Henry, A.; Cola, B. A. *Nature Nanotechnology* **2014**.

(36) Geng, R.; Roy, A.; Zhao, W.; Subedi, R. C.; Li, X.; Locklin, J.; Nguyen, T. D. *Advanced Functional Materials* **2016**, n/a.

(37) Advincula.R., B. W., Caster.K., and Ruhe.J **2004**.

(38) Prucker, O.; Naumann, C. A.; Rühe, J.; Knoll, W.; Frank, C. W. *Journal of the American Chemical Society* **1999**, *121*, 8766.

(39) Liu, Y.; Klep, V.; Zdyrko, B.; Luzinov, I. *Langmuir* **2004**, *20*, 6710.

(40) Izuhara, D.; Swager, T. M. *Macromolecules* **2009**, *42*, 5416.

(41) Yamamoto, T.; Wakabayashi, S.; Osakada, K. *Journal of Organometallic Chemistry* **1992**, *428*, 223.

(42) Bialk, M.; Prucker, O.; Rühe, J. *Colloids and Surfaces A: Physicochemical and Engineering Aspects* **2002**, *198–200*, 543.

(43) Henze, M.; Mädge, D.; Prucker, O.; Rühe, J. *Macromolecules* **2014**, *47*, 2929.

CHAPTER 2

RAPID ELECTROCHEMICAL REDUCTION OF Ni(II) GENERATES REACTIVE MOOLAYERS FOR CONJUGATED POLYMER BRUSHES IN ONE

[1] Roy, A.; Gao, J.; Bilbrey, J. A.; Huddleston, N. E.; Locklin, J. **2014**, *Langmuir*, *30*, 10465.

Abstract

This article reports the development of a robust, one-step electrochemical technique to generate surface-bound conjugated polymers. The electrochemical reduction of arene diazonium salts at the surface of a gold electrode is used to generate tethered bromobenzene monolayers quickly. The oxidative addition of reactive Ni(0) across the aryl halide bond is achieved in situ through a concerted electrochemical reduction of Ni(dppp)Cl_2. This technique limits the diffusion of Ni(0) species away from the surface and overcomes the need for solution deposition techniques which often require multiple steps that result in a loss of surface coverage. With this electrochemical technique, the formation of the reactive monolayer resulted in a surface coverage of 1.29×10^{14} molecules/cm^2, which is a 6-fold increase over previously reported results using solution deposition techniques.

Introduction

Poly(3-alkyl thiophenes) (P3ATs) are often used in organic electronic devices, such as field-effect transistors and photovoltaics, because of their unique physical properties including crystallinity and high carrier mobility.[1–4] Traditional methodologies for the synthesis of these materials proceed through a step-growth mechanism to generate polymers of broad molecular weight distribution and uncontrolled end group functionality.[5,6] However, advancements in Kumada catalyst transfer polycondensation (KCTP), also known as Grignard metathesis polymerization (GRIM), have afforded conjugated polymers of controlled molecular weight and low dispersity.[7–9] KCTP employs aromatic bifunctional (AB-type) monomers with halide and metalating moieties that are polymerized with the aid of a zero-valent nickel catalyst.[8] The cross-coupling reaction proceeds through a cycle of oxidative addition, transmetalation, and reductive elimination, followed by the intramolecular addition of the catalyst, which forms a π complex with the growing chain and does not diffuse away.[10–12] As the chain-growth mechanism involves continued association of the nickel catalyst with the growing polymer chain, KCTP can be amended to surface-initiated polymerizations.[1,13–17] Surface-initiated KCTP (SI-KCTP) forms polymer that is covalently attached to the surface, which imparts improved mechanical stability and, to date, has been used as a charge injection layer in organic photovoltaic devices.[1] Additionally, covalent immobilization prevents the delamination of the films and therefore offers increased versatility in device manufacturing. Initiation from a conducting surface, such as a metal electrode, was previously achieved through functionalization with aryl bromide monolayers, where Ar-Ni(II)-Br is formed by the oxidative addition of Ni(COD)2 in the presence of a bidentate ligand.[13,18,19] $Ni(COD)_2$ was used as the source of Ni(0) for its facile dissociation of COD in the presence of σ- donating ligands; however, this facile dissociation limits the lifetime of $Ni(COD)_2$

as it is prone to degradation. Other analogous Ni(0) catalysts that could possibly be used directly for oxidative addition to nonactivated aryl halides such as $Ni(dppp)_2$ are not reactive enough.[15] This brought about a need to perform an extra ligand-exchange step to associate and exchange different ligand systems with the nickel catalyst during the generation of the initiator monolayer, providing a more stable catalyst system. We have shown that 2,2′-bipyridine (bpy) ligands promote enhanced surface coverage and spatial homogeneity of the initiator moieties.[13] However, bpy was found to hinder chain-growth characteristics;13 thus, additional ligand exchange with a strong σ-donating bidentate ligand, such as 1,3-bis(diphenylphosphino)propane (dppp), is necessary to achieve controlled polymerization. Competitive side reactions during the ligand exchange step have been shown to limit surface initiator coverage by early termination through disproportionation.[20] Disproportionation on the surface presumably occurs due to the close proximity of nickel moieties, which undergo interfacial homocoupling to reduce the number of active initiator sites. Disproportionation can be minimized by using dppp as the ancillary ligand rather than other bidentate phosphines such as 1,2-bis(diphenylphosphino)ethane (dppe) or 1,4-bis(diphenylphosphino)- butane (dppb).[21] However all of these ligand−catalyst combinations involve the extra step of ligand exchange, which causes a substantial loss of surface initiator coverage.[13] Therefore, a need arises to develop a technique that can circumvent this ligand exchange step, which could lead to an increased initiator surface coverage as well as a reduction in the number of synthetic steps. The present work details a new method to generate surface bound, catalytic Ni(0) species. We fabricated bromobenzene monolayers by the electrochemical reduction of corresponding diazonium salts. This initiator monolayer is further activated for oxidative addition by the electrochemical reduction of Ni- (dppp)Cl2, which occurs in one pot and avoids ligand exchange. Zero-valent nickel is generated in situ from a two electron reduction that occurs

at distinct reduction potentials: Ni(II) to Ni(I) at −1.3 V vs Ag/Ag+ (silver wire pseudoreference electrode) followed by Ni(I) to Ni(0) at −2.1 V vs Ag/Ag+ (silver wire pseudoreference electrode).[16,22] Using this method, initiator formation occurs in seconds as opposed to several hours as is necessary with previous solution deposition methods.[13] Electrochemical deposition of the catalytic species overcomes the need for ligand exchange reactions which resulted in a loss of total coverage. Previously, a variety of techniques were used to probe the dynamics of interfacial binding events on surface-bound thin films, including ellipsometry, Raman spectroscopy, ATR/FTIR, and surface plasmon resonance (SPR).[23−25]In particular, SPR is a noninterfering technique that provides high sensitivity and can be coupled with other techniques, allowing real-time analysis for a variety of systems.[26−29] In the present study, SPR is combined with cyclic voltammetry (CV) using a three electrode system in which a gold-coated substrate acts as the working electrode.[30] In situ SPR-CV elucidates the dynamics of reduction of bromobenzene diazonium tetrafluoroborate (BDTB) on a gold surface. P3MT films were successfully grown on a gold electrode, and the properties of the resultant films were investigated by cyclic voltammetry and atomic force microscopy. The polymer films obtained are of similar qualities to those produced by solution deposition techniques.[13] With this new one-pot synthesis technique, the entire process of active initiator monolayer generation occurs extremely fast and avoids a ligand exchange step. Most importantly, we have achieved a 6-fold increase in initiator coverage compared to the coverage of existing solution deposition techniques.

Experimental

Materials:

Dichloro(1,3-bis(diphenylphosphino)propane)nickel, 4-bromobenzene diazonium tetrafluoroborate, tetrabutylammonium hexafluorophosphate were obtained from Sigma Aldrich. Omnisolv acetonitrile (ACN) was obtained from EMD Chemicals. Tetrahydrofuran (THF) was obtained from Sigma Aldrich and purified with an MBRAUN Solvent purification system. All other chemicals were purchased from TCI, Oakwood and Acros Organics and all chemicals were used as received unless mentioned otherwise.

Synthetic Methodology.

All syntheses were carried out under an inert atmosphere of purified argon or nitrogen, using standard Schlenk techniques or a glovebox (Unilab BP with an MB10 purification system, MBraun, Inc.). NMR spectra were recorded using a 300 MHz Varian Mercury NMR spectrometer. Chemical shifts are reported relative to an internal 2 tetramethylsilane standard in CDCl3. The synthesis of 2-ferrocenyl-5-bromothiophene, 2-bromo-3-methyl-5-iodothiophene, along with magnesiation of 2-ferrocenyl-5-bromothiophene and 2-bromo-5-iodo-3-methylthiophene were carried out using synthetic procedures reported previously.[1]

Electrochemical measurements.

Electrochemical measurements were obtained using a CH Instruments bipotentiostat equipped with a platinum counter electrode and a silver wire pseudo reference electrode. The gold substrates were used as the working electrode. Tetrabutylammonium hexafluorophospate in DCM (0.1M, degassed) was used as the supporting electrolyte for all electrochemical measurements. All scans are recorded at a rate of 100 mV/sec.

Electrografting of 4-bromobenzene diazonium tetrafluoroborate.

The gold electrode was polished thoroughly and rinsed with acetone before use. A 10 mM solution of bromobenzene diazonium tetrafluoroborate in acetonitrile was prepared with supporting electrolyte at the same concentration. To form the monolayer, the gold electrode was submersed in the prepared solution and potential was applied from 0.5 V to –0.9 V for two cycles. After deposition, the electrode was extensively rinsed with acetone to remove any physisorbed material, and then dried over argon. Bromobenzene monolayers, which are stable to harsh electrochemical and sonication treatments, were formed by electrochemical reduction of bromobenzene diazonium tetrafluoroborate. This method, however, has the potential to generate multilayers due to the facile generation of reactive bromobenzene radical species.[2] The diazonium reduction to form monolayers and the oxidative addition of nickel to form the initiator complex were studied by [3] surface plasmon resonance (SPR) coupled with cyclic voltammetry to monitor the processes in-situ.

Formation of initiator complex.

In the glove box, a 2 mM solution of $Ni(dppp)Cl_2$ was made in THF. Supporting electrolyte was added in the same concentration and the three electrode system was then set up inside the glove box The gold electrode fabricated with the monolayer was then immersed in the solution and potential was applied from 0 V to -2.1 V. After the second reduction wave at -1.89 V, the gold electrode was immediately taken out of the solution, rinsed in THF, and immersed into the monomer solution. This was kept overnight in the glove box, and the following day, the electrode was rinsed extensively before subjecting to cyclic voltammetry and other characterizations.

Fabrication of Gold Substrate.

A 47 nm gold film was deposited on glass substrate (n = 1.72) using thermal deposition system at 0.5 Å/s after deposition of a 3 nm chromium adhesion layer.

Instrumentation.

For the SPR measurement, the Kretschmann configuration was set up and the apparatus consisted of a HeNe laser with wavelength at 632.8 nm, a high refractive index (n = 1.72) prism, gold substrate, a motorized goniometer, and a photodiode with focusing lens. A three-electrode system was used to carry out cyclic voltammetry, where the gold substrate was the working electrode, a silver wire was the reference electrode, and a platinum wire was counter electrode. A Teflon flow cell filled with experimental solutions was in contact with gold surface. Angular scans were performed under Reflectivity Scan mode. In-situ study was performed under Reflectivity Tracking mode at picked angles. The flow cell was enveloped by an argon gas atmosphere during all electrochemical reactions. SPR fits were performed on Winspall. The ^{4} electrolytic solutions for the SPR coupled CV experiments were of the same concentration as previously used for film formation. Cyclic voltammetry scans were taken in pure ACN electrolyte solutions in order to obtain background information for the blank electrolyte, followed by adding 4-bromobenzene diazonium tetrafuloroborate and Ni(dppp)Cl_2. Meanwhile, Reflectivity Tracking mode was utilized to investigate the reaction mechanism by monitoring the refractivity, and thus thickness, changes of an organic layer on the gold surface. The aryl bromide monolayer was deposited on a gold substrate electrochemically by applying a potential sweep of 0.5 V to –0.9 V for two cycles, where angle of incidence was at 55.5°. Oxidative addition of Ni(0) was conducted by applying a potential sweep of 0 V to –2.1 V to form the initiator complex.

Result and discussion

Monolayer Fabrication by the Reduction of BDTB. Figure 2.1 outlines the electrografting of BDTB on a gold electrode to generate the bromobenzene monolayer.[31, 32]

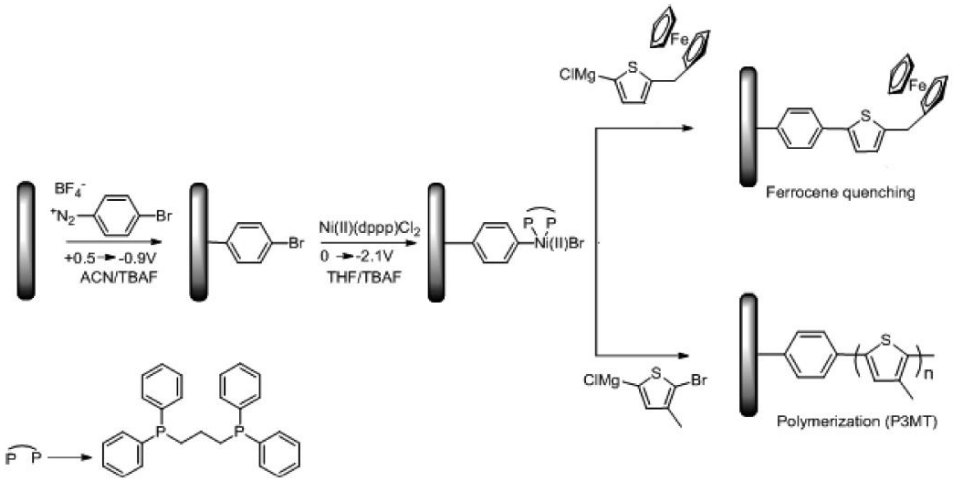

Figure 2.1. Synthesis Process for the Generation of the Surface-Bound Monolayer, Oxidative Addition of the Nickel Initiator, and Surface-Initiated Polymerization of Poly(3-methylthiophene) (P3MT)

Using cyclic voltammetry, a solution of BDTB is subjected to a potential window of 0.5 to −0.9 V over two cycles, as shown in Figure 2.2(a).

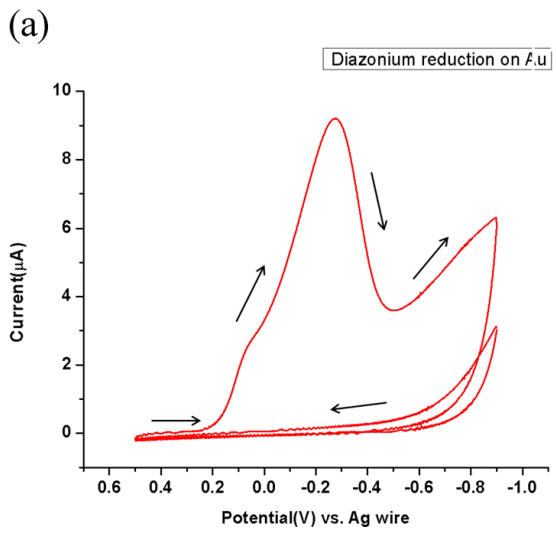

Figure 2.2 (a) Cyclic voltammogram (two cycles) showing the reduction of diazonium salt on a gold electrode to form a bromobenzene blocking layer (0.5 to −0.9 V), where the scan direction is indicated by arrows

In the first cycle, BDTB shows a distinct reduction wave at −0.3 V vs Ag/Ag+ (silver wire pseudoreference electrode), corresponding to the heterolytic cleavage of the C− N bond of the aryl diazonium salt to generate a reactive bromobenzene radical and N_2.[16] The radical species reacts with the gold electrode to form a covalently attached monolayer.[31,33,34] The second cycle shows only charging current and no BDTB reduction, which corresponds to the formation of a blocking layer and prevents further access of the diazonium species to the electrode surface.[32] The diazonium reduction and monolayer formation on gold was monitored by surface plasmon resonance coupled with cyclic voltammetry (SPR-CV, Figure 2.2b).

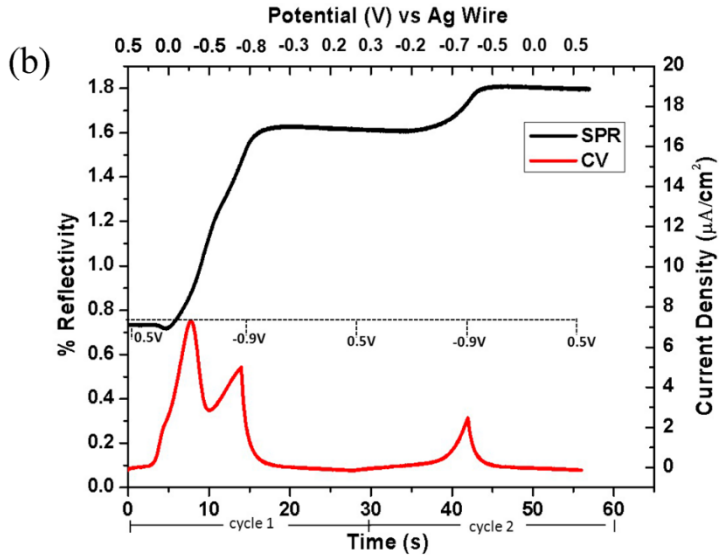

Figure 2.2 (b) in situ SPR-CV monitoring the monolayer formation on a gold substrate over the same potential window. For SPR, the percentage reflectivity from the gold surface is plotted with time. For CV, the current density is plotted with potential applied across the electrode surface.

In SPR, two modes that are used in order to investigate surface binding events are angular scan and reflectivity tracking modes. Using the angular scan mode, we measured the comparative reflectivity with respect to the angle of incidence, whereby the thickness of the organic layer deposited on the gold surface is calculated by accompanying software (Winspall). In reflectivity tracking mode, the comparative reflectivity is monitored with time at a fixed angle of incidence in the high-contrast linear region of the SPR curve. Here, the reflectivity change is proportional to the change in thickness of the organic layers, assuming that the thicknesses and refractive indices of all other layers are fixed.[35] Figure 3.2(b) shows the change in comparative reflectivity when a potential from 0.5 to −0.9 V is applied across the gold substrate (the working electrode) over two cycles. In each cycle, the reflectivity increases at around 0.04 and −0.5 V with the formation of

the bromobenzene radicals. We did not observe complete blocking of the monolayer during the second cycle, though the current was reduced substantially, and only a slight increase in thickness on the order of 2 nm occurred. This observation of incomplete blocking is probably due to the production of some oligomeric material, commonly observed in electrografting.[36] These oligomers may hinder the approach of some of the incoming bromobenzene radicals toward the reactive initiator sites, thereby blocking these sites from further reaction. Also, in our CV-SPR setup (Figure 2.3), the counter electrode has a much lower surface area (ca. 0.11 cm^2) than the working electrode (gold substrate with an area of 1.26 cm^2), unlike in the setup used in Figure 2.2(a), where the sizes of all three electrodes are comparable.

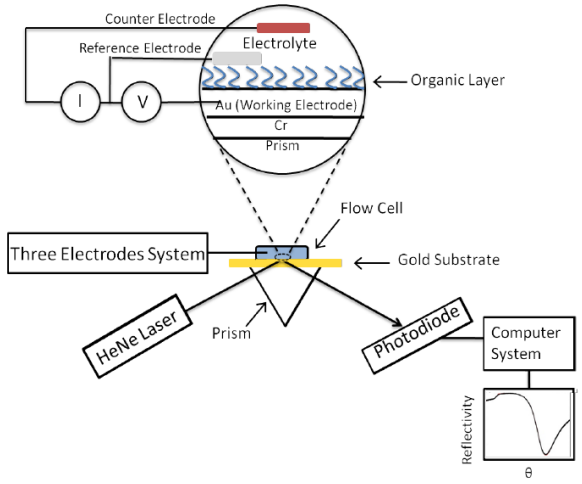

Figure 2.3. Schematic of experimental setup for SPR coupled with CV

The surface area difference between the working and counter electrodes limits the half-reaction occurring at the counter electrode, thereby prohibiting complete diazonium reduction in the first cycle, which likely accounts for the observation of a reduction current in the second cycle. The small pre-wave reduction shoulder at 0.08 V in cycle 1 may be due to either the reduction of a small amount of the ortho-substituted DBTB that is possibly present as a minor impurity with para-DBTB or the reduction at different crystallographic faces inherent in gold.[37]

In the second cycle, the reflectivity plateaus at around −0.4 V, showing no further thickness increase. On the basis of the ratio of reflectivity changes in the in situ SPR curve after each reaction cycle, the thickness of the organic layer increased by 8.8 and 2.0 nm for the first and second cycles, respectively. By comparing SPR angular scans before and after the electrochemical reaction, we calculated the thickness of the thin film to be 8.8 nm (Figure 2) after rinsing with acetonitrile. When the film is rinsed further with THF, a better solvent for the oligomeric material, the thickness decreases from 8.8 to 1.3 nm, which indicates the removal of physisorbed layers loosely bound to the substrate surface.

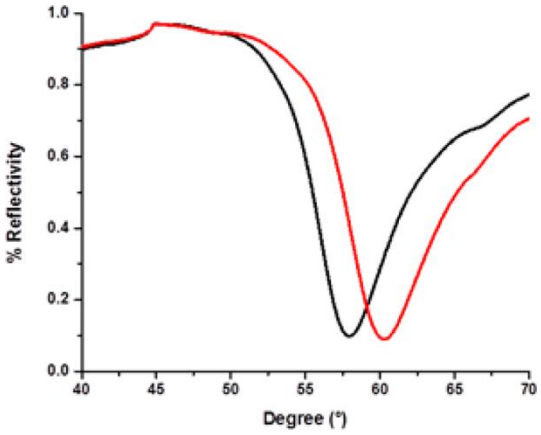

Figure 2.4. SPR angular scans before (black line) and after (red line) surface initiator formation after rinsing with acetonitrile. The film thickness is 8.8 nm.

Measurement	Thickness (nm)	Δ % reflectivity
After CV cycle 1	8.8	0.894
After CV cycle 2	10.8	0.179
After rinse with acetonitrile and THF	1.3	N/A*

*Angular scan was taken *ex situ* after rinsing with ACN and THF.

Table 2.1. Table listing thickness and reflectivity change after each CV cycle for monolayer formation.

Fabrication of Initiator Complex**.**

Zero-valent nickel, which undergoes oxidative addition to the bromobenzene monolayer, was formed through electrochemical reduction. Under an inert atmosphere, a gold electrode functionalized with bromobenzene was submerged in a 0.1 M solution of Ni(dppp)Cl2 in THF/TBAF. Using cyclic voltammetry (Figure 3.5), we reduced Ni(II) to Ni(0) in two successive

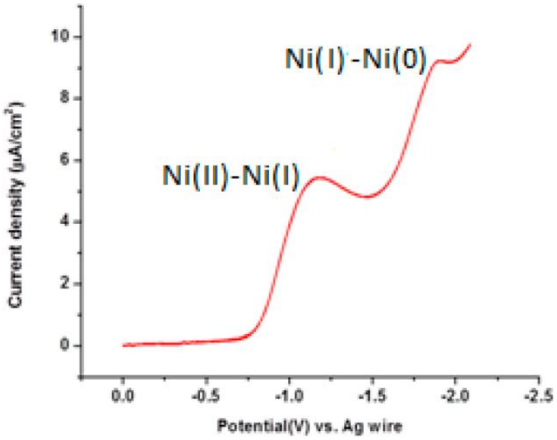

one-electron reductions over a potential window of 0 to −2.1 V.

Figure 2.5. Reduction wave exhibiting the generation of reactive species Ni(0) at −1.89 V.

The first cathodic peak was observed at −1.16 V, corresponding to the reduction of Ni(II) to Ni(I), and the second appeared at −1.89 V, which corresponds to the reduction of Ni(I) to

Ni(0).[22] Once Ni(0) is generated, oxidative addition to the aryl halide bond in the monolayer forms surface-bound initiator complex ArNi(II)Br.[33]

Quantitative Characterization of Immobilized Ni(II) Complexes.

Surface-bound initiator coverage was quantified by cyclic voltammetry using a Grignard-functionalized ferrocene moiety as an indirect electrochemical probe. The ferrocene derivative was chosen for its stable reversible redox couple and ability to couple to the surface through a magnesium halogen exchange reaction.[18] The density of initiators on the surface was quantified through integration of the oxidation and reduction waves, which resulted in the percent yield of the coupling reaction.[13] The cyclic voltammogram obtained after ferrocene quenching of the active

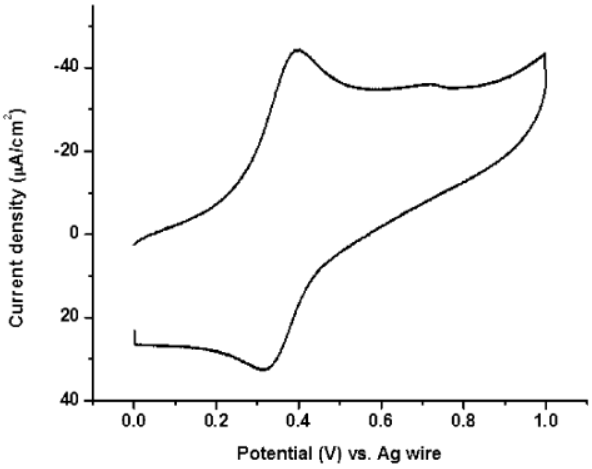

substrate is shown in Figure 2.6.

Figure 2.6. Cyclic voltammogram for ferrocene quenching of the gold electrode, where the integration of oxidation and reduction waves was used to determine initiator complex coverage.

In this system, a coverage of 1.29×10^{14} molecules/cm2 was obtained. Our previously reported work using solution deposition techniques showed an optimized maximum coverage of 0.22×10^{14} molecules/cm^2.[13] Thus, the electrochemical methodology reported here provides an almost 6-fold increase in coverage. An upper bound of the total possible surface coverage can be

approximated by modeling Ni(dppp) units in our initiated monolayer as hexagonally close-packed spheres. Using the reported cone and bite angles[38] we calculated the radius of a spherical Ni(dppp) moiety to be 3.3 Å, which gives a hexagonal surface coverage of 2.6×10^{14} molecules/cm^2 (Figure and following calculations).

Estimation of Ni(dppp) packing.

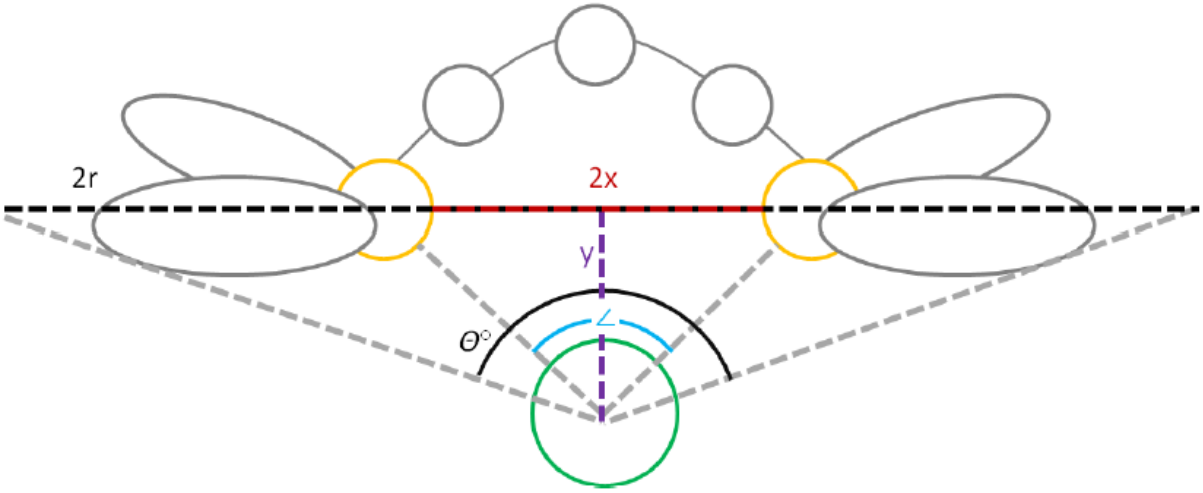

Figure 2.7. Diagram depicting the parameters for modeling Ni(dppp) as a sphere, assuming the Tolman cone angle (θ) = 127° and bite angle (∠) = 87.3°.3

Tolman cone angle (θ) = 127° and bite angle (∠) = 87.3°.3We assume Ni(dppp) has the largest width when measured from the phosphorus side chains. In order to calculate this width a dummy atom is placed in between the phosphorus atoms at a distance y from nickel. Using the bite angle of the complex, which has been reported as 87.3°, the distance y can be determined by:

$$\cos\left(\frac{\angle}{2}\right) = \frac{y}{2.28\ \text{Å}}$$

to give y = 1.65 Å. Next, the radius of the sphere can be found using y and the Tolman cone angle (θ), reported as 127°, by

$$\tan\left(\frac{\theta}{2}\right) = \frac{r}{y},$$

to give r = 3.31 Å (3.31 x 10–8 cm).

Finally, the packing of Ni(dppp) modeled as a circle can be found by calculating the area of a single molecule with the formula area = πr^2 , which gives 3.44 x 10-15 cm ^{2} /molecule. Taking the reciprocal of this gives the coverage on a 1 cm2 substrate to be 2.91 x 10^{14} molecules/cm^2. As the packing density of a closely packed hexagonal surface is 0.9069, meaning 90.69% of the surface is atom and the remaining 9.31% is empty space, the total possible coverage of hexagonally packed nickel is 2.64 x 1014 molecules/cm^2.

Since our method resulted in a total coverage of 1.29 × 1014 molecules/cm^2, our minimum coverage is only 50%, assuming nickel is hexagonally close packed. However, since Ni(dppp) is bound to the bromobenzene monolayer, in order to refine our model we can assume that Ni(dppp) lies directly above the bound molecule (Figure 2.8).

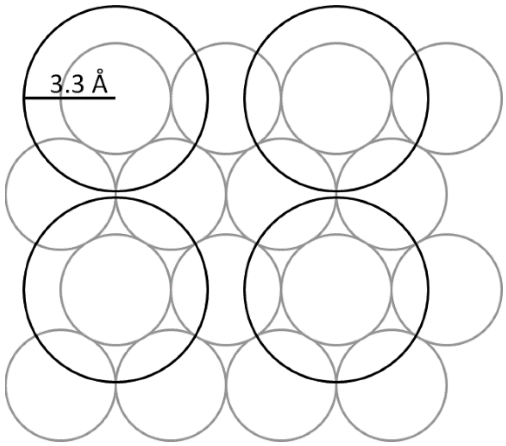

Figure 2.8. Pictorial representation of Ni(dppp) (black spheres) on a hexagonally close-packed bromobenzene monolayer (gray spheres).

As Ni(dppp) is larger than a single bromobenzene unit, steric hindrance prevents the nickel from being hexagonally close packed. If the monolayer is hexagonally close packed, as suggested by the absence of pinhole defects, then we can expect a maximum of 25% functionalization of Ni(dppp) on bromobenzene. Polymerization of 3-methylthiophene was carried out on the initiated gold electrode by immersing it in monomer solution in an inert atmosphere overnight. The electrode was then rinsed with THF extensively to remove any physisorbed material. A bronze-red tinge was observed on the gold electrode surface, indicating the presence of a polymer film. Films were characterized by cyclic voltammetry, where the gold electrode acted as the working electrode. The resulting cyclic voltammogram is shown in Figure 2.9, where distinct doping−dedoping waves of the polymer film can be observed at an anodic (doping) potential of 0.76 V and a cathodic (dedoping) potential of 0.42 V.

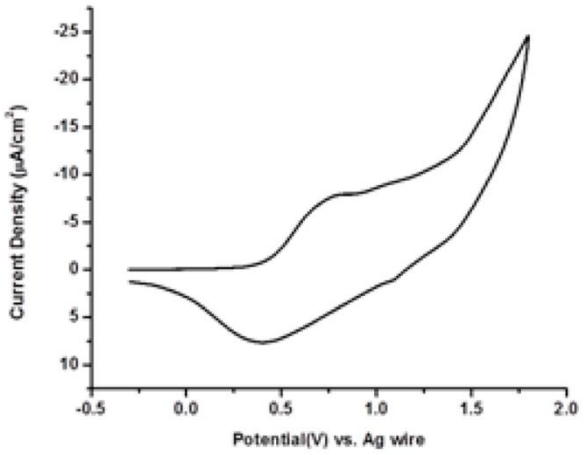

Figure 2.9. Cyclic voltammogram showing the doping and dedoping of P3MT.

The P3MT film remained unchanged over multiple cycles, showing the stability of the generated P3MT film (Figure 2.10).

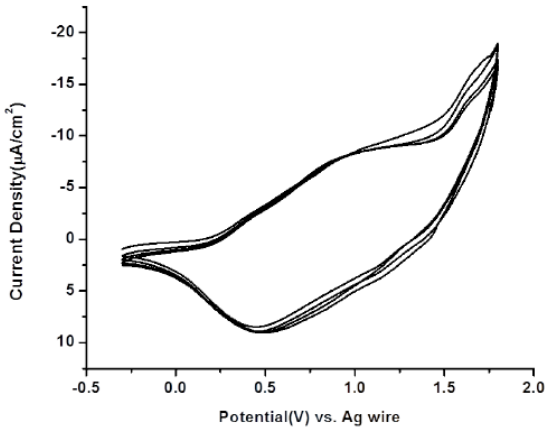

Figure 2.10. Cyclic Voltammetric plot showing doping-dedoping of P3MT for multiple cycles

In order to compare films obtained by electrodeposition methods, we grew a P3MT film by directly electropolymerizing 3-methylthiophene on a gold electrode without the use of an initiating monolayer. Cyclic voltammetry of the resulting film shows doping−dedoping waves at similar potentials to that of a surface-immobilized film (Figure 2.11).

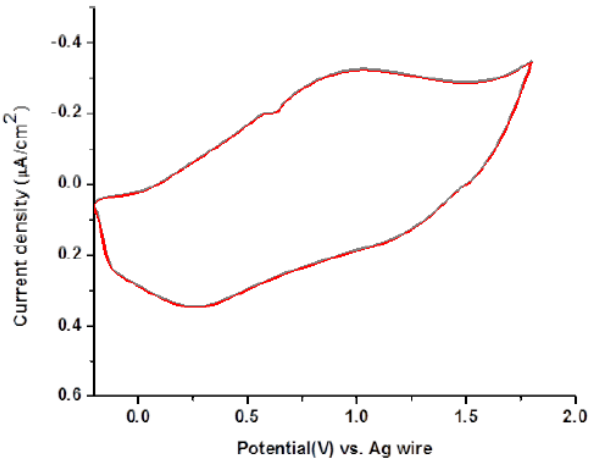

Figure 2.11. Cyclic voltammetry of P3MT grown electrochemically on Gold electrode from 3-methyl thiophene.

We also used larger gold substrates to grow P3MT. The thickness of the polymer film grown on the gold substrate was observed to be 25 nm as measured by spectroscopic ellipsometry.

Atomic force microscopy of the P3MT film shows a uniform morphology with an rms roughness of 5 nm, similar to previously reported films grown by SI-KCTP (Figure 2.12).[18]

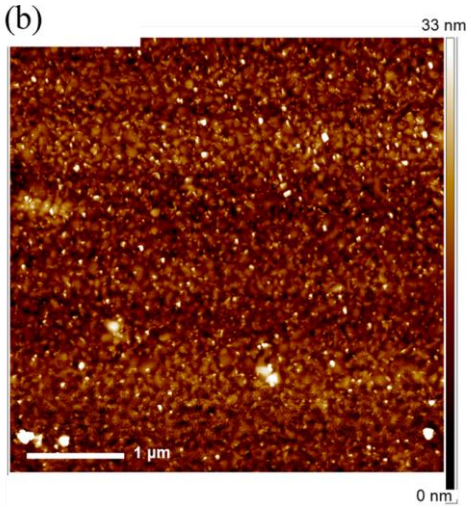

Figure 2.12. Atomic force microscopy of the P3MT film on a gold substrate (5 µm)

Conclusion

We have developed a simple and robust method for depositing surface-initiated monolayers for SI-KCTP which results in a large increase in surface coverage. The method involves electrodepositing bromobenzene monolayers through the reaction of an arene diazonium salt with the gold surface. Reactive Ni(0) is generated in situ by the electrochemical reduction of $Ni(dppp)Cl_2$ in two mechanistic steps: Ni(II) to Ni(I) followed by Ni(I) to Ni(0). The facile addition of nickel to the monolayer limits the diffusion of Ni(0) species away from the surface as compared to the previously used solution deposition technique with Ni(COD)bpy. We have found that electrochemically generated initiator complexes provide a coverage of 1.29×10^{14} molecules/cm^2, which provides a 6- fold increase in coverage compared to those obtained from solution-generated complexes.[13] The electrochemical process of monolayer formation, oxidative addition, and degradation was monitored by surface plasmon resonance coupled with cyclic voltammetry to provide further evidence of the possible mechanism of the process. The electrogeneration process overcomes the need for solution deposition, which suffers from instability of the Ni(0) source, $Ni(COD)_2$, as well as the need for an additional ligand substitution reaction that results in a reduced coverage. Our electrochemical deposition method provides a simple, high-yielding process for generating reactive Ni(0), which, with the addition of monomer, results in the surface-bound polymerization of thiophenes.

References:

(1) Yang, L.; Sontag, S. K.; LaJoie, T. W.; Li, W.; Huddleston, N. E.; Locklin, J.; You, W. Surface Initiated Poly(3-methylthiophene) as a Hole-Transport Layer for Polymer Solar Cells with High Performance. ACS Appl. Mater. Interfaces 2012, 4, 5069−5073.

(2) Sung, A.; Ling, M. M.; Tang, M. L.; Bao, Z.; Locklin, J. Correlating Molecular Structure to Field-Effect Mobility: The Investigation of Side-Chain Functionality in Phenylene−Thiophene Oligomers and Their Application in Field Effect Transistors. Chem. Mater. 2007, 19, 2342−2351.

(3) Hong, Z.; Michelle, L. S.; Mark, E. R.; Colin, R.; Abhijit Basu, M.; Stefan, C. B. M.; Zhenan, B.; Jason, L. In Organic Field-Effect Transistors; CRC Press: Boca Raton, FL, 2007; pp 159−228.

(4) Hou, J.; Chen, T. L.; Zhang, S.; Huo, L.; Sista, S.; Yang, Y. An Easy and Effective Method To Modulate Molecular Energy Level of Poly(3-alkylthiophene) for High-Voc Polymer Solar Cells. Macromolecules 2009, 42, 9217−9219.

(5) Cheng, Y. J.; Yang, S. H.; Hsu, C. S. Synthesis of Conjugated Polymers for Organic Solar Cell Applications. Chem. Rev. 2009, 109, 5868−5923.

(6) Beinhoff, M.; Appapillai, A. T.; Underwood, L. D.; Frommer, J. E.; Carter, K. R. Patterned Polyfluorene Surfaces by Functionalization of Nanoimprinted Polymeric Features. Langmuir 2006, 22, 2411−2414.

(7) Osaka, I.; McCullough, R. D. Advances in Molecular Design and Synthesis of Regioregular Polythiophenes. Acc. Chem. Res. 2008, 41,1202−1214.

(8) Miyakoshi, R.; Yokoyama, A.; Yokozawa, T. Development of catalyst-transfer condensation polymerization. Synthesis of π-conjugated polymers with controlled molecular weight and low polydispersity. J. Polym. Sci., Part A: Polym. Chem. 2008, 46, 753−765.

(9) Yokoyama, A.; Miyakoshi, R.; Yokozawa, T. Chain-Growth Polymerization for Poly(3-hexylthiophene) with a Defined Molecular Weight and a Low Polydispersity. Macromolecules 2004, 37, 1169−1171.

(10) Iovu, M. C.; Sheina, E. E.; Gil, R. R.; McCullough, R. D. Experimental Evidence for the Quasi-"Living" Nature of the Grignard Metathesis Method for the Synthesis of Regioregular Poly(3-alkylthiophenes). Macromolecules 2005, 38, 8649−8656.

(11) Miyakoshi, R.; Yokoyama, A.; Yokozawa, T. Catalyst-Transfer Polycondensation. Mechanism of Ni-Catalyzed Chain-Growth Polymerization Leading to Well-Defined Poly(3-hexylthiophene). J. Am. Chem. Soc. 2005, 127, 17542−17547.

(12) Sontag, S. K.; Bilbrey, J. A.; Huddleston, N. E.; Sheppard, G. R.; Allen, W. D.; Locklin, J. π-Complexation in Nickel-Catalyzed Cross- Coupling Reactions. J. Org. Chem. 2014, 79, 1836−1841.

(13) Sontag, S. K.; Sheppard, G. R.; Usselman, N. M.; Marshall, N.; Locklin, J. Surface-Confined Nickel Mediated Cross-Coupling Reactions: Characterization of Initiator Environment in Kumada Catalyst-Transfer Polycondensation. Langmuir 2011, 27, 12033−12041.

(14) Doubina, N.; Jenkins, J. L.; Paniagua, S. A.; Mazzio, K. A.; MacDonald, G. A.; Jen, A. K. Y.; Armstrong, N. R.; Marder, S. R.; Luscombe, C. K. Surface-Initiated Synthesis of Poly(3-methylthiophene) from Indium Tin Oxide and its Electrochemical Properties.
Langmuir 2011, 28, 1900−1908.

(15) Senkovskyy, V.; Khanduyeva, N.; Komber, H.; Oertel, U.;Stamm, M.; Kuckling, D.; Kiriy, A. Conductive Polymer Brushes of Regioregular Head-to-Tail Poly(3-alkylthiophenes) via Catalyst-Transfer Surface-Initiated Polycondensation. J. Am. Chem. Soc. 2007, 129, 6626−6632.

(16) Marshall, N.; Locklin, J. Reductive Electrografting of Benzene (p-Bisdiazonium Hexafluorophosphate): A Simple and Effective Protocol for Creating Diazonium-Functionalized Thin Films.Langmuir 2011, 27, 13367−13373.

(17) Senkovskyy, V.; Sommer, M.; Tkachov, R.; Komber, H.; Huck, W. T. S.; Kiriy, A. Convenient Route To Initiate Kumada Catalyst-Transfer Polycondensation Using Ni(dppe)Cl2 or Ni(dppp)Cl2 and Sterically Hindered Grignard Compounds. Macromolecules 2010, 43, 10157−10161.

(18) Sontag, S. K.; Marshall, N.; Locklin, J. Formation of conjugated polymer brushes by surface-initiated catalyst-transfer polycondensation. Chem. Commun. 2009, 3354−3356.

(19) Marshall, N.; Sontag, S. K.; Locklin, J. Surface-initiated polymerization of conjugated polymers. Chem. Commun. 2011, 47, 5681−5689.

(20) Yamamoto, T.; Wakabayashi, S.; Osakada, K. Mechanism of C□C coupling reactions of aromatic halides, promoted by Ni(COD)2 in the presence of 2,2′-bipyridine and PPh3, to give biaryls. J. Organomet. Chem. 1992, 428, 223−237.

(21) Bilbrey, J. A.; Sontag, S. K.; Huddleston, N. E.; Allen, W. D.; Locklin, J. On the Role of Disproportionation Energy in Kumada Catalyst-Transfer Polycondensation. ACS Macro Lett. 2012, 1, 995−1000.

(22) Amatore, C.; Jutand, A. Rates and mechanism of biphenyl synthesis catalyzed by electrogenerated coordinatively unsaturated nickel complexes. Organometallics 1988, 7, 2203−2214.

(23) Ohtsuka, T.; Sato, Y.; Uosaki, K. Dynamic Ellipsometry of a Self-Assembled Monolayer of a Ferrocenylalkanethiol during Oxidation-Reduction Cycles. Langmuir 1994, 10, 3658−3662.

(24) Mangolini, F.; Rossi, A.; Spencer, N. D. Chemical Reactivity of Triphenyl Phosphorothionate (TPPT) with Iron: An ATR/FT-IR and XPS Investigation. J. Phys. Chem. C 2010, 115, 1339−1354.

(25) Bryant, M. A.; Pemberton, J. E. Surface Raman scattering of self assembled monolayers formed from 1-alkanethiols at silver [electrodes].J. Am. Chem. Soc. 1991, 113, 3629−3637.

(26) Nelson, B. P.; Frutos, A. G.; Brockman, J. M.; Corn, R. M. Near-Infrared Surface Plasmon Resonance Measurements of Ultrathin Films. 1. Angle Shift and SPR Imaging Experiments. Anal. Chem. 1999,71, 3928−3934.

(27) Meyer, S. A.; Le Ru, E. C.; Etchegoin, P. G. Combining Surface Plasmon Resonance (SPR) Spectroscopy with Surface-Enhanced Raman Scattering (SERS). Anal. Chem. 2011, 83, 2337−2344.

(28) Fujii, E.; Koike, T.; Nakamura, K.; Sasaki, S.-i.; Kurihara, K.; Citterio, D.; Iwasaki, Y.; Niwa, O.; Suzuki, K. Application of an Absorption-Based Surface Plasmon Resonance Principle to the Development of SPR Ammonium Ion and Enzyme Sensors. Anal.Chem. 2002, 74, 6106−6110.

(29) Koutsioubas, A. G.; Spiliopoulos, N.; Anastassopoulos, D. L.; Vradis, A. A.; Priftis, G. D. Formation of alkane-phosphonic acid selfassembled monolayers on alumina: an in situ SPR study. Surf. Interface Anal. 2009, 41, 897−903.

(30) Taranekar, P.; Baba, A.; Fulghum, T. M.; Advincula, R. Conjugated Polymer Network Films from Precursor Polymers: Electrocopolymerization of a Binary Electroactive Monomer Composition. Macromolecules 2005, 38, 3679−3687.

(31) Liu, G.; Böcking, T.; Gooding, J. J. Diazonium salts: Stable monolayers on gold electrodes for sensing applications. J. Electroanal. Chem. 2007, 600, 335−344.

(32) Gui, A. L.; Liu, G. Z.; Chockalingam, M.; Le Saux, G.; Harper, J. B.; Gooding, J. J. A Comparative Study of Modifying Gold and Carbon Electrode with 4-Sulfophenyl Diazonium Salt. Electroanalysis 2010, 22,1283−1289.

(33) Laforgue, A.; Addou, T.; Bélanger, D. Characterization of the Deposition of Organic Molecules at the Surface of Gold by the Electrochemical Reduction of Aryldiazonium Cations. Langmuir 2005,21, 6855−6865.

(34) Laurentius, L.; Stoyanov, S. R.; Gusarov, S.; Kovalenko, A.; Du, R.; Lopinski, G. P.; McDermott, M. T. Diazonium-Derived Aryl Films on Gold Nanoparticles: Evidence for a Carbon−Gold Covalent Bond. ACS Nano 2011, 5, 4219−4227.

(35) Shumaker-Parry, J. S.; Campbell, C. T. Quantitative Methods for Spatially Resolved Adsorption/Desorption Measurements in Real Time by Surface Plasmon Resonance Microscopy. Anal. Chem. 2004,76, 907−917**.**

(36) Kariuki, J. K.; McDermott, M. T. Formation of Multilayers on Glassy Carbon Electrodes via the Reduction of Diazonium Salts. Langmuir 2001, 17, 5947−5951.

(37) Pinson, J. Aryl Diazonium Salts; Wiley-VCH: Weinheim, Germany, 2012; pp 1−35.(38) Tolman, C. A. Steric effects of phosphorus ligands in organometallic chemistry and homogeneous catalysis. Chem. Rev.1977, 77, 313−348.

CHAPTER 3

DEVELOPMENT OF OPTIMAL REACTIVE INITIATOR MONOLAYER FOR GROWING POLY(3-METHYLTHIOPHENE BRUSHES) BY DETAILED INVESTIGATION OF THEIR STRUCTURE PROPERTY RELATIONSHIP

[1] Roy, A.; DeLongchamp, D.; McNeil, C.; Orski, S.; Locklin, J. To be submitted to *Langmuir*

Abstract

In this work, a detailed investigation of the structure property relationship of reactive initiator monolayers towards growth of P3MT brushes has been performed. The structures of phosphonic acid based aryl halide monolayers were systematically varied in order to analyze how the difference in monolayer geometry affects the grafting density and directionality of the P3MT brushes. Through exhaustive characterization of all monolayers and corresponding brushes using electrochemical and spectroscopic techniques like UV-VIS, NEXAFS, XPS, it was perceived that the optimal balance between grafting density and orientation of P3MT brushes can be brought about by the phenyl hexylphosphonic acid (PHPA) based monolayer. Comparing with the characteristics of the monolayers gives an insight into understanding what physical parameters of the monolayers are responsible for optimal brush growth with respect to grafting density and directionality. This can be utilized to make P3MT brushes suitable for fabricating efficient organic electronic devices.

Introduction:

A significant amount of research has been done on developing polymerization techniques for growing conjugated polymers in solution as well as their immobilization from surface. This is primarily due to their immense potential for being used in various organic electronic and organic photovolatic devices such as solar cells, fuel cells, sensors, organic spintronic devices as they show several interesting electronic and optical properties.[1-7] Most of these devices have active layers composed of thin films of conjugated polymers covalently grafted from conducting electrode surfaces. Covalent grafting prevents delamination of films and gives extra stability in devices where multiple layers need to be employed.[8] However, covalent grafting by itself doesn't imply efficient performance of devices. The nature of organization, orientation and grafting density of individual polymer chains altogether play very important roles in determining efficiency of a device and can give rise to interesting optical and electronic properties.

Organic electronic devices require the organic layer to have specific thickness ranges from several nanometers to few hundreds of nanometers. However, film thickness is not the sole parameter that influences device performance and efficiency.[9] In devices with polymer films grafted from substrate surface, orientation of the conjugated polymer chains plays a crucial role by improving anisotropy of charge transfer.[10] The film thickness, grafting density and directionality of the polymer chains together define the device performance. Commonly used solution processing techniques like spin coating or drop casting produces highly amorphous polymer films without any degree of alignment. This reduces the efficiencies of the devices fabricated. Polymer brushes grafted from surface provide a better way to create more order in the organic layer and generate better and controlled interfaces.[8,11-14] Perpendicular orientation of polymer chains is the preferred orientation for maximizing charge transport as it permits more intra molecular charge transport

rather than intermolecular hopping of carriers among the chains.[15] Even though grafting density can be better controlled in grafted polymer brushes, achieving orientation perpendicular to substrate is very difficult to date. An appropriate balance between thickness and orientation is required to maximize device efficiency. Very few methods exist to obtain certain degree of perpendicular orientation. This is owing to the incomplete understanding of the influence of structural parameters of initiator monolayers on the polymer brush growth. Also due to lack of complete control over several reaction parameters like competitive side reactions and other interaction parameters of the growing chains, the process becomes extremely arduous and hard to manipulate. This study aims at performing a detailed investigation of the structure-property relationship of reactive initiator monolayers towards brush growth in order to efficiently manipulate reaction parameters to develop optimal P3MT brushes.

One of the most important methods of synthesizing conjugated polymers is by KCTP (Kumada catalyst transfer polycondensation) or GRIM (Grignard metathesis polymerization). This method has been proven to be very versatile due to its ability to show chain growth characteristics (as initially observed by McCullough and Yokozawa) thereby providing control over molecular weight, dispersity and end group functionality.[7,16,17] Further KCTP was developed for covalently grafting conjugated polymer directly from the surface of conducting substrates (Surface initiated-KCTP).[8,9,14,18] SI-KCTP proceeds through a pathway involving (1) oxidative addition of zerovalent Nickel catalyst across aryl halide bond of a surface bound phosphonic acid monolayer, (2) transmetallation with bifunctional A-B type monomer and (3) reductive elimination of the zerovalent nickel catalyst which stays associated with the growing chain and "ring walks" to intramolecularly adds across the nearest aryl halide bond.[19,20] This process continues in a chain growth fashion and produces a polymer in the "brush" regime at high grafting densities. However,

there are certain problems associated with this process that lowers the efficiency of this reaction. A competitive side reaction, namely disproportionation, causes Ni sites in close proximity, to disproportionate due to the excessive reactivity of Ni catalyst.[21] This results in the formation of several "dead" initiator sites leading to a reduction in grafting density of the polymer. Along with the polymer brush thickness, it could also indirectly influence the directionality of the brushes. The aim of this study is to systematically vary the geometry of the phosphonic acid based aryl halide monolayers to analyze the influence of monolayers' geometry and pattern of assembly on a surface, on the grafting density and directionality of the P3MT brushes. To the best of our knowledge, till date, no such detailed study has been done which could possibly lead to a better understanding of the interplay of the various factors leading to P3MT brush growth. Hereon, we synthesized several monolayers by varying two structural parameters on phosphonic acid based aryl halide monolayers: (a) substituents on the benzene ring and (b) alkyl chain spacer length between the benzene ring and the phosphonic acid head group. The significance of varying the substituent patterns on the benzene rings was an attempt to physically space out the monolayers grafted from the surface. Manipulating the spacer length was to evaluate if there is any change in the interaction parameters e.g van der waal interactions between the monolayers that could also have an impact on the packing geometry of the brushes. This could modify the packing of the monolayers at the surface thereby influencing the directionality of brush growth.

It would also determine if the rates of competitive side reactions like disproportionation reaction will be affected during SI-KCTP, hence altering the grafting densities. We found the initiator monolayer with no substituents on benzene ring and 6 carbon spacers (phenyl hexyl phosphonic acid, PHPA) gave the perfect balance between grafting density and directionality, producing optimal P3MT films that can be applied to fabricate organic electronic devices.

Experimental

Grafting of Poly(3-methylthiophene) from ITO substrates

Materials:

Isopropylmagnesium chloride solution (2.0M in THF) and ferrocene were obtained from Acros Organics, and Bis(cyclooctadiene)nickel(0),Bis(tri-tert-butylphosphine)palladium(0) were obtained from Strem Chemicals. Tetrahydrofuran (THF) and Toluene were obtained from Sigma Aldrich and purified with an MBRAUN Solvent purification system. ITO substrates were purchased from Thin Film Devices (Anaheim, California). All other chemicals were purchased from TCI, Oakwood and Acros Organics. All chemicals were used as received unless mentioned otherwise.

Synthetic Methodology:

All syntheses were carried out under an inert atmosphere of purified argon or nitrogen, using standard Schlenk techniques or a glovebox (Unilab BP with an MB10 purification system, MBraun, Inc.).

The synthesis of 2-bromo-3-methyl-5-iodothiophene, along with magnesiation of 2-bromo-5-iodo-3-methylthiophene were carried out using synthetic procedures reported previously.[8] All NMR spectra were recorded using a Varian Mercury 300MHz spectrometer. Trimethylsilane internal standard was used to report relative chemical shifts.

Electrochemical measurements:

Electrochemical measurements were obtained using a CH Instruments bipotentiostat equipped with a platinum counter electrode and a silver wire pseudo reference electrode with Fc/Fc+ used as an internal standard (- vs. Ag wire electrode). The ITO substrates were used as the working electrodes. Tetrabutylammonium hexafluorophospate in DCM (0.1M, degassed)

was used as the supporting electrolyte for all electrochemical measurements. All scans were recorded at a rate of 100 mV/sec.

Preparation of substrates:

The ITO substrates were cleaned using standard cleaning procedures reported previously.

Monolayer deposition:

6.5 mM solutions of all phosphonic acid monolayers were prepared in ethanol and freshly ozone-cleaned substrates were immersed in 10 mL of these solutions overnight. Following day, substrates were dried under a stream of nitrogen , and annealed at 150^{o}C overnight under inert atmosphere. The next day, substrates were cooled under nitrogen atmosphere. They were rinsed thoroughly with water, methanol and dichloromethane (DCM). They were again dried under nitrogen and taken into the glove box for grafting P3MT by SI-KCTP. All the substrates were stored under inert atmosphere in the glove box until used for surface initiated polymerization.

Polymerization of 3MT from ITO surface.

Formation of initiator complex with Ni(0) catalyst:

In the glove box , 30mg of Ni(COD) and 17mg of bipyridine (bpy) were weighed out into a scintillation vial and 10ml of toluene was added to make a solution. The freshly cleaned substrates were then placed into the vial for 2.5 hours. These substrates were then washed with toluene and THF, before putting into a solution of diphenylphosphinopropane (dppp) ligand (0.1g in THF) for one hour for ligand exchange. This was followed by polymerization overnight.

Formation of initiator complex with Pd(0) catalyst:

In the glove box, 51mg of $Pd(P(^{t}Bu_3)_2$ was weighed out into a scintillation vial and 10ml toluene was added to it to make a solution and ITO substrates were placed in them. The vial was

then heated at 70^{o}C for three hours and rinsed with fresh toluene before polymerization performed at 40^{o}C overnight.

Polymerization of 3MT from ITO surface.

After formation of initiator complexes, the substrates were rinsed with Toluene and THF and then immersed into 10ml (0.1M) monomer (3-methyl-5-chloromagnesio thiophene) solution overnight. Following day, the substrates appeared bright red and a huge quantity of red polymer in solution was observed. The substrates were rinsed extensively with water, methanol and dichloromethane (DCM), sonicated in DCM for 10 mins and then dried under a stream of nitrogen before proceeding with extensive characterizations.

UV-VIS measurements.

UV-vis spectra of P3MT brushes on ITO were taken using a Cary Scan 50 UV-vis spectro-photometer from Varian. Polarized UV-VIS was measured using a custom-built setup, containing a substrate holder attached to a rotatable polarizing filter.

AFM measurements.

AFM measurements were taken on a Bruker Nanoscope V atomic force microscope in tapping mode using silicon tips with a spring constant 40 N/m and a resonant frequency of 300 kHz.

Result and discussion:

The P3MT brushes were characterized thoroughly in order to understand how polymer brush growth is affected by manipulation of various structural parameters of the initiator monolayers. The difference in geometry of the initiator monolayers could affect the way in which the catalyst sites are arranged, possibly influencing the rates of disproportionation reaction occurring at the surface.[21] This can modify the grafting densities of polymer chains. We also hypothesize that the difference in steric and Van der Waal interactions that arise due to difference in geometries of initiator monolayers could influence the way in which monolayers pack. This in turn could influence the directionality of the polymer chains grafted. We found that monolayers PHPA and DMPHPA (Refer Table 3.1) seem to show strikingly different behavior compared to the rest of the monolayers, therefore we chose to focus on the two. After performing a detailed analysis, we infer that PHPA is the most ideal monolayer candidate to grow P3MT brushes suited to potentially fabricate various organic electronic devices. After fabrication of the monolayers, they were tested for pinhole defects on surface by performing cyclic voltammetry (CV) (Figure.3.1).[22]

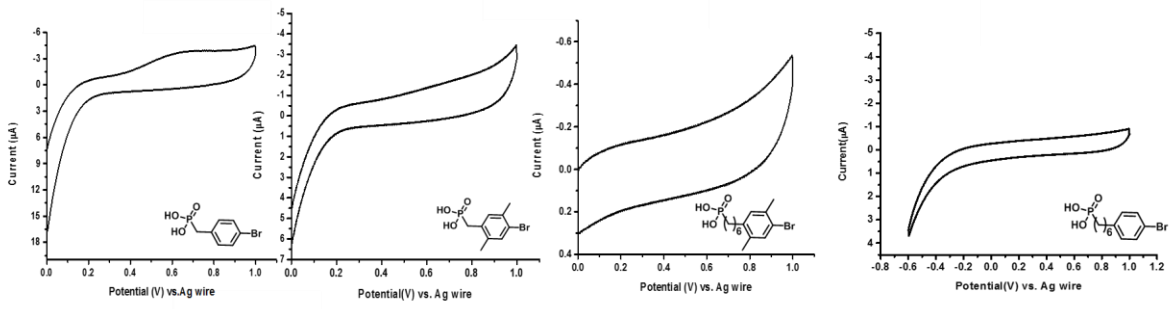

Figure 3.1. Cyclic voltammograms performed on all the monolayers to investigate pinhole defects on the monolayers grafted from ITO substrates.

We observed that all the monolayers were perfectly blocking. Only a small charging current was observed and there was no evidence of any redox activity on the substrate surface. The contact angles of the monolayers are listed in Table 3.1 below.

MONOLAYER	CONTACT ANGLE	STRUCTURE
DMPHPA (6-(4-bromo-2,5-dimethylphenyl)hexyl)phosphonic acid	106.93	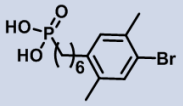
PHPA (6-(4 bromophenyl)hexyl)phosphonic acid	89.4	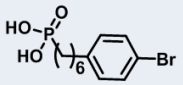
BPA (4-bromobenzyl)phosphonic acid	87.2	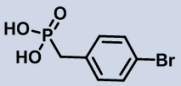
DMBPA (4-bromo-2,5-dimethylbenzyl)phosphonic acid	82.2	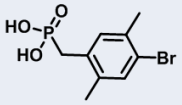

Table 3.1. Table listing the contact angles and chemical structures of the phosphonic aids used to make monolayers.

DMPHPA shows a very high contact angle of 106°, whereas the rest show usual values expected from such monolayers. This is likely due to the combined effects of the dimethyl substituents as well as the alkyl spacer present in DMPHPA, which makes the surface really hydrophobic. It could also be due to a specific packing pattern of the molecules. To investigate more into the packing of monolayers and probe into the consequences of the packing geometry on brush growth, we quantified the catalyst concentration on the initiator monolayers by using ferrocene quenching technique.[8] This previously reported procedure uses ferrocene as an indirect redox active, stable, electrochemical probe that can be attached to monolayers by magnesium-halogen exchange reactions (Figure 3.2).

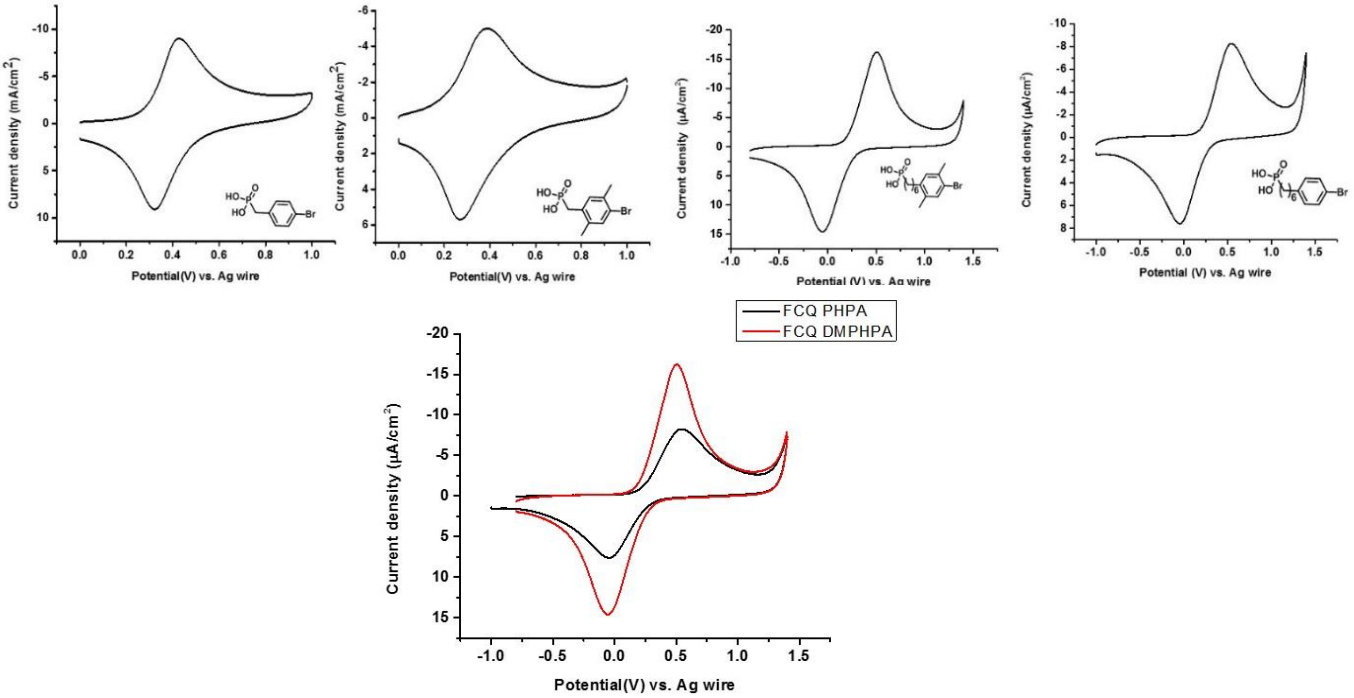

Figure 3.2.(a) Cyclic voltammetry (CV)performed on all the reactive initiator monolayers to account for surface coverage of Ni catalyst on the grafted monolayers on ITO substrates. (b) Overlay of CVs of ferrocene quenched monolayers PHPA and DMPHPA.

On integration of the redox peaks obtained from CV of these ferrocene quenched monolayers, we find that ferrocene quenched DMPHPA gives an extremely high coverage value of 80%, followed by PHPA (38%). The rest show nominal coverage of (15-20%) as is expected and reported in literature for P3MT brushes. On performing XPS (X-ray photoelectron spectroscopy) analysis on the ferrocene quenched monolayers (Figure 3.3), we observed that the ferrocene content was comparatively higher in DMPHPA, proving indirectly the presence of a high quantity of Nickel catalyst on the surface.

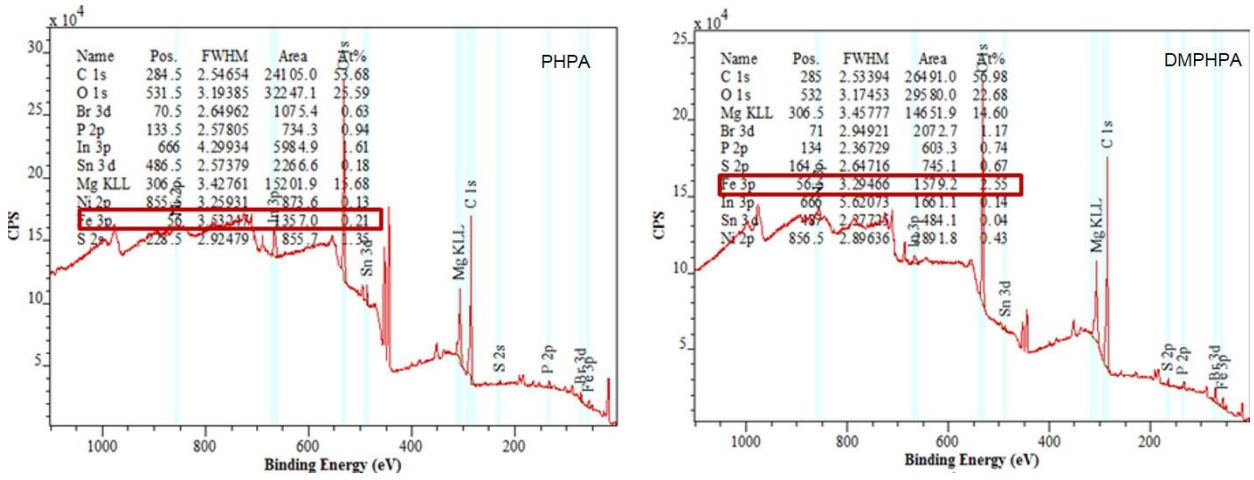

Figure 3.3. XPS of ferrocene quenched PHPA and DMPHPA.

This was followed by PHPA with a Nickel coverage of 38% which is significantly lower than DMPHPA, but high enough to generate high grafting density of polymer brushes. This unique result led us to look deeper into the packing geometry of the two monolayers to analyze if they have any characteristic difference in their packing. We chose to perform NEXAFS analysis as it is a very powerful technique to obtain sensitive information on orientation of absorbed molecules on the surface (Figure 3.4.).

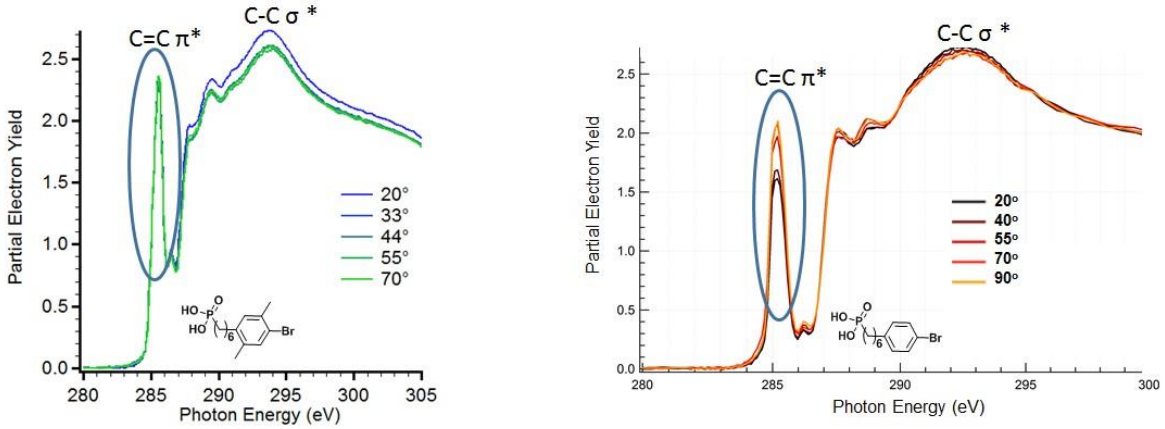

Figure 3.4. NEXAFS of monolayers (a) DMPHPA and (b) PHPA; the angular dependence of π-π*absorptions for PHPA in comparison to DMPHPA shows the preferred directionality in monolayer packing in PHPA

We studied the carbon-K-edge orientation scans and compared the C=C π-π* absorptions of the two monolayers in question, at various angles from (0-90^{o}). We observed that PHPA showed a clear angular dependence in the C=C π-π* absorptions with absorption maximum being at 90^{o} and minimum being at 20^{o}. This was in complete contrast to DMPHPA where there was no angular dependence in C=C π-π* absorption at the measured angles. This indicates that the molecules of PHPA have a higher order of crystallinity and pack in a characteristic manner, whereas DMPHPA molecules are randomly packed at the surface of ITO (Indium tin oxide) substrates.[23, 24]

We believe that although the DMPHPA molecules do not pack to form crystalline monolayers, the dimethyl substituents on the benzene ring must space out the catalyst sites in such a way that the rate of disproportionation is very low. Also the released Ni(0) might be able to reinitiate the initiator sites that were previously inaccessible due to the random packing of the monolayer. These are the possible reasons to observing such high ferrocene quenching coverage of 80% inspite of having very disordered monolayer packing in DMPHPA. However the PHPA

monolayer with its more crystalline packing still leads to retention of sufficiently high but not extreme amounts of catalyst on the surface. This produces high enough grafting densities. With this understanding, polymerization of 3-methylthiophene was performed from the two monolayers to evaluate if there is any evident differences in terms of directionality or grafting densities of the P3MT brushes (Figure 3.5).

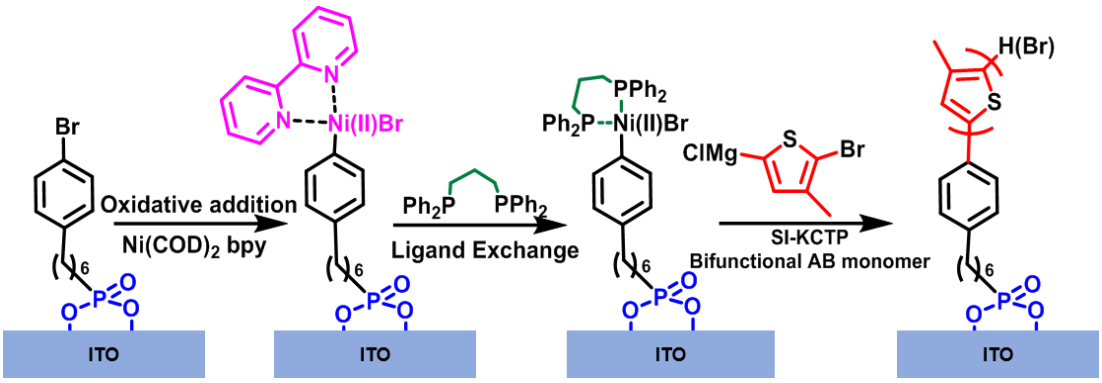

Figure 3.5. Schematic of the grafting procedure of P3MT brushes on ITO substrates by SI-KCTP

The P3MT brushes showed very uniform morphology as expected, on characterization by AFM (Figure 3.6).

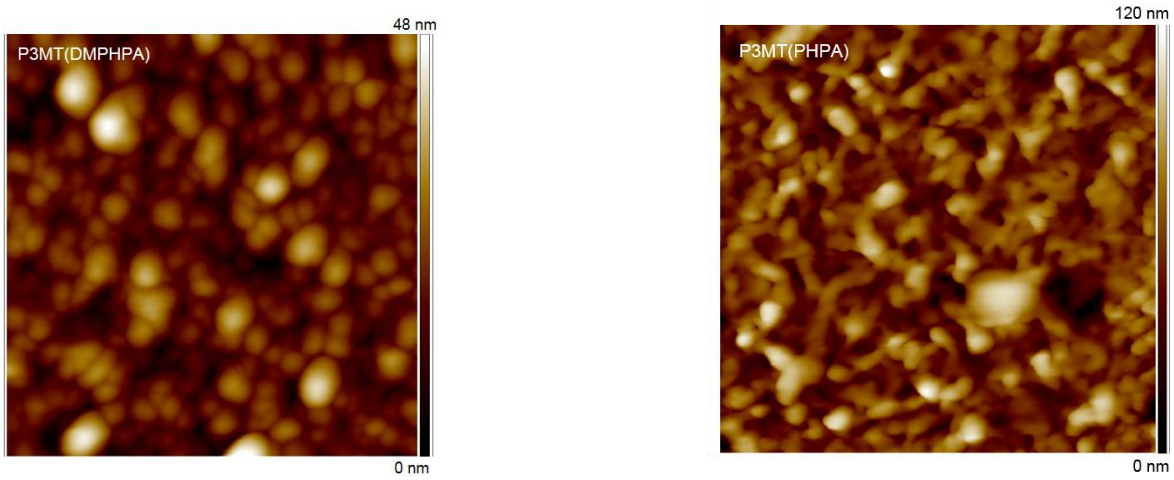

Figure 3.6. AFM images of P3MT brushes grown from monolayers DMPHPA and PHPA

Both monolayers formed thick brushes with DMPHPA giving slightly greater thickness than PHPA (~35nm from PHPA and ~45nm from DMPHPA). The polymer brushes were further

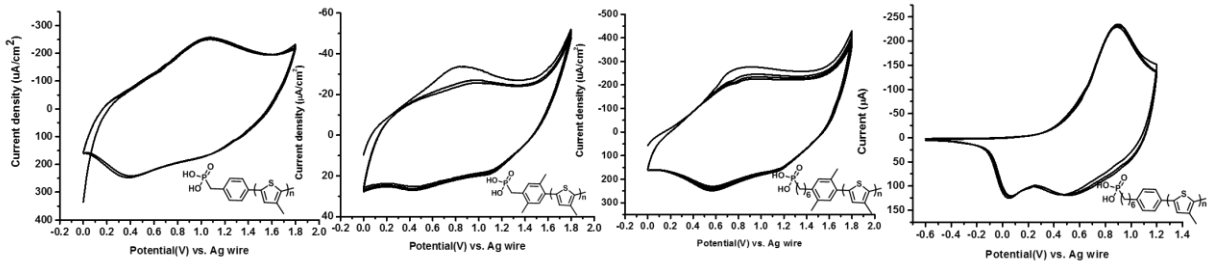

checked for their stability by performing multiple doping and dedoping cycles by (CV) (Figure 3.7.).

Figure 3.7. CV (dope-dedope test) performed on all the polymer (P3MT) brushes to account for stability of the films over multiple redox cycles.

No degradation in the brushes was observed over multiple doping-dedoping cycles exhibiting the stability of these brushes. We also observed that P3MT(PHPA) showed very sharp and distinct redox peaks exhibiting kinetic homogeneity, an attribute that is not observed in any of the other brushes. To observe any characteristic difference in orientation/directionality in the brush geometry, we examined the brushes with UV-VIS and polarized UV-VIS spectroscopy (Figure 3.8(a) and 3.8(b)).

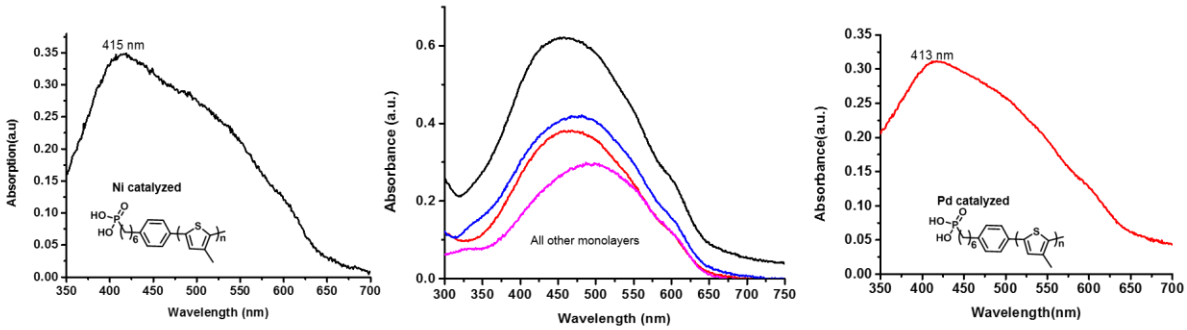

Figure 3.8(a). UV-VIS absorption spectra of (a) Ni catalyzed P3MT from monolayer PHPA; (b) Ni catalyzed P3MT from monolayers A, C, D, E; (c) Pd catalyzed P3MT from monolayer PHPA. No orientation/H-aggregation is seen in P3MT films from all monolayers except PHPA.

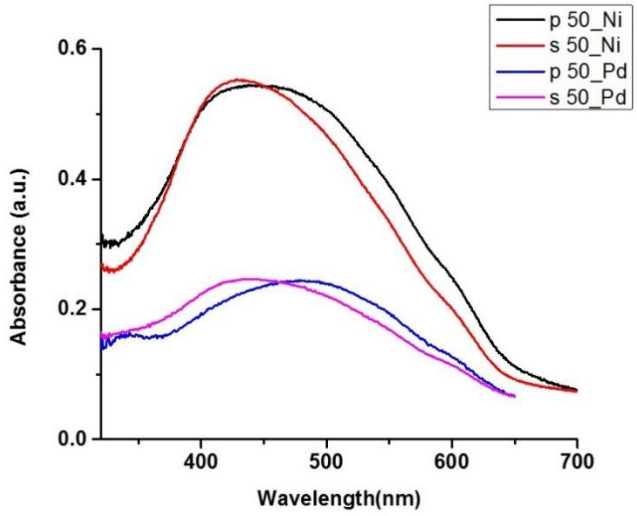

Figure 3.8(b). Polarized UV-VIS data for P3MT film from PHPA monolayer catalyzed by Ni and Pd. The pronounced blue shift in absorption of the λmax at 50^0 shows presence of H-aggregation in the film.

We consistently observed that λmax for the P3MT(PHPA) brushes are remarkably blue shifted to 415 nm while the rest have 465 nm λmax, as is expected for an unoriented P3MT brush (Figure 7(a)). This characteristic blue shift of λmax in P3MT(PHPA) brushes shows that there is substantial increase in H-aggregation of polymer chains in these brushes. This phenomenon is observed even when polymerization is catalyzed by Nickel catalyst.[9] This is notable as well since this is the first example of obtaining orientation in P3MT brushes, grown by SI-KCTP using Ni catalyst. In previous report, only very expensive palladium catalyst could give certain degree orientation/H-aggregation.[9] We further did polarized UV-VIS studies on PHPA(P3MT) brushes catalyzed by Pd and we can infer that the brushes are oriented at an average angle of 55^o (Figure 3.8(b)).[25-28] We consistently observe this behavior for P3MT(PHPA) and not from P3MT(DMPHPA) or P3MT from the other monolayers. Keeping in mind they are all grown from

the same monomer solution in one pot, we therefore believe that PHPA must pack in a very unique manner. The unique packing retains catalyst in the optimum amount to produce oriented polymer brushes at high grafting density. This is in contrast to DMPHPA, which is a randomly oriented monolayer, but sterically spaces out the catalyst sites with its dimethyl substituents in a way to drastically reduce the rate of disproportionation. The ortho substituents on the benzene ring also act to stabilize catalyst sites.[8, 29-31] Even though this randomly oriented monolayer provides very high grafting density, it fails to provide the optimum catalyst concentration needed for achieving orientation in P3MT brushes.

This is a very promising result and we can begin to understand the influence of certain structural features in an initiating monolayer responsible for growing aligned polymer brushes with a decent grafting density. One of the important aspects of this study is to provide insight into designing monolayers that are ideal to make polymer brushes suited for fabrication of organic electronic devices.[32] Since PHPA seemed to be the ideal target monolayer to grow P3MT brushes with orientation and high grafting density, we utilized P3MT(PHPA) to fabricate organic spin valve devices. In this device, the non-magnetic spacer layer was fabricated by grafting P3MT(PHPA) brushes from ferromagnetic LSMO substrate. On performing device characterization, we obtained a very large magnetoresistance response from this device, whereas the other monolayers failed to produce successful spin valve devices. This proves that PHPA is an ideal candidate and has a potential for fabricating efficient organic electronic devices.[32]

Conclusion:

A detailed investigation was performed to probe the P3MT brush growth characteristics in order to attain high grafting density and directionality. We found that the structure of initiator monolayer chosen to grow P3MT brush plays a very important role in increasing the grafting density and optimizing directionality in the brush. Several phosphonic acid based monolayers were analyzed. 6-(4-bromophenyl)hexylphosphonic acid (PHPA) stood out to be the most ideal monolayer providing the perfect balance between grafting density and orientation to the brush. P3MT brushes obtained from PHPA consistently showed high grafting densities and a high degree of H-aggregation, even on catalyzing the polymerization with Ni catalyst. We believe that PHPA monolayer packs in a more crystalline manner, whereby it provides the optimal spacing between the reactive initiator sites, reducing disproportionation and providing high grafting densities (38% catalyst coverage). This unique packing also gives the polymer brush a degree of orientation, average angle of orientation being at 55^0 from the plane of the substrate. This broadens the scope of application of these polymer brushes for fabricating high performance organic electronic devices.

References:

(1). McQuade, D. T.; Pullen, A. E.; Swager, T. M., Conjugated Polymer-Based Chemical Sensors. *Chem. Rev.* **2000,** *100* (7), 2537-2574.

(2). Calabrese Barton, S.; Gallaway, J.; Atanassov, P., Enzymatic Biofuel Cells for Implantable and Microscale Devices. *Chem. Rev.* **2004,** *104* (10), 4867-4886.

(3). Günes, S.; Neugebauer, H.; Sariciftci, N. S., Conjugated Polymer-Based Organic Solar Cells. *Chem. Rev.* **2007,** *107* (4), 1324-1338.

(4). Iovu, M. C.; Jeffries-El, M.; Sheina, E. E.; Cooper, J. R.; McCullough, R. D., Regioregular poly(3-alkylthiophene) conducting block copolymers. *Polymer* **2005,** *46* (19), 8582-8586.

(5). Loewe, R. S.; Khersonsky, S. M.; McCullough, R. D., A Simple Method to Prepare Head-to-Tail Coupled, Regioregular Poly(3-alkylthiophenes) Using Grignard Metathesis. *Adv. Mater.* **1999,** *11* (3), 250-253.

(6). Ma, W.; Yang, C.; Gong, X.; Lee, K.; Heeger, A. J., Thermally Stable, Efficient Polymer Solar Cells with Nanoscale Control of the Interpenetrating Network Morphology. *Adv. Funct. Mater.* **2005,** *15* (10), 1617-1622.

(7). McCullough, R. D.; Lowe, R. D., Enhanced electrical conductivity in regioselectively synthesized poly(3-alkylthiophenes). *J. Chem. Soc., Chem. Commun.* **1992,** (1), 70-72.

(8). Sontag, S. K.; Sheppard, G. R.; Usselman, N. M.; Marshall, N.; Locklin, J., Surface-Confined Nickel Mediated Cross-Coupling Reactions: Characterization of Initiator Environment in Kumada Catalyst-Transfer Polycondensation. *Langmuir* **2011,** *27* (19), 12033-12041.

(9). Huddleston, N. E.; Sontag, S. K.; Bilbrey, J. A.; Sheppard, G. R.; Locklin, J., Palladium-Mediated Surface-Initiated Kumada Catalyst Polycondensation: A Facile Route Towards Oriented Conjugated Polymers. *Macromolecular Rapid Communications* **2012,** *33* (24), 2115-2120.

(10). Sirringhaus, H.; Brown, P. J.; Friend, R. H.; Nielsen, M. M.; Bechgaard, K.; Langeveld-Voss, B. M. W.; Spiering, A. J. H.; Janssen, R. A. J.; Meijer, E. W.; Herwig, P.; de Leeuw, D. M., Two-dimensional charge transport in self-organized, high-mobility conjugated polymers. *Nature* **1999,** *401* (6754), 685-688.

(11). Sontag, S. K.; Marshall, N.; Locklin, J., Formation of conjugatedpolymer brushes by surface-initiated catalyst-transfer polycondensation. *Chem. Commun.* **2009,** (23), 3354-3356.

(12). Yang, L.; Sontag, S. K.; LaJoie, T. W.; Li, W.; Huddleston, N. E.; Locklin, J.; You, W., Surface-Initiated Poly(3-methylthiophene) as a Hole-Transport Layer for Polymer Solar Cells with High Performance. *ACS Applied Materials & Interfaces* **2012,** *4* (10), 5069-5073.

(13). Doubina, N.; Jenkins, J. L.; Paniagua, S. A.; Mazzio, K. A.; MacDonald, G. A.; Jen, A. K. Y.; Armstrong, N. R.; Marder, S. R.; Luscombe, C. K., Surface-Initiated Synthesis of Poly(3-methylthiophene) from Indium Tin Oxide and its Electrochemical Properties. *Langmuir* **2012,** *28* (3), 1900-1908.

(14). Marshall, N.; Sontag, S. K.; Locklin, J., Surface-initiated polymerization of conjugated polymers. *Chem. Commun.* **2011,** *47* (20), 5681-5689.

(15). Collini, E.; Scholes, G. D., Coherent Intrachain Energy Migration in a Conjugated Polymer at Room Temperature. *Science* **2009,** *323* (5912), 369-373.

(16). Miyakoshi, R.; Yokoyama, A.; Yokozawa, T., Catalyst-Transfer Polycondensation. Mechanism of Ni-Catalyzed Chain-Growth Polymerization Leading to Well-Defined Poly(3-hexylthiophene). *J. Am. Chem. Soc.* **2005,** *127* (49), 17542-17547.

(17). Sheina, E. E.; Liu, J.; Iovu, M. C.; Laird, D. W.; McCullough, R. D., Chain Growth Mechanism for Regioregular Nickel-Initiated Cross-Coupling Polymerizations. *Macromolecules* **2004,** *37* (10), 3526-3528.

(18). Roy, A.; Gao, J.; Bilbrey, J. A.; Huddleston, N. E.; Locklin, J., Rapid Electrochemical Reduction of Ni(II) Generates Reactive Monolayers for Conjugated Polymer Brushes in One Step. *Langmuir* **2014,** *30* (34), 10465-10470.

(19). Tkachov, R.; Senkovskyy, V.; Komber, H.; Sommer, J.-U.; Kiriy, A., Random Catalyst Walking along Polymerized Poly(3-hexylthiophene) Chains in Kumada Catalyst-Transfer Polycondensation. *J. Am. Chem. Soc.* **2010,** *132* (22), 7803-7810.

(20). Beryozkina, T.; Senkovskyy, V.; Kaul, E.; Kiriy, A., Kumada Catalyst-Transfer Polycondensation of Thiophene-Based Oligomers: Robustness of a Chain-Growth Mechanism. *Macromolecules* **2008,** *41* (21), 7817-7823.

(21). Yamamoto, T.; Wakabayashi, S.; Osakada, K., Mechanism of C□C coupling reactions of aromatic halides, promoted by Ni(COD)2 in the presence of 2,2′-bipyridine and PPh3, to give biaryls. *J. Organomet. Chem.* **1992,** *428* (1), 223-237.

(22). Yuan, M.; Zhan, S.; Zhou, X.; Liu, Y.; Feng, L.; Lin, Y.; Zhang, Z.; Hu, J., A Method for Removing Self-Assembled Monolayers on Gold. *Langmuir* **2008,** *24* (16), 8707-8710.

(23). Ma, J.; Hashimoto, K.; Koganezawa, T.; Tajima, K., End-On Orientation of Semiconducting Polymers in Thin Films Induced by Surface Segregation of Fluoroalkyl Chains. *J. Am. Chem. Soc.* **2013,** *135* (26), 9644-9647.

(24). Gliboff, M.; Sang, L.; Knesting, K. M.; Schalnat, M. C.; Mudalige, A.; Ratcliff, E. L.; Li, H.; Sigdel, A. K.; Giordano, A. J.; Berry, J. J.; Nordlund, D.; Seidler, G. T.; Brédas, J.-L.; Marder, S. R.; Pemberton, J. E.; Ginger, D. S., Orientation of Phenylphosphonic Acid Self-Assembled Monolayers on a Transparent Conductive Oxide: A Combined NEXAFS, PM-IRRAS, and DFT Study. *Langmuir* **2013,** *29* (7), 2166-2174.

(25). Rikukawa, M.; Rubner, M. F., Fabrication of Langmuir-Blodgett films of poly(3-hexylthiophene) and metal-substituted phthalocyanines. *Langmuir* **1994,** *10* (2), 519-524.

(26). Xu, G.; Bao, Z.; Groves, J. T., Langmuir−Blodgett Films of Regioregular Poly(3-hexylthiophene) as Field-Effect Transistors. *Langmuir* **2000,** *16* (4), 1834-1841.

(27). Zhang, Z.; Verma, A. L.; Yoneyama, M.; Nakashima, K.; Iriyama, K.; Ozaki, Y., Molecular Orientation and Aggregation in Langmuir−Blodgett Films of 5-(4-N-Octadecylpyridyl)-10,15,20-tri-p-tolylporphyrin Studied by Ultraviolet−Visible and Infrared Spectroscopies. *Langmuir* **1997,** *13* (16), 4422-4427.

(28). Locklin, J.; Shinbo, K.; Onishi, K.; Kaneko, F.; Bao, Z.; Advincula, R. C., Ambipolar Organic Thin Film Transistor-like Behavior of Cationic and Anionic Phthalocyanines Fabricated Using Layer-by-Layer Deposition from Aqueous Solution. *Chem. Mater.* **2003,** *15* (7), 1404-1412.

(29). Doubina, N.; Paniagua, S. A.; Soldatova, A. V.; Jen, A. K. Y.; Marder, S. R.; Luscombe, C. K., Steric Effects of the Initiator Substituent Position on the Externally Initiated Polymerization of 2-Bromo-5-iodo-3-hexylthiophene. *Macromolecules* **2011,** *44* (3), 512-520.

(30). Smeets, A.; Van den Bergh, K.; De Winter, J.; Gerbaux, P.; Verbiest, T.; Koeckelberghs, G., Incorporation of Different End Groups in Conjugated Polymers Using Functional Nickel Initiators. *Macromolecules* **2009,** *42* (20), 7638-7641.

(31). Doubina, N.; Ho, A.; Jen, A. K. Y.; Luscombe, C. K., Effect of Initiators on the Kumada Catalyst-Transfer Polycondensation Reaction. *Macromolecules* **2009,** *42* (20), 7670-7677.

(32). Geng, R.; Roy, A.; Zhao, W.; Subedi, R. C.; Li, X.; Locklin, J.; Nguyen, T. D., Engineering of Spin Injection and Spin Transport in Organic Spin Valves Using π-Conjugated Polymer Brushes. *Adv. Funct. Mater.* **2016**, n/a-n/a.

CHAPTER 4

ENGINEERING OF SPIN INJECTION AND SPIN TRANSPORT IN ORGANIC SPIN VALVES USING π CONJUGATED POLYER BRUSHES

[1]Roy, A.; [1]Geng, R.; Zhao, W.; Subedi, R. C.; Li, X.; Locklin, J.; Nguyen, T. D. Accepted by *Advanced Functional Materials*. Reprinted here with permission of John Wiley and Sons.

Abstract

Charge transport in amorphous organic semiconductors is governed by carriers hopping between localized states with small spin diffusion length. Furthermore, the interfacial resistance of organic spin valves (OSVs) is poorly controlled resulting in controversial reports of the magnetoresistance (MR) response. Here, surface-initiated Kumada transfer polycondensation is used to covalently graft π-conjugated poly(3-methylthiophene) brushes from the La0.67Sr0.33MnO3 (LSMO) bottom electrode. The covalent attachment along with the brush morphology allows control over the LSMO/brush interfacial resistance and large spacer mobility. Remarkably, with 15 nm brush spacer layer, an optimum MR effect of 70% at cryogenic temperatures and a MR of 2.7% at 280 K are observed. The temperature dependence of the MR is nearly an order of magnitude weaker than that found in control OSVs made from spin-coated poly (3-hexylthiophene). Using a variety of different brush layer thicknesses, the thickness-dependent MR at 20 K is investigated. A spin diffusion length of 17 nm at −5 mV junction voltage rapidly increased to 48.4 nm at −260 mV.

Introduction

Since the discovery of the spin valve effect in organic semiconductors (OSECs) in 2004, the field of organic spintronics has made significant achievements in basic research as well as advancements in device fabrication.[1,2] An organic spin valve (OSV) is comprised of a thin OSEC layer sandwiched between two ferromagnetic (FM) electrodes where spin injection/ detection by the FM electrodes and spin transport in organic layers have been implicated.[3,4] Since OSECs have reduced spin–orbit coupling due to their lightweight elements, these materials possess a long spin lifetime, on the order of microseconds, which allow for the performance of multiple operations on the spins before they reach equilibrium. This is a necessary condition for realizing spin logic device applications.[5] The spin injection and transport in OSECs have been elucidated using various methods such as low-energy muon-spin spectroscopy,[6] two-photon photoemission,[7] FM resonance spin pumping,[8,9] and spin organic light emitting diodes (spin-OLEDs).[10] In addition, the hyperfine interaction (HFI) has been theoretically and experimentally proven to be the main spin-loss mechanism in OSVs.[11,12] Finally, a large magnetoresistance (MR) of ≈300% has been observed at 10 K with these materials, suggesting that the metal/organic interface might act as a spin filter causing significantly large effective spin polarization at the interface, which is referred to as the spinterface.[13–17] Recently, a large MR of up to 10% at room temperature was reported by several groups, indicating potential future applications of organic valves.[18–20] In addition, sizable MR at a 6 V bias has been observed in double-layer OSVs, which is a good spintronic structure candidate for high performance spin-OLEDs.[21] Beside the above advances, there are still several fundamental challenges for spin injection and spin transport in OSVs.[22] Perhaps, the most convincing demonstration for spin transport in OSECs would be to perform spin precession or the Hanle effect. This experiment has not been achieved in organics, casting doubt for the existence

of spin transport in OSECs.[23–25] It is worth noting that using a ferromagnetic resonance spin pumping technique, Watanabe et al. reported the Hanle effect in the pure spin current of an organic polymer. However, using the same experimental technique, Jiang et al. strongly demonstrated that such an effect might come from the non-uniformity of the microwave magnetic field.[26] Although spin relaxation time in OSECs is significantly long compared to their inorganic counterparts,[3] the spin diffusion length is several orders of magnitudes smaller than in inorganic semiconductors.[2,6,12,27] The most obvious reason for this discrepancy is the low charge mobility caused by hopping transport between localized states in the amorphous organic films.[11,28] Nevertheless, it is not clear whether the electrons hop between majority states or minority defect states in OSVs.[29] Next, since the spin diffusion length in OSECs is short, it is extremely difficult to exhibit nonlocal MR in OSVs where a planar device structure is normally used to reduce the complication of the spin-charge coupling.[30] Finally, it is a challenge to control the spinterface effect in the OSVs due to a lack of microscopic control in organic film fabrication and metal inclusion into soft organic materials during the metal evaporation.[4] In this report, we investigated spin injection and transport in π-conjugated polymer brush-based spin valves where the brushes were grown directly from the surface of the bottom FM electrode, $La_{0.67}Sr_{0.33}MnO_3$ (LSMO), using a covalent grafting technique. Grafted polymer brushes with small torsional degrees of freedom along polymer chains might possess large mobility due to the dominant intrachain charge transport and the reduced positional and energetic disorder. [3,31] In addition, the spinterface at LSMO electrode is well controlled, leading to the same effective spin polarization at the LSMO interface while varying the polymer brush length. Our device structure consists of a self-assembled macromonolayer of conjugated polymer chains, which is similar to that observed in the single molecule electronics field, where the electron orbitals are delocalized throughout the molecular

backbone to achieve high mobility.[32,33] Therefore, the resistance in such device depends on the nature of molecular/metal contacts.[34,35] We studied spin injection and spin diffusion length in the device by fitting the thickness-dependent MR using the modified Julliere model. We observed a large MR of ≈70% at 20 K and nearly 3% at 280 K. The poly (3-methylthiophene) (P3MT) brush-based OSVs show larger conductivity and a smaller MR reduction with temperature in comparison to spin-coated poly(3-hexylthiophene) (P3HT)-based OSVs with the same spacer thickness. However, the spin diffusion length in these brushes is small, ≈17 nm at zero bias voltage, and significantly increases with the applied bias voltage while the effective spin polarization decreases with the junction voltage.

Experimental

Synthetic scheme for 6-(4-bromophenyl)hexylphosphonic acid.

The synthesis of 1 bromo-4-(6-bromohexyl)-benzene was performed according to the previously reported procedure, but slightly modified to improve product yield.[57]

(6-(4- bromophenyl)hexyl)phosphonic acid (Figure 4.1): 2,5-dibromoxylene (5.0g, 21.2 mmol) was added to a three neck flask and purged with Nitrogen. 17.2 mL of dry THF was then added and solution was stirred for 10mins in a dry ice/acetone bath. n-BuLi (1.6M,14.57 mL, 23.32 mmol) was then added to the stirred solution dropwise. This solution was stirred for 30 minutes, and then cannula transferred dropwise to another three neck flask containing 1,6-dibromohexane (6.42 mL, 42.39 mmol) in THF (3mL). This was again stirred for two hours in dry ice/acetone bath and then warmed to room temperature. 20 mL of diethylether was then added to the reaction flask. The product was then washed with water twice, dried with MgSO4 and concentrated to obtain a clear oil (5.26 g, 80%). This was then distilled under vacuum to remove excess 1,6- dibromohexane to reveal pure product. 1 H NMR δ =7.40 (d, 2H, J = 7.1Hz), 7.05 (d, 2H, J = 7.7Hz), 3.40 (t, 2H, J = 6.7Hz), 2.57 (t, 2H, J = 7.5Hz), 1.85 (p, 2H, J = 7.8Hz), 1.61(p, 2 2H,J= 8.1Hz), 1.47(p, 2H,J= 7.8Hz), 1.34(p, 2H,J= 7.4Hz). 4.0g of the product was refluxed with excess triethylphosphite overnight at 170^{o}C. Next, excess triethyl phosphite was distilled off to generate the phosphonate ester (quantitative yield). The phosphonate ester was then stirred with TMS-Br (bromotrimethylsilane) overnight. Excess bromotrimethylsilane was distilled off under vacuum and methanol (20ml) was added and refluxed for 4 hours. The methanol was the removed under vacuum to obtain pure 6-(4-bromophenyl)hexylphosphonic acid (quantitative yield). I H NMR (CD3OD, 300MHz)(ppm) δ =7.38 (d, 2H, J = 8.7Hz), 7.07 (d, 2H, J = 8.0Hz), 3.29 (t, 2H, J =

1.7Hz), 2.56 (t, 2H , J = 7.3Hz), 1.72 - 1.25 (m, 10H) ; 13 C NMR (CD3OD, 300MHz)(ppm) 141.71, 129.97, 118.79, 34.71, 30.79, 29.95, 28.30, 27.50, 22.44, 22.38.

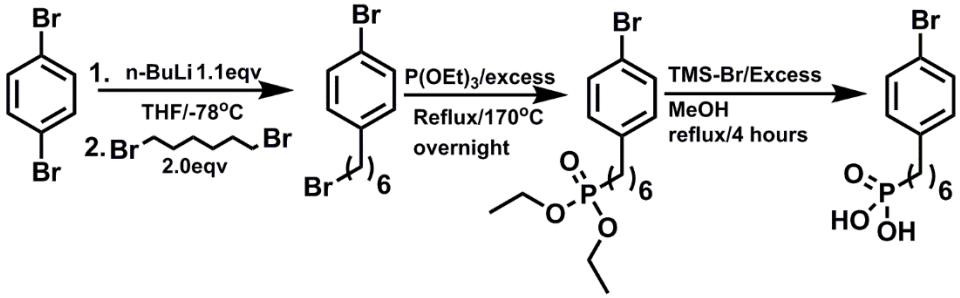

Figure 4.1. Synthetic scheme for 6-(4-bromophenyl)hexylphosphonic acid

Topographical characterization.

Atomic force microscopy was performed to analyze the morphology of the surface of the P3MT films on LSMO. The surface of bare LSMO is very smooth with RMS (root mean square) roughness of 0.83 nm. The 30nm P3MT film on LSMO shows densely packed uniform morphology with RMS roughness of 3.61 nm consistent with P3MT films grown on ITO in previous studies. For comparison, the morphology of spincasted P3HT films was analyzed by AFM as well. To our surprise, the roughness of the spin coated P3HT was very similar to the the roughness of the P3MT brushes that were covalently immobilized. Roughness of P3HT spin coated film is around 3.67 nm.

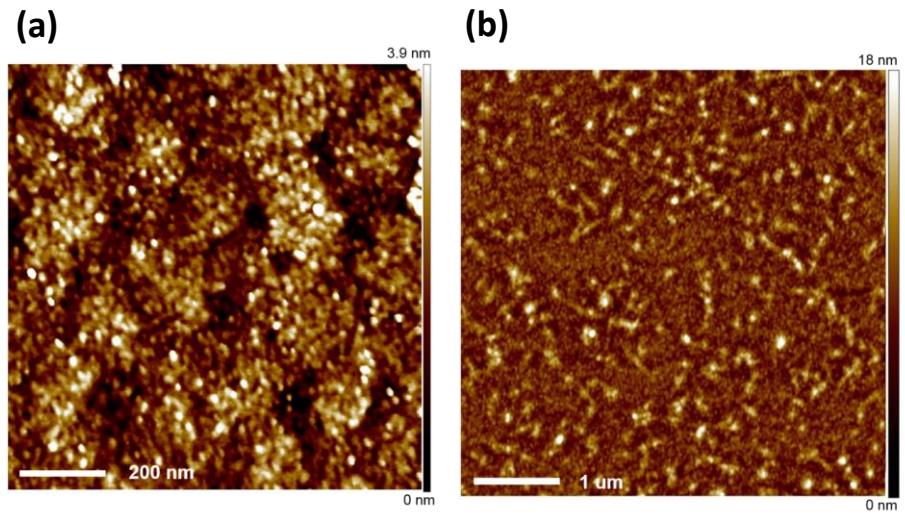

Figure 4.2.(a) AFM topographical images (1µm x 1µm) of bare LSMO and **(b)** spin casted P3HT (5µm x 5µm). RMS roughness of the bare LSMO and P3HT film on LSMO was estimated to be 0.83 nm and 3.67 nm, respectively.

HOMO-LUMO estimation of P3MT film In addition to LSMO substrates, P3MT films were grafted from Indium tin oxide substrates for performing electrochemical and UV-VIS of the films which are difficult to be carried out on patterned LSMO substrates due to lack of transparency of the LSMO film.

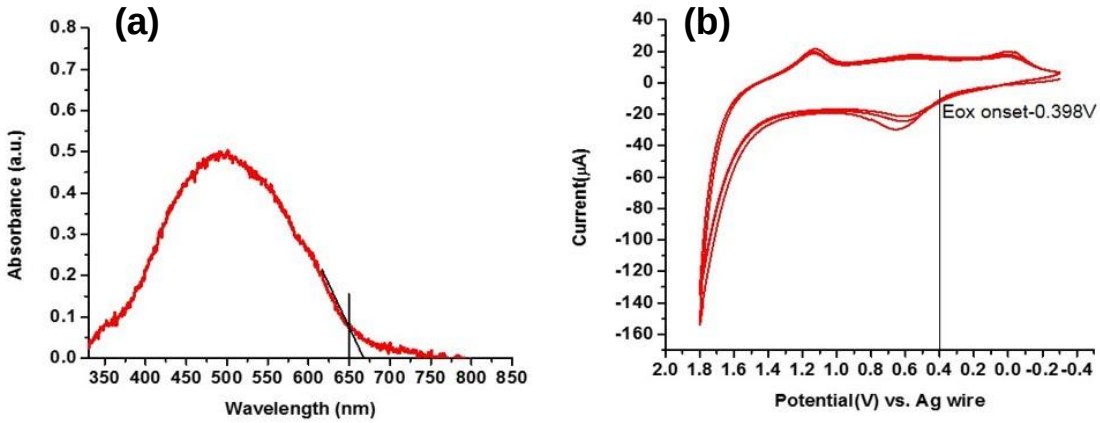

Figure 4.3 . (a) UV-VIS spectra and **(b)** CV of P3MT film on ITO, showing absorption onset at 650 nm and oxidation onset potential at -0.398 V respectively. Ferrocene is used as an internal standard to calculate the energy level of HOMO. From CV of P3MT film on ITO, HOMO energy, E(HOMO)=4.9eV of the brushes can be calculated. In addition, LUMO energy can be estimated from the UV-VIS spectra.

Calculations:

Ferrocene is used as a internal standard to calculate the energy level of HOMO.

HOMO – from Cyclic voltammetry of P3MT film on ITO:

$$E(HOMO) = \left[\left(E_{ox}^{onset} - E_{1/2}Fc\right) + 4.8\right] eV \qquad \text{(S1)}$$

$$E_{1/2}Fc = \frac{(E_{ox} + E_{red})}{2} = \frac{(0.434 + 0.268)}{2} = 0.351\ V \qquad (S2)$$

$$E_{ox}^{onset} = 0.398\ eV$$

$$E(HOMO) = [(0.398 - 0.351) + 4.8] eV \qquad \text{(S3)}$$

$$E(HOMO) = 4.9\ eV$$

LUMO – from UV-VIS spectra of P3MT film on ITO:

$$\lambda\ onset = 650\ nm$$

$$E_g(band\ gap) = \frac{1240}{(\lambda\ onset)} = \frac{1240}{650} = 1.9\ eV \qquad (S4)$$

$$E_g = 1.9\ eV$$

$$E(LUMO) = E(HUMO) - E_g = 4.9 - 1.9 = 3.0\ eV \quad (S5)$$

$$E(LUMO) = 3.0\ eV$$

Maximum magnetoresistance with different P3MT brush thicknesses.

Magnetoresistance (MR) with bias voltage dependence decreases with increasing the bias voltage, which has been explainled in the discussion section. So, in principle, we can achieve larger MR by applying smaller bias voltage. However, due to the resolution of the equipment used for the measurement setup, we can't decrease the bias voltage infinitely. So in order to keep the accuracy of the results, the smallest current we used here is ±100nA, which ensures the experimental results with a very small uncertainty of 5%.

Temperature dependent MR and IV characteristics.

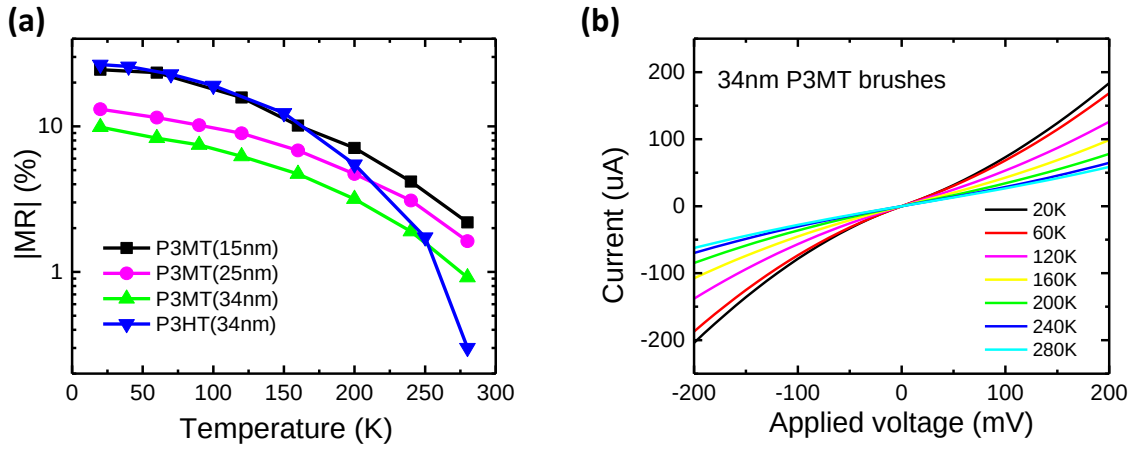

Figure 4.4. (a) The MR response of P3HT film-based OSV and P3MT brush-based OSVs with different spacer thicknesses measured at 20K with bias voltage -5 mV, respectively. (b) Typical temperature dependent IV characteristics of a P3MT with 34 nm thickness.

Ellipsometric measurements.

Measurement of the thickness of the P3MT films on the LSMO substrates were carried out using imaging ellipsometry (Accurion nanofilm_EP4) with a 658nm HeNe laser light source at 65°. Film thickness was obtained by fitting ellipsometric data using EP4 Model software provided by Accurion. Several positions were measured on each substrate and data was averaged. The refractive index parameters, n = 1.7 and k= 0 were used in the model to obtain the thickness of each sample. 8. UV-VIS measurements UV-vis spectra of P3MT on ITO substrates were measured using a Cary 50 UV-vis spectrophotometer from Varian.

UV-VIS measurements.

UV-vis spectra of P3MT on ITO substrates were measured using a Cary 50 UV-vis spectrophotometer from Varian.

Device Fabrication and Measurement.

The OSVs were fabricated using P3MT brushes as the interlayer sandwiched between La0.67Sr0.33MnO3 and cobalt. LSMO films, having thickness of ≈50 nm and area of 5 × 5 mm2, were grown epitaxially on <100> oriented SrTiO3 substrates at 750 °C using magnetron sputtering, with Ar and O2 flux in the ratio of 1:1 in a pressure of 4 Pa. The films were subsequently annealed at 800 °C for 2 h in O2 atmosphere before being slowly cooled to room temperature. The average roughness of LSMO is ≈0.83 nm (**see Figure 4.2(a).** The LSMO films were subsequently patterned using standard photolithography and chemical etching techniques. As the LSMO films are stable against oxidation; they can be cleaned and reused multiple times without serious degradation. The P3MT brushes were covalently grafted onto the surface of the LSMO. Even though the polymer brushes were used for device fabrication almost instantly after they are grown, rinsed, and dried, they were exposed to oxygen for a short period of time during transportation between labs for MR measurement, and we cannot exclude the possibility of some oxidation of the film, which could limit the MR values observed. Then the top electrode layer of Co (15 nm)/Ag (50 nm) was deposited by E-beam evaporation using a shadow mask at room temperature with a high vacuum condition of 1 × 10−6 mbar. The obtained active device area was typically ≈0.2 × 0.4 mm2.

As a control experiment, a P3HT-based OSV was fabricated. The P3HT film was made by solution processing and then was annealed at 140 °C for one hour before the top electrode deposition. All of the fabrication processes were done in inert atmosphere in the glove box, where the oxygen and water levels were less than 0.1 ppm.

The device was then mounted on the cold finger of a closed-cycle helium cryostat located between two poles of an electromagnet. The MR response was measured by using the four-probe technique with an in-plane magnetic field up to 3 KOe. A Keithley 3635B power source was used to apply a constant current, and a Keithley 2000 meter was used to measure the bias voltage across the junction. (see Figure 4.4)

Grafting of Poly(3-methylthiophene) from Patterned LSMO Substrates

Materials.

Isopropylmagnesium chloride solution (2.0 m in tetrahydrofuran (THF)) and ferrocene were obtained from Acros Organics, and Bis(cyclooctadiene)nickel(0) was obtained from Strem Chemicals. THF and toluene were obtained from Sigma- Aldrich and purified with an MBRAUN Solvent purification system. All other chemicals were purchased from Tokyo Chemical Industry Co. Ltd., Oakwood and Acros Organics and all chemicals were used as received unless mentioned otherwise.

Synthetic methodology.

All syntheses were carried out under an inert atmosphere of purified argon or nitrogen, using standard Schlenk techniques or a glovebox (Unilab BP with an MB10 purification system, MBraun, Inc.). The synthesis of 2-bromo-3-methyl-5-iodothiophene, along with its magnesiation, was carried out using synthetic procedures reported previously.[36]

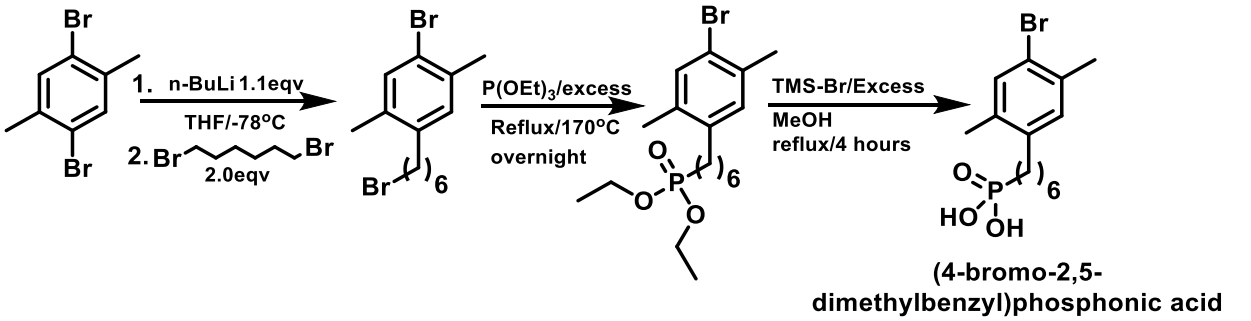

Figure 4.5. Scheme for synthesis of (4-bromo-2,5-dimethylbenzyl)phosphonic acid (PHPA)

To a three neck flask, 1,4-dibromo-2,5-dimethylbenzene (2.0g,7.58 mmol) was added and purged with nitrogen. THF (17.2ml) was added to this flask and the suspension was stirred for 10 mins in a dry ice-acetone bath. n-BuLi (6.16ml, 9.58mmol, 1.6M) was then added dropwise to the reaction mixture. The color of the mixture change from white to colorless. It was stirred further for 30 mins, then 1,6-dibromohexane (2.3 ml,15.15mmol) was added in one lot. The reaction was stirred for two hours and then warmed to room temperature. Approximately 20 ml of diethyl ether was then added and then reaction was worked up by washing with water and brine, followed by drying with $MgSO_4$. Diethyl ether was then removed under vacuum to produce a pale white oil. Excess dibromohexane was then distilled off under vacuum (yield 60%). The product obtained was then refluxed vigorously with triethylphosphite (excess) over 24 hours, and the excess triethylphosphite was distilled off the following day (quantitative yield). Bromotrimethylsilane was then added in excess and stirred overnight, followed by distilling off the excess under vacuum the next day. Methanol (30 mL) was then added and refluxed for 4 hours, and then solvent was removed under vacuum to obtain pure (4-bromo-2,5-dimethylbenzyl)phosphonic acid in quantitative yield.

I H NMR ($CDCl_3$, 300MHz) (ppm) : δ =7.30 (s, 1H), 6.99 (s, 1H), 3.42 (t, 2H, J =7.5Hz), 2.52 (t, 2H, J = 8.4Hz), 2.35 (s, 3H), 2.25 (s, 3H), 1.47 (m, 8H)

Electrochemical Measurements.

Electrochemical measurements were obtained using a CH Instruments bipotentiostat equipped with a platinum counter electrode and a silver wire pseudo reference electrode with Fc/Fc+ used as an internal standard (0.351 V vs Ag wire electrode).

The ITO substrates (used as reference) were used as the working electrodes. Tetrabutylammonium hexafluorophospate in dichloromethane (DCM) (0.1 m, degassed) was used as the supporting electrolyte for all electrochemical measurements. All scans were recorded at a rate of 100 mV s−1.

Preparation of Substrates

The patterned LSMO substrates were sonicated in chloroform for 10 min. This was followed by their immersion in a H2O2:NH4OH:H2O (1:1:5) bath at 85 °C for 30 min.[2] The substrates were then thoroughly rinsed with water, sonicated in isopropanol for 10 min and ozone cleaned for 15 min before final use. ITO substrates were cleaned using previously reported procedures.[36]

Monolayer deposition.

A 6.5 × 10−3 m solution of 6-(4-bromo- 2,5-dimethylphenyl) hexylphosphonic acid in ethanol was prepared and the freshly ozone-cleaned substrates were immersed in 5 mL of this solution overnight. The next day, substrates were dried under nitrogen gas and annealed at 150 °C overnight under inert atmosphere. The following day, substrates were cooled under nitrogen atmosphere and rinsed thoroughly with water, methanol, and DCM. These were then dried under nitrogen before grafting P3MT. All the substrates were stored under inert atmosphere in the glove box until used for surface initiated polymerization.

Formation of Initiator Complex

In the glovebox, 15 mg of Bis(1,5-cyclooctadiene)nickel(0) (Ni(COD)2) and 8.5 mg of 2,2′-bipyridine (bpy) were weighed out in a 20 mL scintillation vial. Toluene (5 ml) was then added to form a homogeneous solution. LSMO substrates fabricated with aryl halide monolayers were then immersed in this solution for 3 h. This was followed by rinsing with toluene and THF before performing ligand exchange with 5 mL of 0.1 m solution of bis-1,3 diphenylphosphinopropane (dppp) in THF. The process of ligand exchange was carried out for one hour and then rinsed with THF before polymerization.

Polymerization of 3MT from LSMO Surface.

The substrates with reactive initiator were immersed in monomer solution. After 2 h, the solution turned bright red and a significant amount of red polymer precipitate was observed in solution. This is very notable, since the usual SI-KCTP process on ITO, SiO2, and Au takes over 12 h for completion.[36,37,64–66] The substrates were taken out of solution, rinsed with water, methanol, and DCM thoroughly, sonicated for 10–15 min in DCM, and dried under nitrogen atmosphere, before being used for device fabrication. The substrates appeared bright red as well after rinsing, a good indication of the grafted P3MT from the substrate surface.

Results and discussion

Schematics and IV Characteristics

P3MT Brushes

Figure 4.6 shows the synthetic scheme for grafting P3MT from the LSMO substrate. The conjugated polymer brushes were covalently grafted from the surface via surface initiated Kumada catalyst transfer polycondensation (SI-KCTP).[36,37] SI-KCTP allows covalent grafting of P3MT from reactive initiator monolayers, by a three-step process of oxidative addition of Ni(0) catalyst across aryl halide bond of monolayer, transmetallation, and carbon bond forming reductive elimination followed directly by an intramolecular oxidative addition of the transient Ni(0) to the nearest aryl halide bond. This process continues through a chain growth mechanism through which the conjugated polymer grows directly from the surface.[36] We note that the grafting density of the polymer brushes is significantly high, which minimizes short circuiting even in ultrathin devices where the top electrode of Co/Ag is deposited. After the fabrication of pinhole-free, aryl halide containing monolayers on LSMO using phosphonic acid head-groups for covalent attachment, we used SI-KCTP to grow films of P3MT with controlled thickness up to 40 nm.[38] The morphology of the P3MT films were analyzed by atomic force microscope (AFM) (see Figure 4.6(b),4.6(c)).

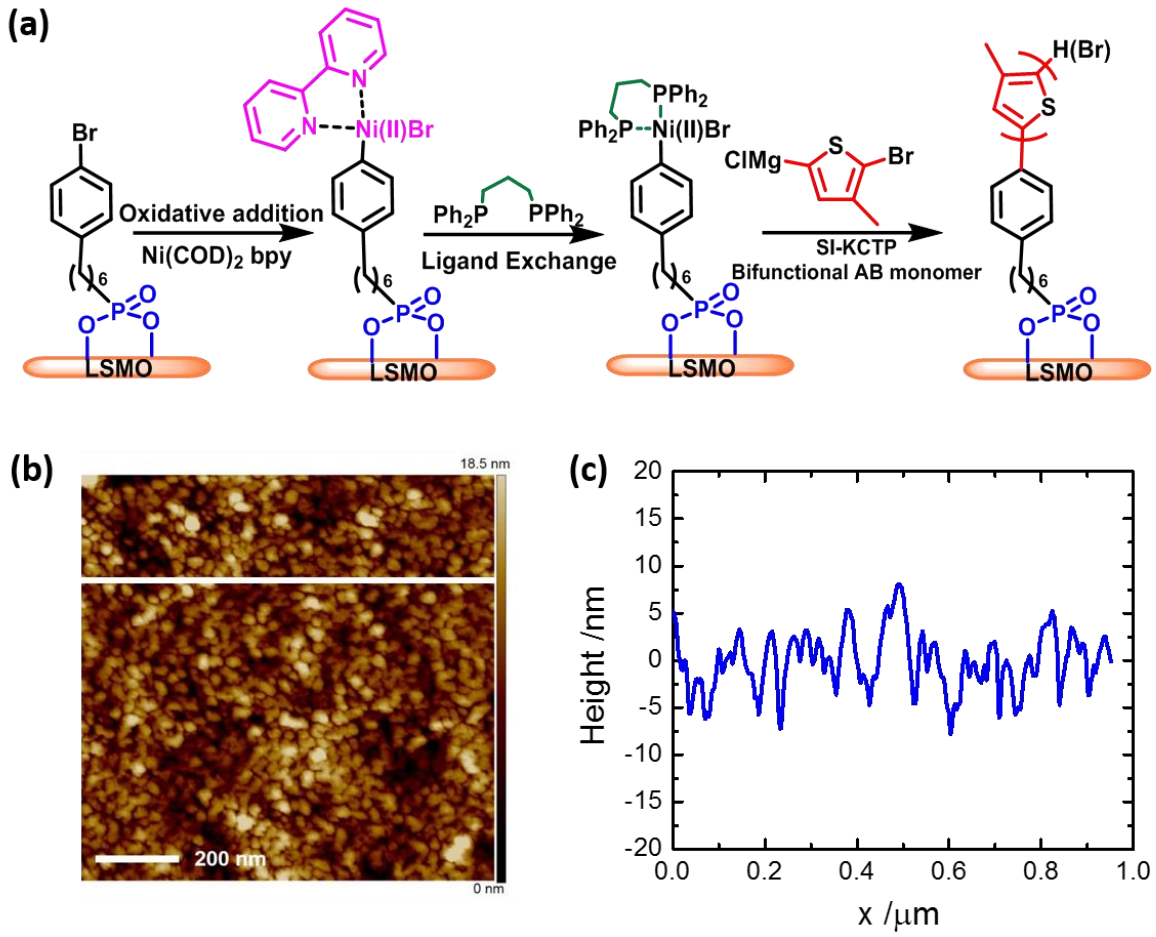

Figure 4.6. (a) Scheme showing the procedure for grafting of poly(3-methylthiophene) from the surface of LSMO substrate via SI-KCTP. (b) AFM topographical image of 30nm P3MT brushes grafted from LSMO substrate. The RMS roughness of the film was 3.61nm. (c) The profile of the highlighted line in (b).

The 30 nm P3MT film on LSMO shows densely packed uniform morphology with root mean squared (RMS) roughness of 3.6 nm consistent with P3MT films grown on indium tin oxide (ITO) in previous studies.[36] In fact, the roughness of these films has a similar quality compared to others used in OSVs where a thin insulating layer is used in the device to prevent the direct tunneling from one electrode to the other.[39,40] The charge transport in these devices can be described using a multiple-step tunneling transport. The covalent attachment to the LSMO provides excellent control

over the interface compared to traditional methods of fabricating organic films by spin casting or thermal evaporation. Therefore, the resistance mismatch problem for the spin injection from the LSMO electrode into the polymers can be overcome by carefully engineering the interface.[41–44] This opens a possibility of tuning the interfacial spin polarization of the electrodes (or spinterface) by tuning the monolayer thickness or resistivity. In the ideal case, the carrier transport mainly occurs along the polymer chains, rather than interchain hopping, leading to a substantial enhancement in carrier mobility in the film. For the same thickness of the films shown in Figure 4.7(d), the polymer brush shows much higher electrical conductivity than amorphous, spin casted films made using P3HT, which indicates a larger carrier mobility in the polymer brushes. It is worth noting that the interfacial resistance caused by the weak van der Waals force between the organic and bottom electrode is quite small compare to the bulk resistance.[45] Therefore, the spin diffusion length in the brushes is expected to be enhanced.[1,3]

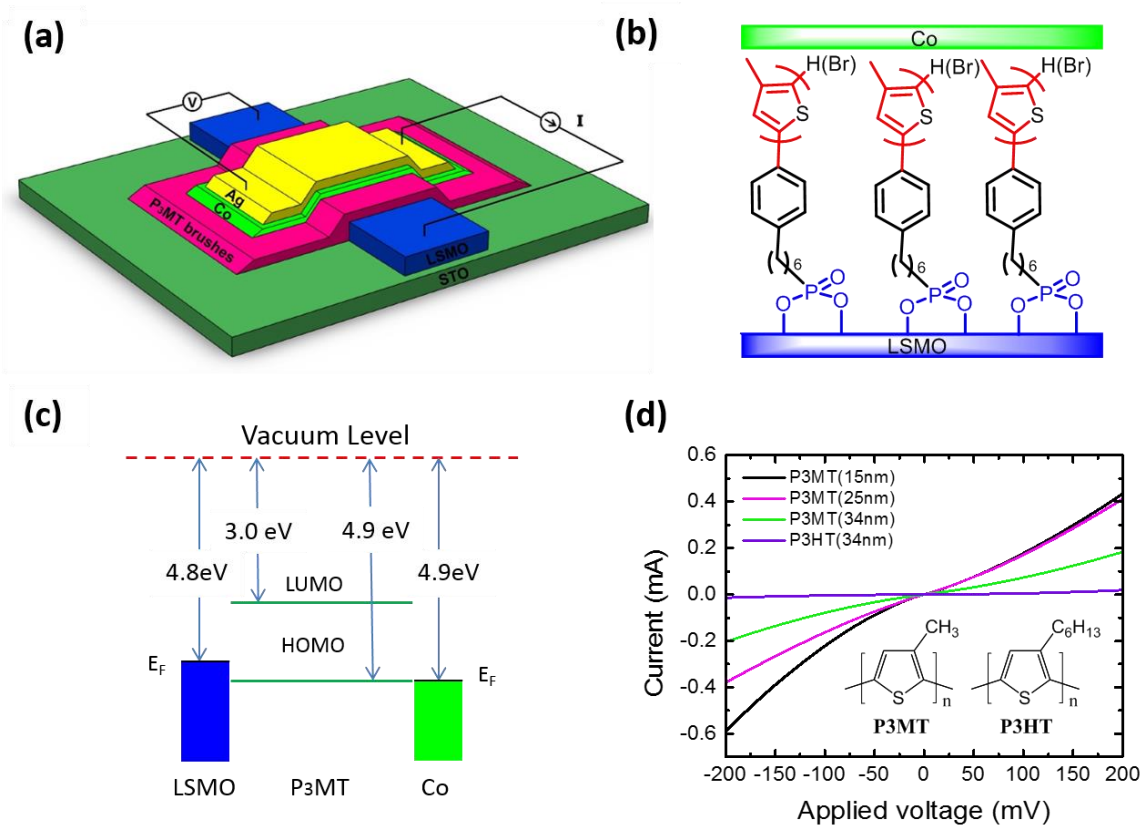

Figure 4.7. (a) Schematic diagram of polymer brush-based OSV with four-probe measurement technique. (b) Schematic diagram of the device cross section showing the P3MT brushes chemically bound to the LSMO surface through phosphonic acid headgroups. (c) The energy band diagram for the device showing the Fermi levels (E_F) and the work functions of LSMO and Co, respectively, and the highest occupied molecular orbital (HOMO) and the lowest unoccupied molecular orbital (LUMO) levels of P3MT brushes. (d) IV-characteristics of the OSVs with different thicknesses measured at 20K. In comparison, the IV curve of P3HT-based OSV with 34nm thickness is also demonstrated (in violet). The inset shows the chemical structure of P3MT and P3HT, respectively.

Organic Spin Valves with Aligned π-Conjugated Polymers and IV Response

Figure 4.8(a) shows a schematic diagram of polymer brush based spin valve device structure where a 50 nm LSMO film with nearly 100% spin polarization (at low temperature) is used as the bottom electrode and a 15 nm Co film with ≈30% spin polarization is used as the top electrode.[2] It is possible to switch the relative magnetization of the FM electrodes between parallel (P) and antiparallel (AP) alignments by sweeping the external magnetic field. The device resistance $R(B)$ at the applied magnetic field B is then dependent on the relative magnetizations. The MR response is commonly defined as $MR(B) = (R\text{AP} - R(B)/R\text{AP}$, where RAP denotes the junction resistance R measured in antiparallel magnetization configuration.[2,46,47] The organic interlayer of P3MT is chemically bonded to the surface of the LSMO electrode as shown in Figure 4.7(b). Using C and ultraviolet-visible (UV–vis) spectroscopy, the highest occupied molecular orbital (HOMO) and the lowest unoccupied molecular orbital (LUMO) energy levels of the brushes were estimated (Figure 4.3). The energy band diagram is shown in Figure 4.7(c) where the energy levels of LSMO, P3MT, and Co are well matched.[2,48] It should be noted that due to the chemical adsorption at the interfaces, the surface work functions of both Co and LSMO may change from the values described in the figure.[49] The HOMO of P3MT was calculated to be 4.9 eV using CV and the LUMO was estimated using UV–vis spectroscopy to be 3.0 eV. The band gap (Eg) of P3MT was therefore estimated to be 1.9 eV, which is similar to energy level values for P3MT found in literature.[50] Figure 4.8(d) shows the I–V characteristics of OSVs with three different thicknesses of the polymer brushes. The IVs show nonohmic behavior, indicating that the devices have no short circuit connection between two electrodes. In addition, the resistance of the device is relatively small compared to resistance of a controlled OSV made by amorphous P3HT film with the same spacer thickness (see Figure 4.7d). The best comparison would be an

OSV using amorphous P3MT film made by spin casting as a control device for evaluating the spin/charge injection and transport of the P3MT brushes-based OSVs. However, it is not possible to spin-cast P3MT solution on substrates due to its extremely low solubility in any organic solvent. In contrast, P3HT is an ideal candidate for comparison because of its excellent solubility for solution processing, and both polymers consist of thiophene repeat units, essentially causing the same spin-related-interactions including HFI and spin–orbit coupling. In addition, the HOMO and LUMO energy levels are similar for both polymers. Interestingly, the resistances of devices made with different brush lengths are quite similar.

This dependence on thickness is weaker than that in OSVs using amorphous organic films.[14,39,51] This might be because of the large mobility of brushes together with the presence of an insulating alkyl spacer monolayer, which causes a certain interfacial resistance. We note that in the single molecule electronics devices, the resistance of the contacts defines the

resistance of the whole device; therefore the IV characteristic is insensitive to the molecular chain length.[34,35] This indicates that the charge transport in our films is governed by both interchain hopping and intrachain transport. Unfortunately, the presence of the interface resistance complicates the behavior of the IV characteristics and we are not able to fit the IV characteristics with the space charge limited current (SCLC) equation for extracting the charge mobility.[52,53] In addition, since the device resistance is quite small, the interfacial resistance of the Co and LSMO contacts may play an important role to reduce MR magnitude.

Magnetoresistance of OSVs

Magnetoresistance Loops

Figure 4.8(a) shows a typical MR loop obtained in the OSV with a 15 nm P3MT brush thickness; a large MR magnitude of ≈70% was observed at 20 K with the applied current of −100 nA. The original MR is shown in Figure 4.5(a). The arrows show the sweeping trace of the magnetic field, and the insets indicate the relative magnetizations of the two FM electrodes. Remarkably, a large MR of ≈2.7% was obtained at 280 K with −105 μV junction voltage shown in Figure 4.8b, while the P3HT-based OSV shows its maximum measurable MR value of 0.3% at 280 K (inset in Figure 4.8(b). The temperature- dependent MR magnitude of the devices with different thicknesses and typical temperature-dependent IVs are shown in Figure4.4). In Figure 4.8(c), magnetooptic Kerr effect (MOKE) measurements performed on LSMO electrode of the device in Figure4.7(a), indicate that the coercive field of the LSMO film is Hc1 ≈ 37 Oe at 20 K. Although the Co electrode of the device is not accessible to MOKE owing to the Ag top contact and opaqueness of LSMO film, the coercive field of a 15 nm Co film deposited on the top of P3MT brush (15 nm)/ITO substrate under the same condition, was measured to be Hc2 ≈ 350 Oe at 20 K from the transparent ITO side. The normalized temperature-dependent MR of the P3MTbased OSVs with different thicknesses clearly shows nearly an order of magnitude weaker dependence than that in the amorphous P3HT film-based OSV (see Figure 4.8(d).

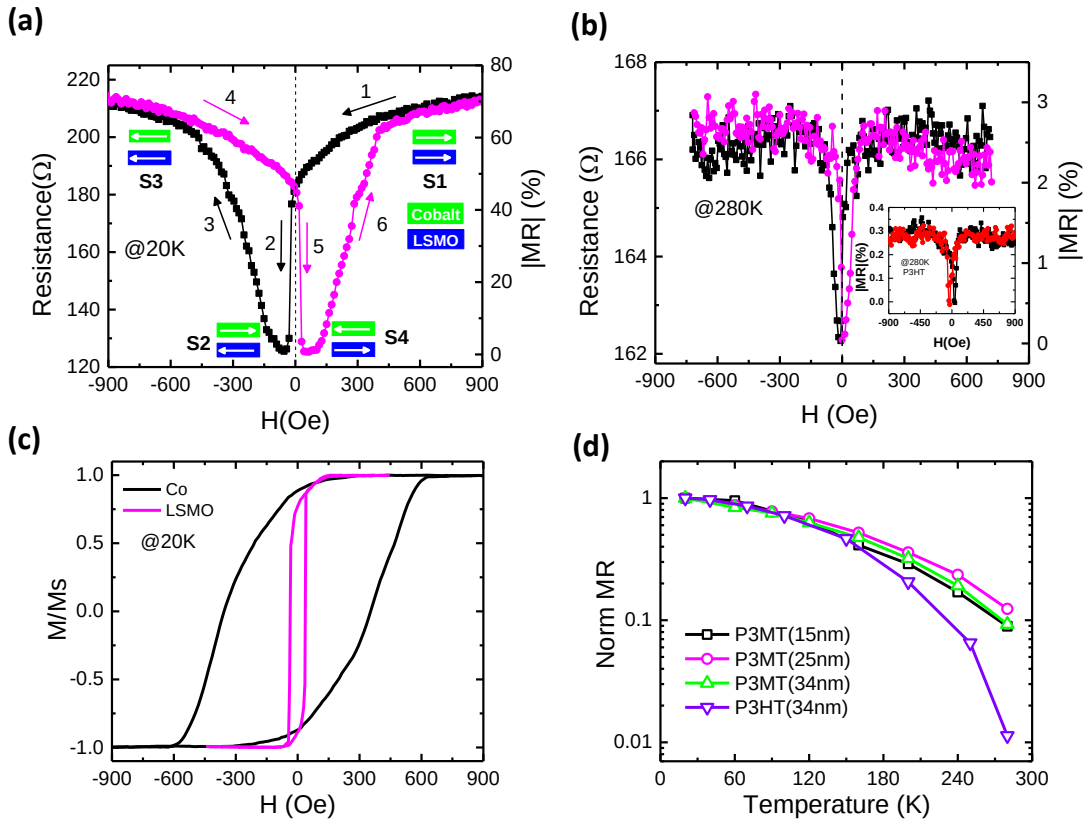

Figure 4.8. The magneto-resistance (MR) response of the polymer brush-based OSVs. The MR loops of LSMO/P3MT(15nm)/Co(15nm)/Ag(50nm) OSV measured (a) at 20K with a current of -100nA and (b) at 280K with current of -0.63uA, respectively. The magnetizations of the electrodes are shown as insets when the external magnetic field is sweeping from positive field to negative field, which is demonstrated by the directional arrows. The inset in (b) shows the MR of LSMO/P3HT(34nm)/Co/Ag at 280K. (c) The magnetic hysteresis loops of LSMO substrate and the structure of ITO/P3MT(15nm)/Co(15nm)/Ag at 20K, respectively. (d) Temperature dependent normalized MR comparison of 34nm P3HT film-based OSV (violet down triangle), and P3MT brush-based OSVs with different thicknesses of 15nm (black square), 25nm (magenta circle) and 34nm (green up triangle), respectively.

There are two scenarios to explain the weaker temperature dependence in the P3MT-based OSVs.[1] The introduction of the monolayer (tunneling barrier) for the covalent bond between the P3MT brush and the LSMO may aid in overcoming the resistance mismatch problem at high temperature and therefore causes a weaker MR decay of the effective spin polarization at the LSMO interface.[41–44] It is worth noting that the resistance mismatch problem can be overcome by using either an appropriate insulator at the interface or an electrode material with 100% spin polarization.[54] The resistance mismatch problem, in principle, is suppressed at cryogenic temperature since the LSMO possesses nearly 100% spin polarization. The tunneling barrier from the monolayer does not play an active role at low temperature. However, since LSMO has low Curie temperature of ≈350 K, the spin polarization is smaller at higher temperature and is almost dismissed at room temperature. The tunneling barrier at high temperature may reduce the conductivity mismatch problem resulting in a better effective spin polarization of LSMO electrode.[2] The interfacial spin polarization of the LSMO might be modified during the monolayer deposition on the LSMO surface.

Thickness Dependence

Figure 4.9(a) shows the bias voltage dependence of MR measured at 20 K with different brush spacer layers that vary in thickness.

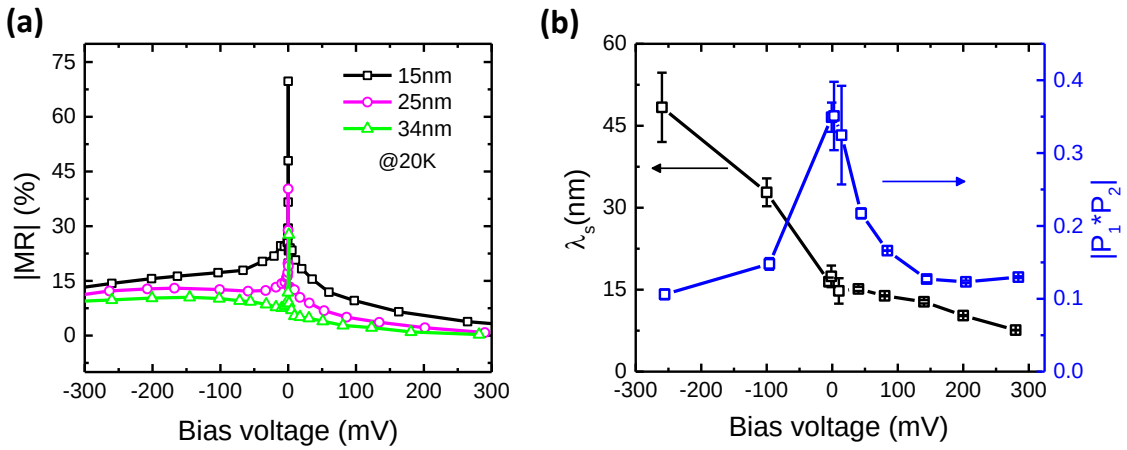

Figure 4.9 (a) Bias voltage dependence of MR with different P3MT thickness at 20K. (b) Spin diffusion λ_s length and the effective spin polarization $|\mathbf{P_1} \cdot \mathbf{P_2}|$with bias voltage dependence at 20K.

The IV characteristics are shown in Figure 4.7(d). Generally, the thicker the interlayer, the smaller the MR magnitude, due to the decay of spin polarization. MR magnitude is large at low bias voltage and then decays rapidly at higher bias voltage. The MR reduction with bias voltage dependence could be explained by two possible mechanisms: (1) the Fermi energy, which decides the density of state of majority and minority spin injection, might be shifted under a relatively large bias voltage; therefore the effective spin polarization of LSMO and/or Co could be modified.[55,56,2] It was suggested that there are two different tunneling processes from the FM electrode into the organic layer; a direct tunneling occurring at low junction bias voltage that conserves spin, and a two-step tunneling via a defect state such as magnetic impurity at the interface occurring at high junction bias voltage that does not conserve spin.[57] Since the relatively

large contact resistance leads to a considerable voltage drops at the junction, the former is more likely to explain the voltage-dependent MR than the latter.[55,56] The asymmetric behavior of MR versus bias voltage has been commonly observed by many groups.[56,58] In addition, the MR magnitudes with thickness dependence in Figure 4a could be fitted using the Julliere model where λs is the effective spin diffusion length of P3MT interlayer; $P1$ and $P2$ are the effective spin polarizations (not the bulk spin polarization) of LSMO and Co, respectively; and d is thickness of the P3MT interlayer. The two free fitting parameters, λs and $P1\_P2$ are shown in Figure 4b. The product of $\_\ P1\ P2$ reduces at large bias voltage due to the modification of the effective spin polarizations of the FM electrodes by the bias voltage as discussed above. Surprisingly, the spin diffusion length λs increases from 17 nm at low junction bias up to 48.4 nm with −260 mV junction bias. This tendency of bias voltage dependence to spin diffusion length may be due to the fact that the drift velocity of the carrier becomes faster at higher applied voltage or electric field. Therefore, the hyperfine interaction becomes less efficient due to the fast charge transit time. This has been theorized by Bobbert et al.[11] Similarly, Yu found that the spin diffusion length increases strongly with increasing charge density of the device in his exchange coupling theory for spin transport in OSECs.[23] However, the spin diffusion length in our devices is smaller with larger positive voltage. This is likely due to the fact that LSMO has a slightly different work function compared to that of the Co layer, resulting in the small negative built-in voltage, Vbi of a few hundred mV. As the result, the internal electric field does not change its direction even when the applied voltage is positive. In principle, the existence of Vbi would cause considerable asymmetric IV characteristics. However, this is not observed in most OSVs.[18,29,59,60] We note that the small spin diffusion length obtained by the fitting is against our expectation. There might be two reasons that Equation (1) might not be used to accurately extract the spin diffusion length from thickness-dependent MR.[1]

The effective spin polarization may change with respect to the chain length since the resistance ratio of the brushes over the LSMO resistance varies with the length.[61] However, this may not be a case since the insulating monolayer is used at the interface and is the same for each brush thickness.[2] The spin relaxation time is dependent on the chain length of the P3MT brush layer. Specifically, the hyperfine interaction is dependent on the extension of the electron orbital wave function or the delocalization of the electron within the P3MT layer.[62,63] It is worth noting that the connection between the HFI strength and the electron delocalization has not been examined in OSECs. The demonstration of the Hanle effect in these polymer brush layers will be a proper method to evaluate the spin diffusion length, and this is currently under investigation. It is worth noting that there were two unsuccessful demonstrations of Hanle effect experiments in vertical OSVs using amorphous OSEC films.[24,25] The reason for the missing effect may be associated with a slow hopping time (due to low mobility) compared to the fast spin precession time.

Conclusion

We have shown that a large MR at room temperature can be obtained in OSVs by covalently immobilizing P3MT to LSMO bottom electrodes using SI-KCTP. To the best of our knowledge, this is the first example of fabricating OSVs with covalently immobilized polymer brushes. After studying the spin injection and transport in these devices, it was observed that the LSMO/polymer brush spinterface is more defined and the brush shows much larger charge carrier mobilities in comparison to spin casted films. The temperature dependence of MR for the brush configuration was also thoroughly studied and observed to be one order lower in magnitude than spin casted films. In conclusion, we believe that this device fabrication method provides a new dimension to the field of OSV devices, where conjugated polymer brushes can be covalently grafted to the electrode surface to improve the spinterface and spin transport in unique ways, thereby greatly enhancing the MR response.

References:

(1) T. D. Nguyen, E. Ehrenfreund, Z. V. Vardeny, *MRS Bull.* **2014**, *39*, 585.

(2) Z. H. Xiong, D. Wu, Z. Valy Vardeny, J. Shi, *Nature* **2004**, *427*, 821.

[(3) W. J. M. Naber, S. Faez, W. G. van der Wiel, *J. Phys. D* **2007**, *40*, R205.

(4) V. A. Dediu, L. E. Hueso, I. Bergenti, C. Taliani, *Nat. Mater.* **2009**, *8*, 707.

(5) S. Datta, B. Das, *Appl. Phys. Lett.* **1990**, *56*, 665.

(6) A. J. Drew, J. Hoppler, L. Schulz, F. L. Pratt, P. Desai, P. Shakya, T. Kreouzis, W. P. Gillin, A. Suter, N. A. Morley, V. K. Malik, A. Dubroka, K. W. Kim, H. Bouyanfif, F. Bourqui, C. Bernhard, R. Scheuermann, G. J. Nieuwenhuys, T. Prokscha, E. Morenzoni, *Nat. Mater.* **2009**, *8*, 109.

(7) M. Cinchetti, K. Heimer, J. Wustenberg, O. Andreyev, M. Bauer, S. Lach, C. Ziegler, Y. Gao, M. Aeschlimann, *Nat. Mater.* **2009**, *8*, 115.

(8)] K. Ando, S. Watanabe, S. Mooser, E. Saitoh, H. Sirringhaus, *Nat. Mater.* **2013**, *12*, 622.

(9) S. Watanabe, K. Ando, K. Kang, S. Mooser, Y. Vaynzof, H. Kurebayashi, E. Saitoh, H. Sirringhaus, *Nat. Phys.* **2014**, *10*, 308.

(0) T. D. Nguyen, E. Ehrenfreund, Z. V. Vardeny, *Science* **2012**, *337*, 204.

(11) P. A. Bobbert, W. Wagemans, F. W. A. v. Oost, B. Koopmans, M. Wohlgenannt, *Phys. Rev. Lett.* **2009**, *102*, 156604.

(12) T. D. Nguyen, G. Hukic-Markosian, F. Wang, L. Wojcik, X. Li, E. Ehrenfreund, Z. V. Vardeny, *Nat. Mater.* **2010**, *9*, 345.

(13) D. Sun, L. Yin, C. Sun, H. Guo, Z. Gai, X. G. Zhang, T. Z. Ward, Z. Cheng, J. Shen, *Phys. Rev. Lett.* **2010**, *104*, 236602.

(14) C. Barraud, P. Seneor, R. Mattana, S. Fusil, K. Bouzehouane, C. Deranlot, P. Graziosi, L. Hueso, I. Bergenti, V. Dediu, F. Petroff, A. Fert, *Nat. Phys.* **2010**, *6*, 615.

(15) T. D. Nguyen, E. Ehrenfreund, Z. V. Vardeny, *Synth. Met.* **2013**, *173*, 16.

(16) S. Sanvito, A. R. Rocha, *J. Comput. Theor. Nanosci.* **2006**, *3*, 624.

(17) F. Djeghloul, F. Ibrahim, M. Cantoni, M. Bowen, L. Joly, S. Boukari, P. Ohresser, F. Bertran, P. Le Fevre, P. Thakur, F. Scheurer, T. Miyamachi, R. Mattana, P. Seneor, A. Jaafar, C. Rinaldi, S. Javaid,J. Arabski, J. P. Kappler, W. Wulfhekel, N. B. Brookes, R. Bertacco,
A. Taleb-Ibrahimi, M. Alouani, E. Beaurepaire, W. Weber, *Sci. Rep.* **2013**, *3*, 1272.

(18) X. Zhang, S. Mizukami, T. Kubota, Q. Ma, M. Oogane, H. Naganuma, Y. Ando, T. Miyazaki, *Nat. Commun.* **2013**, *4*, 1392.

(19) X. Sun, M. Gobbi, A. Bedoya-Pinto, O. Txoperena, F. Golmar, R. Llopis, A. Chuvilin, F. Casanova, L. E. Hueso, *Nat. Commun.* **2013**, *4*, 2794.

(20) Y. Kawasugi, T. Ujino, H. Tada, *Org. Electron.* **2013**, *14*, 3186.

(21) S. H. Liang, R. Geng, Q. T. Zhang, L. You, R. C. Subedi, J. Wang, X. F. Han, T. D. Nguyen, *Org. Electron.* **2015**, *26*, 314.

(22) C. Boehme, J. M. Lupton, *Nat. Nanotechnol.* **2013**, *8*, 612.

(23) Z. G. Yu, *Phys. Rev. Lett.* **2013**, *111*, 016601.

(24) A. Riminucci, M. Prezioso, C. Pernechele, P. Graziosi, I. Bergenti, R. Cecchini, M. Calbucci, M. Solzi, V. Alek Dediu, *Appl. Phys. Lett.* **2013**, *102*, 092407.

(25) M. Grunewald, R. Gockeritz, N. Homonnay, F. Wurthner, L. W. Molenkamp, G. Schmidt, *Phys. Rev. B* **2013**, *88*, 085319.

(26) S. W. Jiang, S. Liu, P. Wang, Z. Z. Luan, X. D. Tao, H. F. Ding, D. Wu, *Phys. Rev. Lett.* **2015**, *115*, 086601.

(27) J. Rybicki, R. Lin, F. Wang, M. Wohlgenannt, C. He, T. Sanders, Y. Suzuki, *Phys. Rev. Lett.* **2012**, *109*, 076603.

(28) Z. G. Yu, *Phys. Rev. Lett.* **2011**, *106*, 106602.

(29) Z. G. Yu, *Nat. Commun.* **2014**, *5*, 4842.

(30) I. Žutic´, J. Fabian, S. Das Sarma, *Rev. Mod. Phys.* **2004**, *76*, 323.

(31) V. Coropceanu, J. Cornil, D. A. da Silva Filho, Y. Olivier, R. Silbey,
J.-L. Bredas, *Chem. Rev.* **2007**, *107*, 926.

(32) M. A. Reed, C. Zhou, C. J. Muller, T. P. Burgin, J. M. Tour, *Science* **1997**, *278*, 252.

(33) T. Dadosh, Y. Gordin, R. Krahne, I. Khivrich, D. Mahalu, V. Frydman, J. Sperling, A. Yacoby, I. Bar-Joseph, *Nature* **2005**, *436*, 677.

(34) X. D. Cui, A. Primak, X. Zarate, J. Tomfohr, O. F. Sankey,
A. L. Moore, T. A. Moore, D. Gust, G. Harris, S. M. Lindsay, *Science* **2001**, *294*, 571.

(35) K. W. Hipps, *Science* **2001**, *294*, 536.

(36) S. K. Sontag, G. R. Sheppard, N. M. Usselman, N. Marshall, J. Locklin, *Langmuir* **2011**, *27*, 12033.

(37) N. Doubina, J. L. Jenkins, S. A. Paniagua, K. A. Mazzio, G. A. MacDonald, A. K. Y. Jen, N. R. Armstrong, S. R. Marder, C. K. Luscombe, *Langmuir* **2012**, *28*, 1900.

(38) M. Yuan, S. Zhan, X. Zhou, Y. Liu, L. Feng, Y. Lin, Z. Zhang, J. Hu, *Langmuir* **2008**, *24*, 8707.

(39) T. L. A. Tran, T. Q. Le, J. G. M. Sanderink, W. G. van der Wiel, M. P. de Jong, *Adv. Funct. Mater.* **2012**, *22*, 1180.

(40) J. J. H. M. Schoonus, P. G. E. Lumens, W. Wagemans, J. T. Kohlhepp, P. A. Bobbert, H. J. M. Swagten, B. Koopmans, *Phys. Rev. Lett.* **2009**, *103*, 146601.

(41) M. Yunus, P. P. Ruden, D. L. Smith, *J. Appl. Phys.* **2008**, *103*, 103714.

(42) D. L. Smith, R. N. Silver, *Phys. Rev. B* **2001**, *64*, 045323.

(43) J. D. Albrecht, D. L. Smith, *Phys. Rev. B* **2002**, *66*, 113303.

(44) E. I. Rashba, *Phys. Rev. B* **2000**, *62*, R16267.

(45) T. D. Nguyen, Y. Sheng, J. Rybicki, G. Veeraraghavan, M. Wohlgenannt, *J. Mater. Chem.* **2007**, *17*, 1995.

(46) M. Julliere, *Phys. Lett. A* **1975**, *54*, 225.

(47) J. S. Moodera, L. R. Kinder, T. M. Wong, R. Meservey, *Phys. Rev. Lett.* **1995**, *74*, 3273.

(48) F. Li, T. Li, F. Chen, F. Zhang, *Sci. Rep.* **2015**, *5*, 9355.

(49) F. Li, Y. Zhan, T.-H. Lee, X. Liu, A. Chikamatsu, T.-F. Guo, H.-J. Lin, J. C. A. Huang, M. Fahlman, *J. Phys. Chem. C* **2011**, *115*, 16947.

(50) S. V. Kamat, J. B. Yadav, V. Puri, R. K. Puri, O. S. Joo, *Appl. Surf. Sci.* **2011**, *258*, 482.

(51) R. Lin, F. Wang, J. Rybicki, M. Wohlgenannt, K. A. Hutchinson, *Phys. Rev. B.* **2010**, *81*, 195214.

(52) M. Lu, H. T. Nicolai, G.-J. A. H. Wetzelaer, P. W. M. Blom, *J. Polym. Sci., Part B: Polym. Phys.* **2011**, *49*, 1745.

(53) P. W. M. Blom, M. C. J. M. Vissenberg, *Mater. Sci. Eng., R* **2000**, *27*, 53.

(54) S. Sanvito, *Chem. Soc. Rev.* **2011**, *40*, 3336.

(55) J. M. De Teresa, A. Barthelemy, A. Fert, J. P. Contour, F. Montaigne, P. Seneor, *Science* **1999**, *286*, 507.

(56) S. W. Jiang, D. J. Shu, L. Lin, Y. J. Shi, J. Shi, H. F. Ding, J. Du, M. Wang, D. Wu, *New J. Phys.* **2014**, *16*, 013028.

(57) J. Zhang, R. M. White, *J. Appl. Phys.* **1998**, *83*, 6512.

(58) F. Wang, Z. V. Vardeny, *J. Mater. Chem.* **2009**, *19*, 1685.

(59) J.-W. Yoo, H. W. Jang, V. N. Prigodin, C. Kao, C. B. Eom, A. J. Epstein, *Phys. Rev. B* **2009**, *80*, 205207.

(60) X. Zhang, Q. Ma, K. Suzuki, A. Sugihara, G. Qin, T. Miyazaki, S. Mizukami, *ACS Appl. Mater. Interfaces* **2015**, *7*, 4685.

(61) A. Fert, H. Jaffres, *Phys. Rev. B* **2001**, *64*, 184420.

(62) I. A. Merkulov, A. L. Efros, M. Rosen, *Phys. Rev. B* **2002**, *65*, 205309.

(63) S. John, K. Alexander, L. Daniel, *J. Phys.: Condens. Matter* **2003**, *15*, R1809.

(64) A. Roy, J. Gao, J. A. Bilbrey, N. E. Huddleston, J. Locklin, *Langmuir* **2014**, *30*, 10465.

(65) N. E. Huddleston, S. K. Sontag, J. A. Bilbrey, G. R. Sheppard, J. Locklin, *Macromol. Rapid Commun.* **2012**, *33*, 2115.

(66) I. Barlow, S. Sun, G. J. Leggett, M. Turner, *Langmuir* **2010**, *26*, 4449.

CHAPTER 5

THERMAL CONDUCTANCE OF POLY(3-METHYLTHIOPHENE) BRUSHES

[1]Anandi Roy, [1] Thomas L. Bougher, Rugang Geng, Jason Locklin, Baratunde A. Cola[*]. Submitted to *Applied Materials and Interfaces*, 04/13/2016

Abstract

A wide variety of recent work has demonstrated that the thermal conductivity of polymers can be improved dramatically through the alignment of polymer chains in the direction of heat transfer. Most of the polymeric samples exhibit high conductivity in either the axial direction of a fiber or in the in-plane direction of a thin film, while the most useful direction for thermal management is often the cross-plane direction of film. Here we show poly(3-methylthiophene) brushes grafted from phosphonic acid monolayers using surface initiated polymerization can exhibit through-plane thermal conductivity greater than 2 W/m-K, a six-fold increase compared to spincoated poly(3-hexylthiophene) samples. The thickness of these films (10-40 nm) is somewhat less than that required in most applications, but the method demonstrates a route toward higher thermal conductivity in covalently-grafted, aligned polymer films.

Introduction

Polymers are generally considered thermal insulators with a thermal conductivity around 0.2 W/m-K owing to their high level of disorder in the bulk state.[1] The strong covalent bonding within the backbone of a polymer chain can effectively conduct heat, but when the chains are tangled, a large amount of the vibrational energy must be transferred between the weak inter-chain van der Waals forces, which significantly reduces the thermal conductivity. However, the perception of polymers as thermally insulating is changing with recent experimental results that demonstrate significant enhancements in pure polymers through new processing and nanostructuring. The concept of achieving high thermal conductivity and elastic modulus in polymer films through mechanical drawing has been demonstrated a number of times mainly through the work of C.L. Choy,[2-4] who demonstrated that the thermal conductivity value of ultra-high molecular weight polyethylene (UHMWPE) could exceed 40 W/m-K with draw ratios greater than 300.[4] This one-hundred-fold increase in the in-plane thermal conductivity is caused by increased crystallinity and orientation of the polymer chains within the crystal lamellae in the plane of the film.

Simulations predicting high thermal conductivity for individual polymer chains,[5-7] crystals,[8] and nanofibers[9] have fueled a rapid increase in the research surrounding the thermal conductivity of polymeric materials. The thermal conductivity of a single polyethylene (PE) chain has been predicted to be as high as 350 W/m-K,[6] and the measured thermal conductivity of a PE nanofiber was reported to be 104 ± 28 W/m-K.[10] Even commercially available highly-drawn microfibers were found to have thermal conductivity values as high as 23 W/m-K.[11] Despite the high values of thermal conductivity achieved, these have typically been in single fibers or the in-plane direction of films. For through-plane thermal conductivity, nanoporous templates have been

used to achieve through-plane thermal conductivity between 1-5 W/m-K,[5, 12] which are more amenable to application compared with individually drawn fibers and films, but still not a fully dense film. Recently, isotropic thermal conductivity (1.5 W/m-K) was achieved through optimizing the hydrogen bonding of a polymer blend.[13] Previous work on polymer brushes showed a very small increase (10%) in thermal conductivity for PMMA brushes compared to spincoated films.[14]

Here we demonstrate that the thermal conductivity of grafted brushes of poly(3-methylthiophene) (P3MT) can significantly exceed that of bulk poly(3-hexylthiophene) (P3HT), primarily due to improvement of the interface on covalent grafting of the polymer directly to the substrate surface, which reduces energetic and positional disorder.[15] In addition, we believe that an improvement in polymer brush alignment further enhances the thermal conductivity. We have used Surface Initiated Kumada Catalyst Transfer Polycondensation (SI-KCTP), a technique widely used by our group and others for grafting well defined conjugated polymers (e.g., poly(3-alkylthiophenes) and poly(phenylenes)) in a chain growth fashion, from surfaces in various organic electronic devices (e.g., solar cells, spin valves).[16-17] We use time domain thermoreflectance (TDTR) to measure the thermal conductivity of polymer brushes (15-36 nm) on Indium tin oxide (ITO)-coated Si substrates. The thermal conductivity of P3MT brushes was found to be up to six times higher compared to similar spincoated P3HT layers of comparable thickness.

Experimental

Materials:

Isopropylmagnesium chloride solution (2.0M in THF) was obtained from Acros Organics, and Bis(cyclooctadiene)nickel(0) was obtained from Strem Chemicals. Tetrahydrofuran (THF) and Toluene solvents were obtained from Sigma Aldrich and purified with an MBRAUN Solvent purification system. Aluminum was obtained from Kurt J. Lesker company (Part#: EVMAL50QXQ). All other chemicals were purchased from TCI, Oakwood, Acros Organics, or EMD Chemicals Inc. and all chemicals were used as received unless mentioned otherwise.

Synthetic Methodology:

All syntheses were carried out under an inert atmosphere of purified argon or nitrogen. Standard Schlenk techniques have been used for synthesis and a glovebox (Unilab BP with an MB10 purification system, MBraun, Inc.) was used for performing SI-KCTP on all substrates. The synthesis of 2-bromo-3-methyl-5-iodothiophene, along with magnesiation of 2-bromo-5-iodo-3-methylthiophene were carried out using previously reported synthetic procedures.[16]

Electrochemical measurements:

Electrochemical measurements were obtained using a CH Instruments bipotentiostat equipped with a platinum counter electrode and a silver wire pseudo reference electrode and Fc/Fc+ was used as an internal standard (0.351V vs. Ag wire electrode). ITO on glass substrates were chosen as working electrodes. Tetrabutylammonium hexafluorophospate in DCM (0.1M, degassed) was used as the supporting electrolyte for all electrochemical measurements. All scans were recorded at a rate of 100 mV/sec.

Preparation of substrates:

Silicon substrates (1cm x 1cm) were cleaned by sonication with acetone, water and IPA and then plasma cleaned for 5 minutes and then dried under stream of nitrogen before performing ITO deposition. For ITO deposition, A 50 nm film ITO was deposited by physical vapor deposition (PVD 75, Kurt J. Lesker) using a 90:10 Ar/O_2 mixture (Airgas) at 5 mTorr at RF 100W power with an ITO target (Kurt J. Lesker, 99.99%) for 1 hr. After ITO deposition, the thickness of the ITO layer was measured by modelling using spectroscopic ellipsometry. These substrates were then annealed under nitrogen atmosphere from 0-400^oC at a rate of 3^o/min, subsequently cooling it down to room temperature at the same rate. The thickness of ITO layer was measured again and was found to decrease only slightly (by ~1 nm). The substrates were then rinsed with IPA and plasma cleaned for 5 minutes again before being used for monolayer deposition.

Monolayer deposition:

Two aryl halide monolayers with phosphonic acid head groups were chosen for this study. 6.5 mM solutions of 6-(4-bromo-2,5-dimethylphenyl) hexylphosphonic acid (DMPHPA) and (6-(4-bromophenyl)hexyl)phosphonic acid (PHPA) in ethanol were prepared and the plasma-cleaned substrates were immersed in 5 mL of these solutions overnight. The substrates were then dried under a stream of nitrogen, and annealed at 150^oC overnight under inert atmosphere. The substrates were subsequently cooled under a nitrogen atmosphere, and rinsed thoroughly with water, methanol and dichloromethane (DCM) and dried under a stream of nitrogen. All substrates were stored under inert atmosphere in the glove box until used for surface initiated polymerization.

Grafting of poly(3-methylthiophene) from ITO-Si substrates

Formation of initiator complex:

In the glovebox, 15 mg of $Ni(COD)_2$ Bis(1,5-cyclooctadiene)nickel(0) and 8.5 mg of 2,2'-bipyridine (bpy) were added to a scintillation vial dry, degassed toluene (5 ml) was added to give a homogeneous solution. Aryl halide monolayers on ITO-Si substrates were then immersed in this solution for three hours for oxidative addition. This was followed by rinsing two times with toluene and THF each before performing ligand exchange with 5 mL of 0.1 M solution of Bis-1,3-diphenylphosphinopropane (dppp) in THF. This process was carried out for one hour and subsequently rinsed with THF before polymerization via SI-KCTP.

Polymerization of 3MT by SI-KCTP:

After oxidative addition, the substrates with reactive initiator were immersed in monomer solution. Overnight, the solution turned bright red, where a significant amount of polymer precipitate was observed. Next, substrates were removed from solution, rinsed with water, methanol and DCM thoroughly, and dried under a stream of nitrogen, before being used for thermal conductivity measurements. The substrates were dark purple after polymerization and the color was homogeneous across the substrate, which is a good indicator of uniform P3MT films. To further investigate the stability of the grafted polymer films, we performed cyclic voltammetry (CV) on these brushes grown from monolayers on ITO-glass (used for electrochemical and optical characterization) under identical reaction conditions.[18] The P3MT films are very stable over multiple cycles of doping and de-doping (**Figure 5.1**.) which indicates excellent interfacial and electrochemical stability.

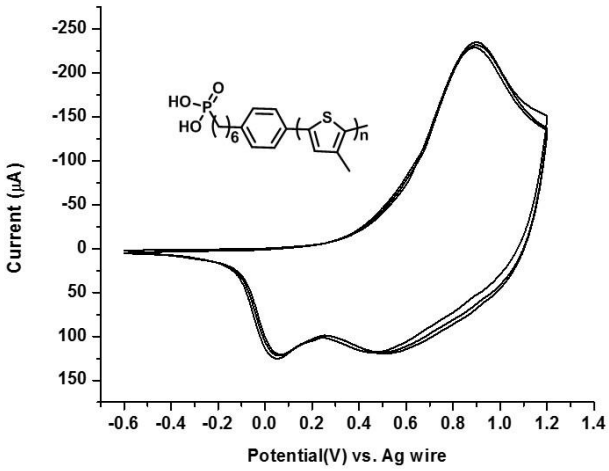

Figure 5.1. CVs over multiple cycles of doping and de-doping, depicting the stability of the P3MT brush grafted on ITO by SI-KCTP starting from monolayer PHPA (inset).

To compare thermal conductivities of systems with covalently grafted and spin coated polymer films, several substrates were prepared using poly(3-hexylthiophene) (P3HT) solutions (10 mg/mL dissolved in *ortho*-dichlorobenzene) that were spin coated onto ITO-Si substrates at 3200 RPM. P3HT was used as a control for solution processing because of the extremely low solubility of P3MT. Both P3MT and P3HT have similar chemical structures, and has been used in our previous work to compare solution based processing to surface grafted layers.[15, 19]

TDTR setup:

TDTR is a pump and probe technique that utilizes an ultra-fast laser with a pulsewidth of less than 1 ps to thermally excite a sample, measure the temperature decay, and extract thermal properties using a diffusive heat conduction model over timescales from 100 to 7000 ps. In the simplest sense the pump beam is a heater and the probe beam is a temperature sensor. The ultra-short laser pulse and high oscillation frequency enable measurement of the temperature decay over short timescales, which allows accurate measurement of thermal properties of thin (sub-hundred

nm) films. In our implementation of TDTR we use a Ti:sapphire laser oscillating at 80.7 MHz with an energy of ~40 nJ/pulse (3 W average power) at a wavelength of 800 nm as described previously.[20] An electro-optic modulator (EOM) is controlled by a function generator and chops the pump beam at a frequency between 3.6 and 11.6 MHz (in this work). The pump pulse is then frequency-doubled to 400 nm using a BiBO crystal so that it is possible to spectrally separate the beams prior to measuring the signal with the photodetector. To focus the beams on to the sample, we use a 5x objective lens with $1/e^2$ diameters of 40 and 14 μm for the pump and probe, respectively.

Results and discussion

Figure 5.2 illustrates the procedure for grafting of P3MT films from ITO-Si substrates via SI-KCTP. The polymerization process involves three consecutive steps of oxidative addition of Ni(0) catalyst across an aryl halide bond of the monolayer, ligand exchange, and monomer addition which proceeds through transmetallation and carbon bond forming reductive elimination, followed by the intramolecular addition of the liberated Ni(0) across the nearest aryl halide bond. This process leads to a chain growth polymerization of polymers directly from the surface.[16-18, 21-22]

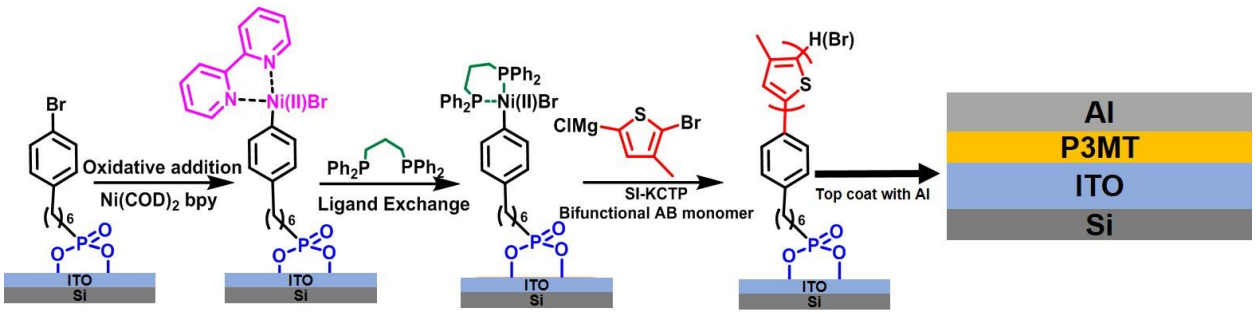

Figure 5.2. Scheme showing grafting of P3MT from PHPA by SI-KCTP on ITO-Si substrate, followed by e-beam deposition of the aluminium transducer layer on top.

After grafting P3MT, the morphology of the films was analyzed by AFM (Figure 5.3(a)). The brushes have a uniform morphology and are densely packed, with an RMS roughness of 5.61 nm, similar to what has been reported in previous studies of P3MT films on ITO.[17, 23]

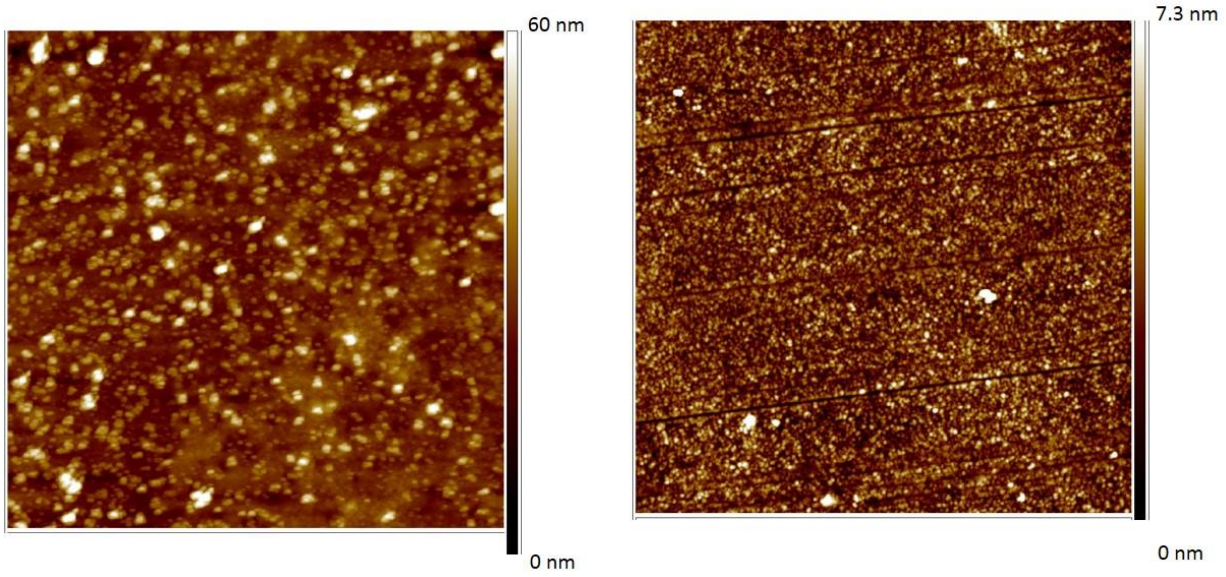

Figure 5.3. AFM topographical images (3um) of (a) 27nm film of P3MT(PHPA) on ITO-Si substrate; RMS roughness of 5.61 nm and (b) bare ITO on Si deposited by thermal evaporation; RMS roughness of 1.05 nm.

The thickness of each polymer layer was also characterized by spectroscopic ellipsometry. After the films were grown, they were coated with a top Al layer by e-beam evaporation with a nominal layer thickness of 90 nm. We did not observe any degradation in performance of these layers after e-beam metal deposition.[15] The exact layer thickness of Al was measured using AFM and picosecond acoustics.[24] The thermal conductivity measurement of multi-layer thin film samples with TDTR can be problematic because of the number of unknown layer and interfacial conductance values. To minimize the number of unknowns we built up the accurate model by isolating each layer separately, first measuring the top Al layer (electrically), and then measuring Al/Si, Al/ITO/Si, and finally Al/P3MT/ITO/Si. Each of the sample configurations was fabricated and metallized with every batch of polymer samples to determine the specific properties of each layer in each sample tested. The thermal conductivity of the Al was determined to be 95 W/m-K

by measuring the electrical resistivity and using the Wiedemann Franz law to estimate the thermal conductivity. The thermal conductivity of the ITO was determined to be 1.35 W/m-K using TDTR and was consistent across multiple batches. Even with isolating the properties of the underlying layers, there can still be difficulty differentiating between interface conductance and layer thermal conductivity as the layer thickness becomes diminishingly small. The ability of a TDTR measurement to measure a specific parameter of interest is typically defined by the sensitivity [25]:

$$S_p = \frac{\partial \ln\left(-V_{in}/V_{out}\right)}{\partial p} \qquad \text{(Eq. 1)}$$

Where S_p is the sensitivity to parameter p, $-V_{in}/V_{out}$ is the normalized TDTR temperature signal, and p is parameter of interest. The larger the absolute value of S_p indicates this parameter can be determined more accurately through the measurement. Figure 2 shows how the sensitivity of the sample thermal conductivity and interface conductance changes with layer thickness and layer thermal conductivity. For thin films, the sensitivity goes up with thermal resistance; therefore thicker and lower conductivity layers are easiest to measure. In this study, this means that the P3HT layers (k ~ 0.3 W/m-K) can be measured with greater accuracy compared with the P3MT brushes (k > 1.0 W/m-K) and values of thermal conductivity above 2 W/m-K cannot be determined with reasonable accuracy due to the diminishing sensitivity. The change in sensitivity with thermal conductivity is captured in the uncertainty, since the sensitivity to model parameters is a direct input for the uncertainty calculation.[26] The sensitivity plots in Figure 2 are shown for 6.3 MHz, while measurements were performed at 3.6 MHz, 6.3 MHz, 8.8 MHz, and 11.6 MHz respectively. In some cases, changes in the heating frequency can dramatically change the sensitivity to different parameters, but since the thin films are fully penetrated by heat at all frequencies considered here, there is not a significant change in sensitivity between frequencies. No systematic trend of thermal

conductivity or total thermal resistance with frequency was observed, and we incorporate the results from all frequencies for the reported values. We used a Monte Carlo simulation to estimate uncertainty as described previously [20] and report the 90th and 10th percentiles as the confidence bounds.

P3MT brushes grafted from two different monolayers were used in this work: (6-(4-bromophenyl)hexyl)phosphonic acid (PHPA), and 6-(4-bromo-2,5-dimethylphenyl) hexylphosphonic acid (DMPHPA) each containing an alkyl spacer length of six carbons. We have observed that varying the substituent pattern on the benzene ring can lead to different packing densities in the monolayers on ITO. This, in turn, influences the rates of competitive side reactions like disproportionation during initiator formation and SI-KCTP, altering the grafting densities and possibly the directionality of the P3MT brushes grown from these layers.[27]

First, cyclic voltammetry was performed using 1 mM $Fe(CN)_6$ in 0.1 M KCl as a solution redox probe, where we observed that both monolayers were perfectly blocking and free of any pinhole defects (Figure 5.4).

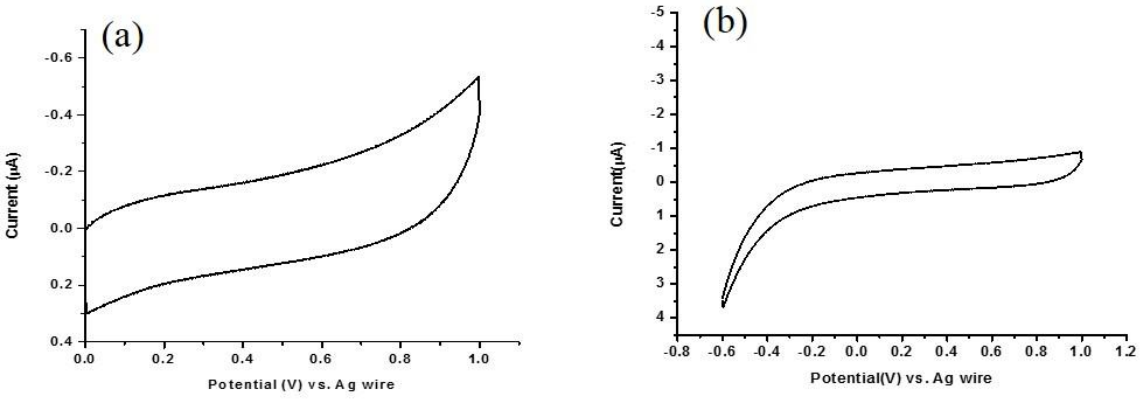

Figure 5.4. Cyclic volatmmograms showing absence of any pinhole defects in the monolayers (a) DMPHPA and (b) PHPA grafted from ITO-glass substrate surface.

We also prepared spin coated P3HT films of similar thickness to compare the thermal conductivity of covalently grafted polymer brushes with that of spin coated polymer films. Since the thermal conductance in the layer is largely dictated by the long P3MT chain rather than the grafted monolayer, it is likely that these monolayers would only affect the layer thermal conductivity by differences in orientation.

The thermal conductivity of the P3MT samples is significantly higher than that of spincoated P3HT in most cases **(Fig. 3(a)),** although within P3MT samples, variations across the samples are observed. When all other properties are equal, a higher ratio of $-V_{in}/V_{out}$ indicates a higher thermal conductance (i.e., lower resistance). The P3HT sample thermal conductivity is 0.32 +/- 0.04/0.06 W/m-K, while the P3MT samples are 0.83 +/- 0.25/0.30 W/m-K and 1.03 +/- 0.13/0.22 W/m-K for P3MT(DMPHPA) and (P3MT)PHPA-Batch 1, respectively (Figure 3(a)). We note that these are the values reported for the data sets in Figure 3a, and not the average for each sample. The thermal conductivity of spincoated P3HT observed is within the range of previously reported values.[28-29] The thermal conductivity for the sample from monolayer PHPA-Batch 2 has thermal conductivity high enough that it cannot be fully determined, but is greater than 2 W/m-K. Multiple spots on the samples from the second batch of monolayer DMPHPA were so highly conductive that the exact values could not be determined for these sub-30 nm films. With such a thin conductive film it is hard to separate the conductance of the layer from the interface.

As discussed previously and shown in Figure 5.5(b) the sensitivity diminishes quickly for higher thermal conductivity because the uncertainty becomes too large.

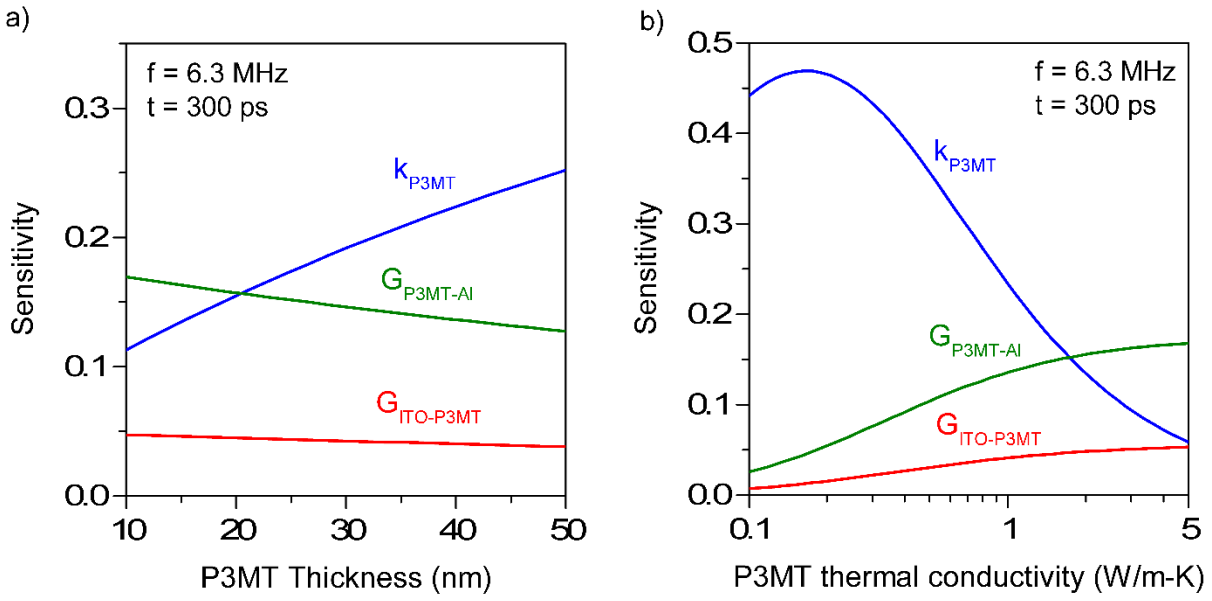

Figure 5.5. Sensitivity of TDTR measurement to polymer thermal conductivity: a) Sensitivity versus polymer layer thickness for k = 0.8 W/m-K b) Sensitivity versus polymer thermal conductivity for 30 nm layer.

In certain cases errors in film thickness can propagate into large errors in the determined thermal conductivity. To check this, we set each layer (Al, P3MT, ITO) to 3 nm less than the determined value, which in each case will lower the fitted thermal conductivity. The resulting P3MT thermal conductivity for these samples is still greater than 2 W/m-K indicating that this is an unlikely Source of the determined high thermal conductivity.

All P3MT samples exhibited a higher degree of variability across the 1 cm^2 sample area compared with the P3HT samples tested. Figure 5.6 b shows three different spots on a P3MT

sample with monolayer PHPA; the three spots are fitted to 1.24 +/- 0.48/0.26 W/m-K, 0.80 +/- 0.12/0.06 W/m-K and 0.34 ± 0.07 W/m-K.

This large variation in thermal conductivity was observed on many of the P3MT samples, while the variation on the P3HT samples was about 10%.

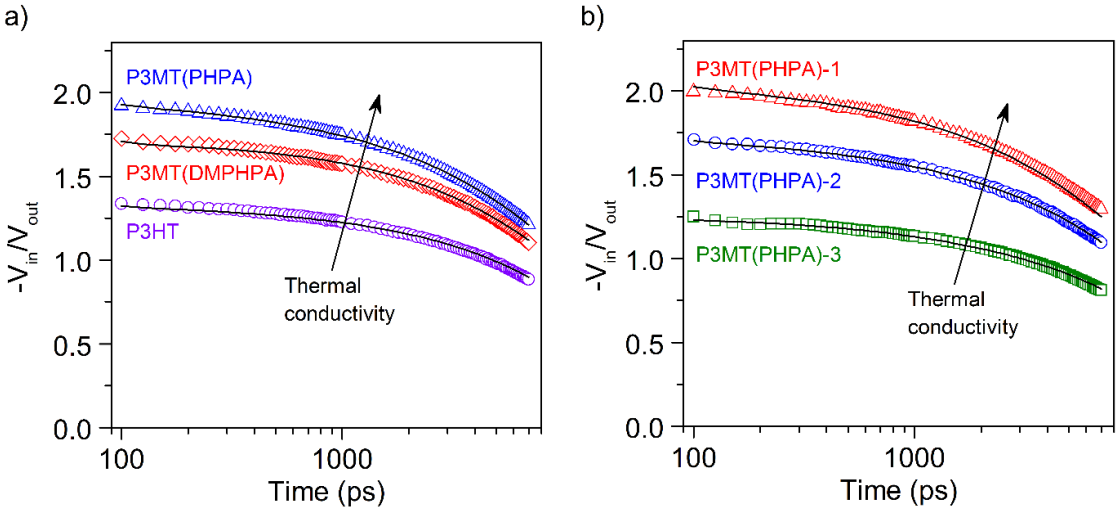

Figure 5.6. TDTR data for P3MT and P3HT films. $-V_{in}/V_{out}$ is the normalized temperature response measured from the Al surface of the sample. a) Comparison of three samples with similar thickness (~35 nm), generally a higher ratio indicates a sample with higher thermal conductivity (k). k_{P3HT} = 0.32 +/- 0.02/0.04 W/m-K, $k_{P3MT\text{-}DMPHPA}$ = 0.75 +/- 0.85/0.19 W/m-K, $k_{P3MT\text{-}PHPA}$ = 1.03 +/- 0.13/0.23 W/m-K b) Comparison of different spots on the same P3MT sample with DMPHPA monolayer, Batch 1. $k_{P3MT\text{-}PHPA}$ (Spot 1) = 1.24 +/- 0.48/0.26 W/m-K, $k_{P3MT\text{-}PHPA}$(Spot 2) = 0.80 +/- 0.12/0.06 W/m-K $k_{P3MT\text{-}PHPA}$ (Spot 3) 0.34 ± 0.07 W/m-K.

We attribute the variability in P3MT samples to local changes in the orientation and alignment of the brush layers. We are probing an area only 1256 μm^2, and the orientation

variability at this length scale may be more than is observed by UV-Vis, where the sample size is an area of $4x10^6$ μm^2 which is about 3000 times larger than the area probed by TDTR.

Because of the high degree of variability within each sample, we do not report a single thermal conductivity value, rather a range as shown in Figure 5.7a.

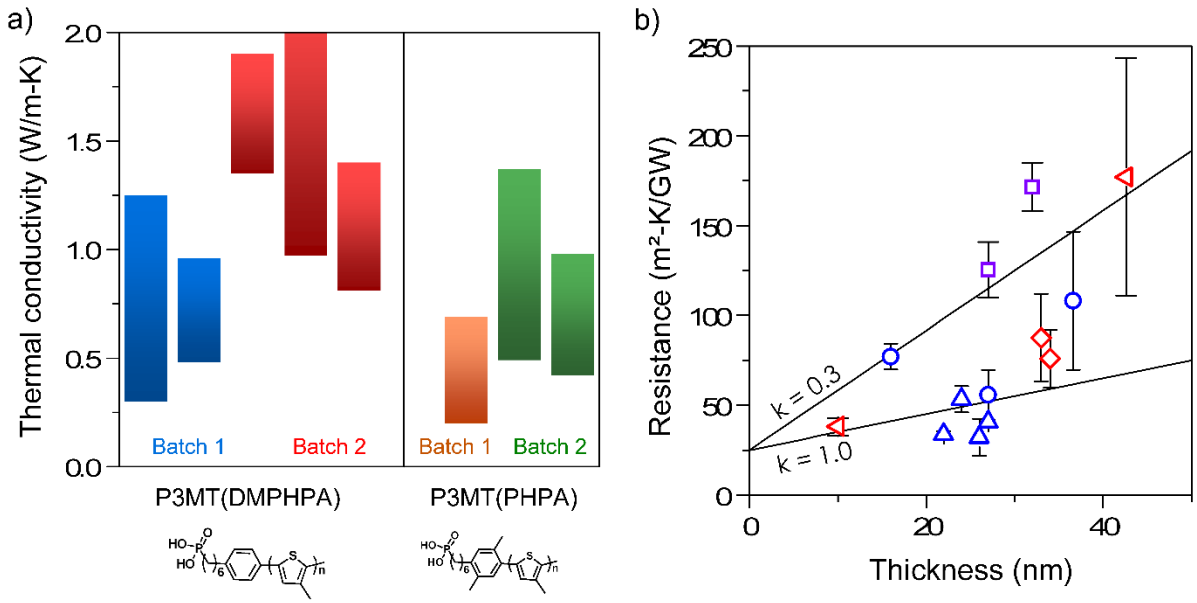

Figure 5.7. a) Thermal conductivity range for P3MT samples. Each bar represents the range of thermal conductivity values measured on a single 1 cm^2 sample, with at least 5 measurements per sample. Batch 1 and batch 2 refer to samples made using the same processing at different times. **b)** Thermal resistance versus polymer film thickness for all samples. Resistance includes the polymer layer resistance and both interfaces (ITO-Polymer and Polymer-Al). Blue circles are P3MT(PHPA), batch 1. Blue triangles are P3MT(PHPA), batch 2. Red sideways triangles are P3MT(DMPHPA), batch 1. Red diamonds are P3MT(DMPHPA), batch 2. Purple squares are spincoated P3HT.

The samples in the second batch exhibited similar variability as batch 1, but were generally more conductive in all cases (Fig. 5.7a). This is likely due to improved uniformity of the polymer brushes grafted on the surface, as measured by spectroscopic ellipsometry. The high conductivity samples (k > 1.5 W/m-K) are at the limit of what we can resolve for sub 30 nm films (**Fig. 2b); but** it is clear the resistance of these samples is very low compared to spincoated P3HT samples. In particular, between the P3MT brushes grown from monolayers PHPA and DMPHPA there is a difference in conductivity observed in every batch, the conductivity of brushes grown from DMPHPA being lower than those grown from PHPA. The most probable reason for such a difference is the degree of orientation/H-aggregation observed in the P3MT(PHPA) brushes as compared to P3MT(DMPHPA) brushes. This is apparent from the UV-VIS data (Figure 5.7) which shows that the λ_{max} for P3MT(PHPA) is more pronounced and blue shifted to 415 nm whereas the λ_{max} of P3MT(DMPHPA) is observed at 465 nm, the typical value for isotropic P3MT brushes.[30-31] (Figure 5.8)

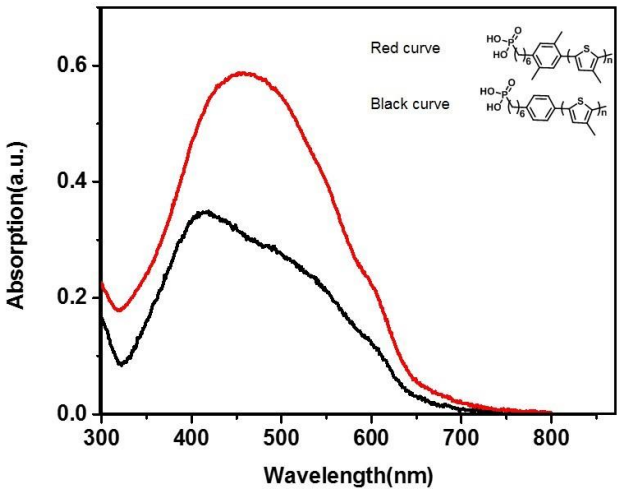

Figure 5.8. UV-VIS measurements of P3MT brushes fabricated from monolayers PHPA (black curve) and DMPHPA(red curve). The film made from PHPA clearly shows H-aggregation as the λ_{max} is blue shifted to a great extent to 415 nm, whereas brush from monolayer DMPHPA doesn't, with λ_{max} being 460 nm.

This preferential alignment of the polymer chains (P3MT(PHPA)) will increase thermal conductivity, since heat can conduct directly up the polymer backbone in many instances. Molecular dynamics simulations have estimated the thermal conductivity of an individual unsubstituted polythiophene chain to be ~40 W/m-K,[5] although the side chain in P3MT may reduce the thermal conductivity somewhat through the increase in scattering of propagating vibrational modes. Even if the single chain thermal conductivity were only 20 W/m-K, it would only take a very modest degree of chain alignment to result in a bulk thermal conductivity of 2 W/m-K as observed in some samples here. Polymer brushes are unique macromolecular monolayers, where some or most of the polymer chains will extend completely from one interface to the other, eliminating the inefficient inter-chain transfer of vibrational energy that is typically the limiting

factor in heat conduction in bulk polymers.[1] Even though the polymer chains in sample DMPHPA have no preferred orientation as measured by polarized UV-vis data, these samples are still benefitting from certain chains that extend vertically through the sample creating some low resistance pathways for conduction. The best samples for monolayer PHPA are about twice as conductive as those for monolayer DMPHPA showing that more chain alignment in the vertical direction will increase thermal conductivity.

The total thermal resistance of the sample includes the resistance at each interface along with the resistance of the layer:

$$R_{total} = \frac{1}{G_{ITO-Polymer}} + \frac{L_{Polymer}}{k_{Polymer}} + \frac{1}{G_{Polymer-Al}}$$

Because of the low sensitivity to the individual interface conductance parameters ($G_{ITO\text{-}polymer}$ and $G_{polymer\text{-}Al}$), we cannot independently extract the value of each interface, rather we can determine the total interface conductance or boundary resistance. The total boundary resistance of all samples was in the range of 17 to 41 m^2-K/GW; there was not a noticeable difference between the spincoated P3HT interfaces and the covalently attached P3MT interfaces, which means either adhesion strength is not the limiting factor of thermal conductance across the ITO-polymer interface or that the Al-polymer interfacial resistance is so large as to mask smaller changes in resistance at the other interface. The total resistance as a function of film thickness is shown in Figure 4b. Along with the measurements, two lines are shown: the resistance for a sample with $R_{interfaces}$ = 25 m^2-K/GW and layer thermal conductivity of either 0.3 or 1.0 W/m-K. The P3HT sample and two of the P3MT samples fall along the k = 0.3 W/m-K line indicating relatively high resistivity. The P3MT samples from batch 2 with both monolayers fall well below the 0.3 W/m-K line with most near or below the 1.0 W/m-K line indicating samples with relatively low resistivity. Previous work on the thermal conductance of PMMA brushes showed that the interfacial resistance

did not become dominate until extremely thin samples (~6 nm) were probed, owing to the low thermal conductivity of the PMMA (~ 0.22 W/m-K).[14] For the k = 1.0 W/m-K line, the layer and interfacial resistances are equal for a thickness of 25 nm, which means that the P3MT brushes from batch 2 can be significantly thicker compared to the PMMA before the layer resistance dominates the sample.

Conclusion

P3MT brushes grafted from ITO were measured with time domain thermoreflectance and found to exhibit exceptional through-plane thermal conductivity values ranging from 0.3 to greater than 2 W/m-K, compared with 0.3 W/m-K for spincoated P3HT films. The thermal conductivity the polymer brushes in this study appear to have variability that we attribute to differences in chain orientation of the polymer backbones. The P3MT(PHPA) samples with better orientation and H-aggregation exhibited higher thermal conductivity, exceeding 2 W/m-K for several samples, although the exact values of the highly conductive samples was difficult to ascertain given the thickness of the films (< 40 nm). Even the P3MT(DMPHPA) samples with no preferred orientation exhibited thermal conductivity above 1 W/m-K in some cases, demonstrating the efficiency of higher order of the covalently grafted extended polymer chains for heat transport, even when they are isotropic. Despite variability, the polymer brush samples have significantly lower thermal resistance compared to spincoated P3HT, indicating this fabrication methodology may be an effective strategy for thermal management in future applications.

References:

(1). Henry, A., Thermal Transport in Polymers. *Ann. Rev. Heat. Transf.* **2013**.

(2). Choy, C. L., Thermal conductivity of polymers. *Polymer* **1977,** *18* (10), 984-1004.

(3). Choy, C. L.; Chen, F. C.; Luk, W. H., Thermal conductivity of oriented crystalline polymers. *J.Polym. Sci. Pol. Phys.* **1980,** *18* (6), 1187-1207.

(4). Choy, C. L.; Wong, Y. W.; Yang, G. W.; Kanamoto, T., Elastic modulus and thermal conductivity of ultradrawn polyethylene. *J. Polym. Sci.B: Polym. Phys.* **1999,** *37* (23), 3359-3367.

(5). Singh, V.; Bougher, T. L.; Weathers, A.; Cai, Y.; Bi, K.; Pettes, M.; Wei, L.; Resler, D. P.; Gattuso, T. R.; Altman, D. H.; Sandage, K. H.; Shi, L.; Henry, A.; Cola, B. A., High Thermal Conductivity of Chain-Oriented Amorphous Polythiophene. *Nat. Nanotechnol.* **2014**.

(6). Henry, A.; Chen, G., High thermal conductivity of single polyethylene chains using molecular dynamics simulations. *Phys. Rev. Lett.* **2008,** *101* (23), 235502.

(7). Liu, J.; Yang, R., Length-dependent thermal conductivity of single extended polymer chains. *Phys. Rev. B* **2012,** *86*.

(8). Henry, A.; Chen, G.; Plimpton, S. J.; Thompson, A., 1D-to-3D transition of phonon heat conduction in polyethylene using molecular dynamics simulations. *Phys. Rev. B* **2010,** *82* (14), 144308.

(9). Zhang, T.; Wu, X.; Luo, T., Polymer Nanofibers with Outstanding Thermal Conductivity and Thermal Stability: Fundamental Linkage between Molecular Characteristics and Macroscopic Thermal Properties. *J. Phys. Chem.* **2014,** *118* (36), 21148-21159.

(10). Shen, S.; Henry, A.; Tong, J.; Zheng, R. T.; Chen, G., Polyethylene nanofibres with very high thermal conductivities. *Nat. Nanotechnol.* **2010,** *5* (4), 251-255.

(11). Wang, X.; Ho, V.; Segalman, R. A.; Cahill, D. G., Thermal Conductivity of High-Modulus Polymer Fibers. *Macromolecules* **2013,** *46* (12), 4937-4943.

(12). Miguel, R.; Jaime, M.; Stéphane, G.; Theodorian, B.-T.; Stefan, D.; Marisol, M.-G., Decrease in thermal conductivity in polymeric P3HT nanowires by size-reduction induced by crystal orientation: new approaches towards thermal transport engineering of organic materials. *Nanoscale* **2014,** *6* (14), 7858.

(13). Kim, G.-H.; Lee, D.; Shanker, A.; Shao, L.; Kwon, M. S.; Gidley, D.; Kim, J.; Pipe, K. P., High thermal conductivity in amorphous polymer blends by engineered interchain interactions. *Nat. Mater.* **2015,** *14* (3), 295-300.

(14). Losego, M. D.; Moh, L.; Arpin, K. A.; Cahill, D. G.; Braun, P. V., Interfacial thermal conductance in spun-cast polymer films and polymer brushes. *Appl. Phy.s Lett.* **2010,** *97* (1), 011908-3.

(15). Geng, R.; Roy, A.; Zhao, W.; Subedi, R. C.; Li, X.; Locklin, J.; Nguyen, T. D., Engineering of Spin Injection and Spin Transport in Organic Spin Valves Using π-Conjugated Polymer Brushes. *Adv. Funct. Mater.* **2016**, n/a-n/a.

(16). Sontag, S. K.; Sheppard, G. R.; Usselman, N. M.; Marshall, N.; Locklin, J., Surface-Confined Nickel Mediated Cross-Coupling Reactions: Characterization of Initiator Environment in Kumada Catalyst-Transfer Polycondensation. *Langmuir* **2011,** *27* (19), 12033-12041.

(17). Sontag, S. K.; Marshall, N.; Locklin, J., Formation of conjugatedpolymer brushes by surface-initiated catalyst-transfer polycondensation. *Chem. Commun.* **2009,** (23), 3354-3356.

(18). Doubina, N.; Jenkins, J. L.; Paniagua, S. A.; Mazzio, K. A.; MacDonald, G. A.; Jen, A. K. Y.; Armstrong, N. R.; Marder, S. R.; Luscombe, C. K., Surface-Initiated Synthesis of Poly(3-

methylthiophene) from Indium Tin Oxide and its Electrochemical Properties. *Langmuir* **2012,** *28* (3), 1900-1908.

(19). Yang, L.; Sontag, S. K.; LaJoie, T. W.; Li, W.; Huddleston, N. E.; Locklin, J.; You, W., Surface-Initiated Poly(3-methylthiophene) as a Hole-Transport Layer for Polymer Solar Cells with High Performance. *ACS Appl.Mater.Interfaces* **2012,** *4* (10), 5069-5073.

(20). Bougher, T. L.; Yates, L.; Lo, C.-F.; Johnson, W.; Graham, S.; Cola, B. A., Thermal boundary resistance in GaN films measured by time domain thermoreflectance with robust Monte Carlo uncertainty estimation. *Nanosc. Microsc. Therm.* **2016,** (just-accepted).

(21). Senkovskyy, V.; Sommer, M.; Tkachov, R.; Komber, H.; Huck, W. T. S.; Kiriy, A., Convenient Route To Initiate Kumada Catalyst-Transfer Polycondensation Using Ni(dppe)Cl2 or Ni(dppp)Cl2 and Sterically Hindered Grignard Compounds. *Macromolecules* **2010,** *43* (23), 10157-10161.

(22). Bilbrey, J. A.; Sontag, S. K.; Huddleston, N. E.; Allen, W. D.; Locklin, J., On the Role of Disproportionation Energy in Kumada Catalyst-Transfer Polycondensation. *Acs Macro. Lett.* **2012,** *1* (8), 995-1000.

(23). Roy, A.; Gao, J.; Bilbrey, J. A.; Huddleston, N. E.; Locklin, J., Rapid Electrochemical Reduction of Ni(II) Generates Reactive Monolayers for Conjugated Polymer Brushes in One Step. *Langmuir* **2014,** *30* (34), 10465-10470.

(24). Hohensee, G. T.; Hsieh, W. P.; Losego, M. D.; Cahill, D. G., Interpreting picosecond acoustics in the case of low interface stiffness. *Rev. Sci. Instrum.* **2012,** *83* (11).

(25). Gundrum, B. C.; Cahill, D. G.; Averback, R. S., Thermal conductance of metal-metal interfaces. *Phys. Rev. B* **2005,** *72* (24), 245426.

(26). Wei, C. D.; Zheng, X.; Cahill, D. G.; Zhao, J. C., Invited Article: Micron resolution spatially resolved measurement of heat capacity using dual-frequency time-domain thermoreflectance. *Rev. Sci. Instrum.* **2013,** *84* (7).

(27). Yamamoto, T.; Wakabayashi, S.; Osakada, K., Mechanism of C□C coupling reactions of aromatic halides, promoted by Ni(COD)2 in the presence of 2,2′-bipyridine and PPh3, to give biaryls. *J. Organomet. Chem.* **1992,** *428* (1), 223-237.

(28). Duda, J. C.; Hopkins, P. E.; Shen, Y.; Gupta, M. C., Thermal transport in organic semiconducting polymers. *Appl. Phys. Lett.* **2013,** *102* (25), 251912.

(29). Sun, J.; Yeh, L. M.; Jung, B. J.; Zhang, B.; Feser, J.; Majumdar, A.; Katz, H. E., Simultaneous Increase in Seebeck Coefficient and Conductivity in a Doped Poly(alkylthiophene) Blend with Defined Density of States. *Macromolecules* **2010,** *43* (6), 28972903.

(30). Huddleston, N. E.; Sontag, S. K.; Bilbrey, J. A.; Sheppard, G. R.; Locklin, J., Palladium-Mediated Surface-Initiated Kumada Catalyst Polycondensation: A Facile Route Towards Oriented Conjugated Polymers. *Macromol. Rapid. Comm.* **2012,** *33* (24), 2115-2120.

(31). Ma, J.; Hashimoto, K.; Koganezawa, T.; Tajima, K., End-On Orientation of Semiconducting Polymers in Thin Films Induced by Surface Segregation of Fluoroalkyl Chains. *J Am Chem Soc* **2013,** *135* (26), 9644-9647.

CHAPTER 6

CONCLUSIONS AND OUTLOOK

In this work, conjugated polymer, P3MT brushes have been grafted from surfaces of variety of substrates by SI-KCTP. This offers a very versatile technique to grow conjugated polymer chains that are covalently immobilized from substrate surface. High grafting density can be attained using this *grafting from* technique as compared to *grafting to* or *grafting through* techniques. This method offers a way to grow polymer chains that have higher order, as compared to polymeric layers deposited by other techniques like spin coating. Spin coating techniques make highly amorphous polymer coatings as polymer chains remain in their random coil configuration, as opposed to *grafting from* techniques, which can make highly ordered and stretched polymer chains. This highly stretched regime is known as the brush regime and polymer brushes show several interesting optical and electronic properties in this regime. This is the regime that has been exploited in all of these reported studies.

The objective of this study was to ultimately grow P3MT brushes that could be used in fabrication of efficient OEDs. So far applications of these brushes towards actual device fabrication is limited. This is owing to the extreme difficulty in growing brushes with an appropriate balance between grafting density as well as directionality, required for efficient carrier transport through the polymer chains in a two terminal device. These difficulties are due to several limitations posed by the surface grafting reactions, e.g., competitive side reactions. The first part of this work is therefore dedicated to improve the efficiency of SI-KCTP reaction by (a) modifying the time consuming reaction procedures, (b) investigating the mechanistic pathways in detail and

analyzing structural parameters required to generate high grafting density films. The second part involves application of the developed polymer brushes in fabricating efficient organic electronic devices.

At the end of this study, uniform P3MT brushes with an empirically optimized balance between grafting density and orientation were synthesized. These were utilized to successfully fabricate organic spintronic devices. Their thermal conductivities were also thoroughly characterized and were proven to have great potential in fabricating heat conducting devices.

Chapter 2 explains how the SI-KCTP reaction conditions are modified from the currently used procedures. With the use of electrochemical reduction techniques on gold substrates, reactive initiator monolayers are generated very rapidly and ligand exchange step is completely avoided. This reduced the rates of disproportionation and we obtained an appreciable 6-fold increase in surface coverage (~21%), the maximum coverage achievable being 25%.

Chapter 3 focuses on the structure-function relationship of the reactive initiator monolayer to the growth of P3MT brushes. Several monolayers were synthesized by varying structural parameters systematically and the polymer brushes from corresponding monolayers were also thoroughly characterized. On detailed analysis, the ideal monolayer was found to be PHPA. This was found to produce high grafting density brushes, and most importantly it induced pronounced H-Aggregation in the polymer brushes that none other monolayers could generate. The brushes were found to be oriented at an average angle of 55^0. This optimum balance between grafting density and directionality made the PHPA monolayer an ideal candidate for application in OEDs.

Chapter 4 demonstrates the usage of P3MT(PHPA) brushes in fabricating organic spin valve devices (OSV). The OSVs fabricated with covalently grafted P3MT(PHPA) brush showed very high magnetoresistance response of 70% at 20K and 3% at RT. In comparison, spin coated

P3HT based OSV showed very low MR response of about 0.3% at RT. This proved the hypothesis that covalently immobilized brushes provide higher degree of ordering the organic layer and more intimate contact with the substrate surface. This improved the spinterface, enhancing spin injection and more efficient transport of electron spins, between two terminals of the OSV.

Chapter 5 further proves that the polymer brushes offer better interfaces and more order when used to fabricate devices. Amorphous polymeric materials are poor thermal conductors. Their disordered state limits efficient transfer of phonons due to voids/entanglements and several coupling spots between the chains. This can now be overcome by using P3MT brushes covalently bound to a substrate surface. On measurement by TDTR, the aligned brushes showed the highest thermal conductivity followed by un-aligned ones, and the least conductivity was shown by the spin coated films. So covalently grafted conjugated polymers can now be used as thermally conducting materials too.

Future work

The work in this dissertation has provided a pathway to generate P3MT brushes by SI-KCTP that can be applied to fabricate organic electron devices. The detailed investigation on the structure-function relationship of initiator monolayers towards polymer brush growth gives an insight into the rationale behind designing monolayers for efficient SI-KCTP. Structural parameters can be tuned systematically based on the properties required in a device. A lot of information has been acquired regarding how the rates of competitive side reactions are altered at different initiator environments. The cumulative analysis of different kinds of interactions between the growing chains in a brush helps in a better understanding of SI-KCTP mechanistic pathways. Monomer scope can also be expanded in future, that can help in tuning bandgap of conjugated polymers. Also the use of expensive Pd catalyst can now be avoided and less expensive Ni catalyst

can be used. Initial success observed in device fabrication has opened up a new dimension where the P3MT brushes can now be successfully applied for fabrication of several other devices like heat conducting devices, organic light emitting diodes (OLEDs), organic solar cell devices with improved efficiencies.

Final remarks

SI-KCTP has proven to be a versatile method to generate surface bound conjugated polymer by the *grafting from* approach. This approach provides a way to generate uniform polymeric coatings on objects with complex geometries. It prevents delamination and provides better interfaces in fabricated devices. The recent improvements in generation of thick and oriented brushes for making devices has shown that this method offers endless possibilities in the field of OEDs. However, even though this method has a lot of potential, certain limitations still lead to decrease in the efficiencies of these reactions. Different devices may have different requirements in terms of grafting densities and brush geometries and this can be achieved by understanding the structure-function relationship. Systematic observation, characterization and manipulation of reaction parameters can help in overcoming limitations of this process. This work is aimed at stimulating interest in the field of conjugated polymers and their immense potential for application towards fabricating high performance OEDs.

APPENDIX A

^{1}HNMR STRUCTURE OF COMPOUNDS

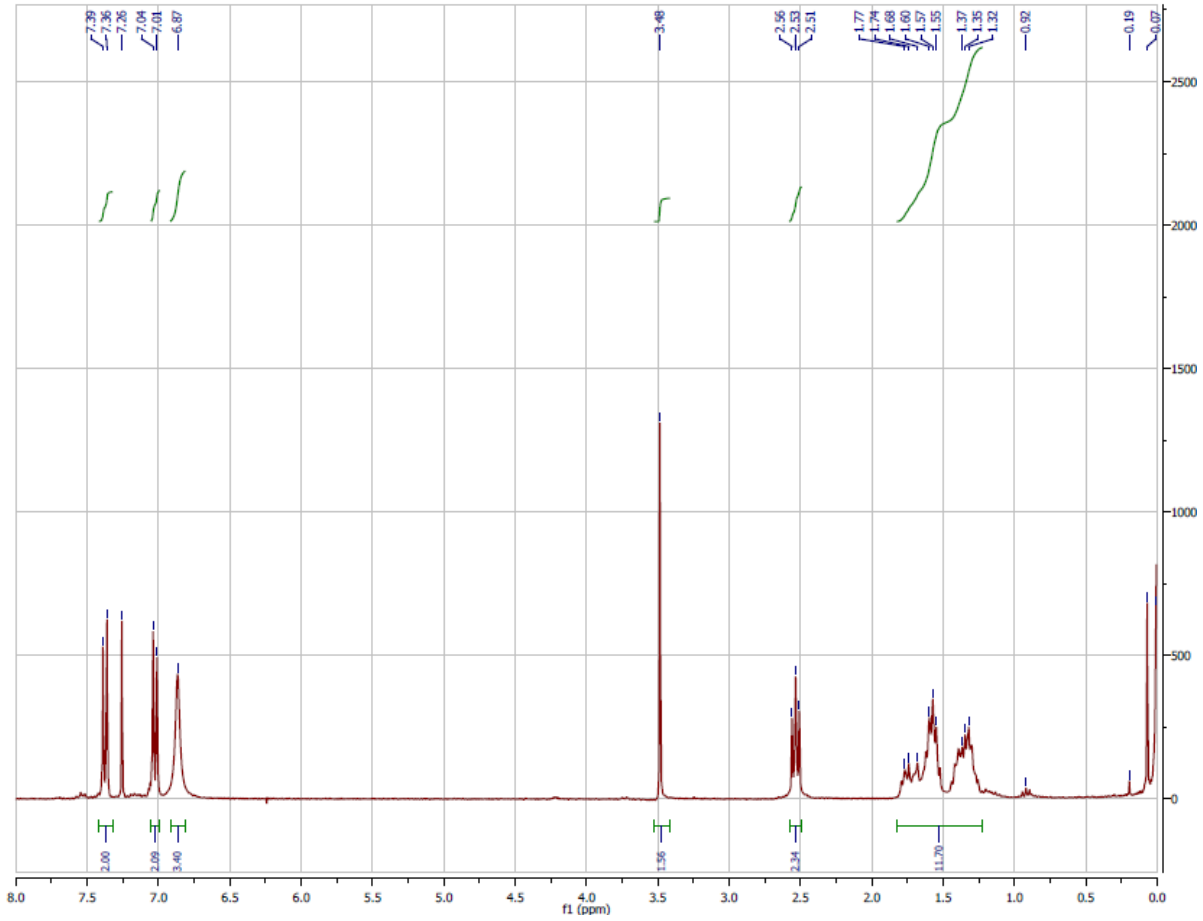

Figure A-1 . ^{1}HNMR of (6-(4-bromophenyl)hexyl)phosphonic acid in $CDCl_3$

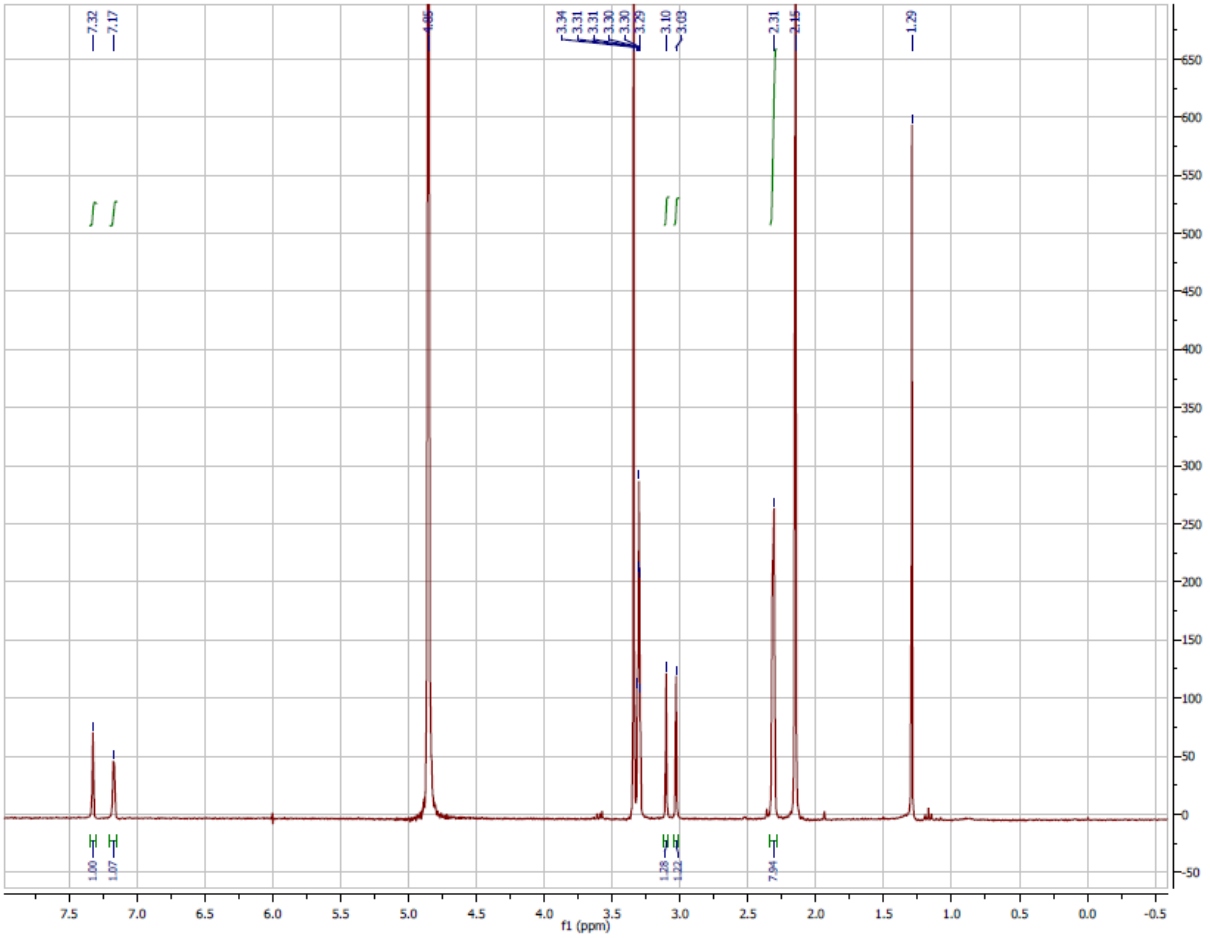

Figure A-2. ^{1}HNMR of (4-bromo-2,5-dimethylbenzyl)phosphonic acid in CD_3OD

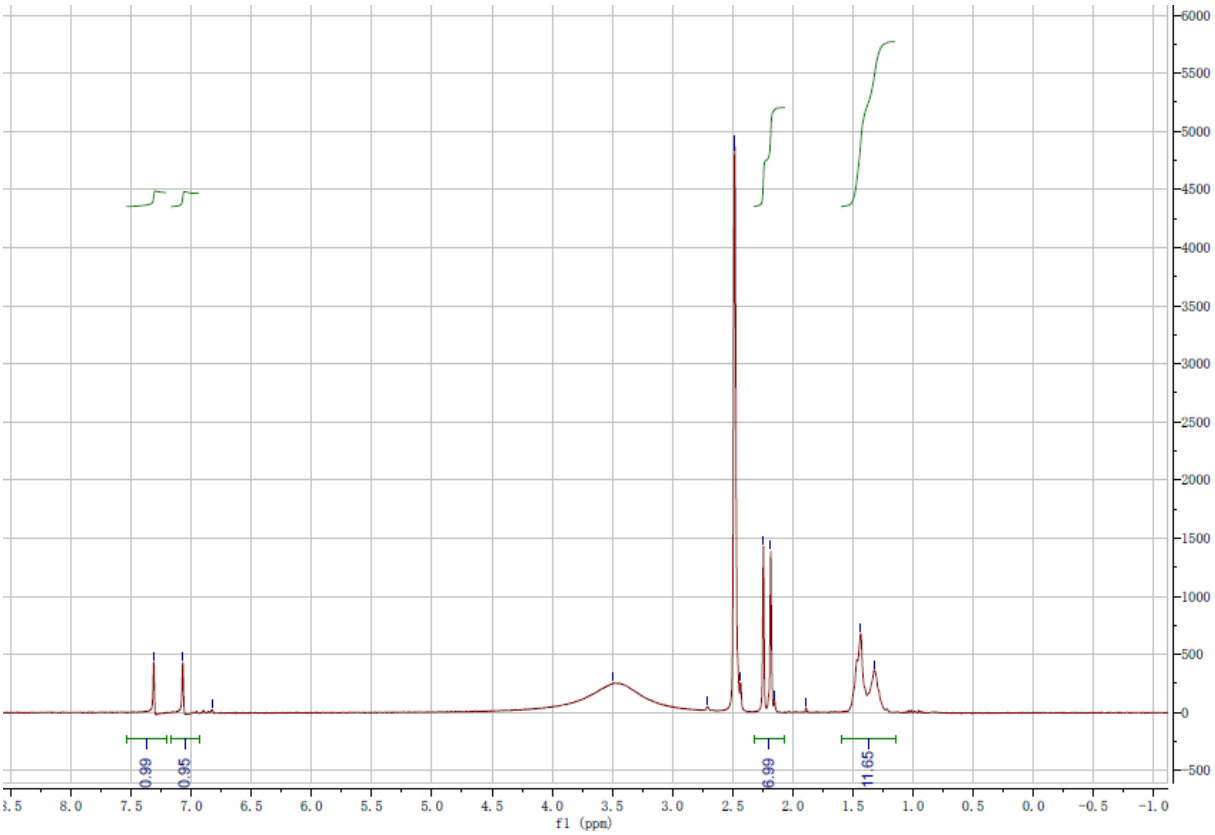

Figure A-3. [1]HNMR of (6-(4-bromo-2,5-dimethylphenyl)hexyl)phosphonic acid in DMSO-d6